Z. Zhao

Shape Design Sensitivity Analysis and Optimization Using the Boundary Element Method

Lecture Notes in Engineering

The Springer-Verlag Lecture Notes provide rapid (approximately six months), refereed publication of topical items, longer than ordinary journal articles but shorter and less formal than most monographs and textbooks. They are published in an attractive yet economical format; authors or editors provide manuscripts typed to specifications, ready for photo-reproduction.

The Editorial Board

Lecture Notes in Engineering

Edited by C. A. Brebbia and S. A. Orszag

62

Z. Zhao

Shape Design Sensitivity Analysis and Optimization Using the Boundary Element Method

Series Editors
C. A. Brebbia · S. A. Orszag

Consulting Editors
J. Argyris · K.-J. Bathe · A. S. Cakmak · J. Connor · R. McCrory
C. S. Desai · K.-P. Holz · F. A. Leckie · G. Pinder · A. R. S. Pont
J. H. Seinfeld · P. Silvester · P. Spanos · W. Wunderlich · S. Yip

Author
Dr. Zhiye Zhao
School of Civil and Structural Engineering
Nanyang Technological University
Nanyang Avenue
Singapore 2263

PREFACE

This book investigates the various aspects of shape optimization of two-dimensional continuum structures, including shape design sensitivity analysis, structural analysis using the boundary element method (BEM), and shape optimization implementation.

The book begins by reviewing the developments of shape optimization, followed by the presentation of the mathematical programming methods for solving optimization problems. The basic theory of the BEM is presented which will be employed later on as the numerical tool to provide the structural responses and the shape design sensitivities.

The key issue of shape optimization, the shape design sensitivity analysis, is fully investigated. A general formulation of stress sensitivity using the continuum approach is presented. The difficulty of the modelling of the adjoint problem is studied, and two approaches are presented for the modelling of the adjoint problem. The first approach uses distributed loads to smooth the concentrated adjoint loads, and the second approach employs the singularity subtraction method to remove the singular boundary displacements and tractions from the BEM equation.

A novel finite difference based approach to shape design sensitivity is presented, which overcomes the two drawbacks of the conventional finite difference method. This approach has the advantage of being simple in concept, and easier implementation.

A shape optimization program for two-dimensional continuum structures is developed, including structural analysis using the BEM, shape design sensitivity analysis, mathematical programming, and the design boundary modelling. Some numerical examples are used to demonstrate the proposed formulations for shape design sensitivity analysis and shape optimization implementation.

ACKNOWLEDGEMENT

Contents

Chapter 1

Introduction

1.1 Introduction

Engineering design is an iterative process, in which the design is continuously modified until it meets the criteria set by the engineers. The traditional design process is carried out by the so called 'trial and error' method, in which the designer uses his experience and intuition to lead the design process. This manual based design process has the advantage that the designer's knowledge can be utilized in the design, and this approach still dominates the design method. But as the design problem becomes more complex, design modification becomes much more difficult. Therefore there is a urgent need for a new tool to guide the design modification.

The optimum design process attempts to use mathematical optimization techniques to meet the above challenge, in which the design problem is transformed into a mathematical optimization problem, and the design is modified automatically toward the best design (or optimum design).

The basic principles of the optimization theory were established a long time ago (17th and 18th centuries). However pure mathematical optimization is sel-

dom used in practical design because of the high idealization of the technique. Since the optimization is an iterative process requiring large computation, the real engineering application of optimization methods has only now become feasible with the advent of high performance digital computers.

The applications of optimization range from science and engineering, to economics and commerce. One application of optimization is the optimum design of structures. For one particular design, there may exist a number of solutions which satisfy the given conditions. The purpose of the optimization method is, instead of simply producing a feasible design, we can search amongst all the possible designs and finally determine the optimum one. Therefore we can define design optimization as 'by using a mathematical technique to determine an optimal design which satisfies the criteria set up by design engineers'.

One important class of problems in structural optimization is shape optimization, which concerns the selection of the geometry parameters of the structure. These geometry parameters, which can change during design modification, are called shape design variables. Besides the design variables, there are two terms frequently used in optimization - the objective and the constraints. The objective is the goal in which the design strives to achieve, for example the minimum material, the minimum stress concentration etc. The constraints are those criteria in which a design must meet. One example of the constraints in shape optimization is that the stress of a structure must not exceed the allowable stress. A large number of optimization problems belong to shape optimization, as in the mechanical design and the aerospace engineering.

The purpose of this thesis is to investigate the various aspects of shape optimization, including the shape design sensitivity analysis, structural analysis using the boundary element method, and shape optimization implementation. The outline of the thesis is as follows.

The introduction chapter gives a literature survey of shape optimization.

The survey follows the developments of shape optimization in the structural design for the last two decades, including the structural optimization using the finite element method and the boundary element method, and shape design sensitivity analysis.

Chapter 2 introduces the basic theory of optimization methods. Various mathematical programming methods for solving optimization problems are listed, and the difficulties related with shape optimization are discussed.

Chapter 3 contains the boundary element formulation of elastostatics. After deriving the basic boundary integral equation, the boundary discretization and the numerical implementation are described.

Chapter 4 investigates shape design sensitivity analysis. First, the two main approaches for sensitivity analysis are compared, and the continuum approach is explained in detail. Secondly, the implementation of the displacement sensitivity analysis by the continuum approach is given. A general formulation for stress sensitivity using the continuum approach is derived, followed by the discussions of the adjoint loads. Two approaches for the modelling of the adjoint problem are presented, one uses the distributed loads to replace the singular loads, and the another employs the singularity subtraction method to remove the singularity from the BEM equation. A new finite difference based approach to shape design sensitivity is derived next, which overcomes the two drawbacks of the conventional finite difference method. A few numerical examples are presented to justify the proposed formulations.

Chapter 5 describes the shape optimization, which includes discussions of the modelling of both the design model and the analysis model, the automatic remeshing method, the implementation of a 2-D shape optimization program, and finally some examples.

1.2   Review of Shape Optimization

The mathematical theory of optimization started as earlier as 17th century. The necessary conditions for unconstrained problems were set by Euler, and constrained problems by Lagrange. In 1638, Galileo Galilei [1] discussed the optimal shape of the beam, and the optimal elastic column was formulated by Lagrange [2]. Historically there were many scholars who were dedicated to optimization, among them were Isaac Newton (1643-1727), Jacob Bernoulli (1655-1705), William Rowan Hamllton (1808-1865), Lagrange (1736-1813), Euler (1707-1783).

Unfortunately, the pure mathematical approach can only solve very simple idealized problems, whereas the practical problems are more complicated. However the mathematical optimization theory provides a foundation for numerical optimization, therefore it is still an important research field.

In the following, a brief review of shape optimization is given with the author's remarks, which includes 3 fields:

1. Shape Optimization by using the finite element method.

2. Shape optimization by using the boundary element method.

3. Shape design sensitivity analysis.

1.2.1   Shape Optimization using the Finite Element Method

Since most of the structural problems can not be solved analytically, engineers searched alternative methods, i.e. the numerical methods. Numerical methods employ various approximation concepts to obtain a numerical solution for the problem. For the last three decades, the finite element method (FEM) has become a powerful tool for structural analysis [3, 4]. As the structural analysis

is an integrated part of shape optimization system, the progress of structural optimization often depends on the development of the FEM.

Schmit [5] was the first person to set forth the general approach of structural optimization in 1960, which indicated the feasibility to couple the FEM and the nonlinear mathematical programming for the optimum structural design. This were followed by the coupling of the FEM and the mathematical programming by Kicher, Gellatly et al. [6, 7, 8]. The introduction of the mathematical programming coupled with the FEM is a milestone in solving practical structure optimization problems, which proved to be the most successful tool for the optimum structural design. One of the first approaches of shape optimization was presented by Zienkiewicz and Campbell [9], in which they used the finite elements to model the problem, and the design variables were the boundary nodes. The numerical solution of the optimization problem was obtained by the sequential linear programming, and the direct differential method for the design sensitivities. Since then many researches have been carried out in the field of shape optimization problems using the FEM [10]-[17].

Schnack [18] presented a method for stress concentration using finite element formulation. Tvergaard [19] formulated a general optimal problem of two-dimensional elastic components, the approaches were related with the minimum volume and minimum stresses (stress concentration). Oda [20] developed a technique for optimum strength shape, he also presented a pattern transformation method to shape optimization, which is based on the stress-ratio method and the proportional transformation of the finite elements constituting the boundary [21].

Ramakrishnan and Francavilla [22] used the similar formulation of Zienkiewicz and Cambell, but employed the penalty function. A function space gradient projection method for two-dimensional elastic bodies was presented by Chun and Haug [23], using the design sensitivity analysis method presented by Rousselet and Haug [24] and the gradient projection method by Haug and Arora

The optimality criteria method was first introduced by Prager et al. [26] for continuum structures and by Berke [27] for the discretized system. Fleury [28] and Braibant [29] introduced the dual formulation in the optimality criteria method. Kunar and Chan [35] used a fully stress criterion to minimize the weight. Dems and Mroz [30, 31, 32] presented a quite general approach of shape optimal design using both the optimality criteria method and the variational calculus, and the optimality conditions were generated for both the conservative and the nonconservative load systems. The variational formulations for shape optimization can be seen in [33, 34]

The three-dimensional shape optimization problems have been presented by Kodiyalam and Vanderplaats [36] using the forced approximation technique. In their approach, the approximate stresses were obtained through linearization of nodal forces rather than by direct linearization of the stresses. The applications of three-dimensional shape optimization can be found in [37]-[40]

1.2.2 Shape Optimization using the Boundary Element Method

Despite the success of FEM in shape optimization, there still remains one main drawback. The FEM is a domain method, which requires the discretization of the whole domain. The remeshing during the iterations of the optimization process is very expensive, especially in three-dimensional cases, which also often causes element distortion near the design boundary.

Recently, the boundary element method (BEM) has been recognized as an alternative numerical method for engineering problems [41, 42]. The BEM discretizes the boundary only, so the remeshing procedure becomes much more easier than FEM. This feature, as well as the fact that BEM usually provides

more accurate structural responses on the boundary, makes BEM a very attractive numerical method in the application of shape optimization. Fig. 1.1 shows an optimum design example of a fillet from Zhao and Adey using BEM [43], and Yang, Choi and Haug [44] using FEM. Fig. 1.1(a) and Fig. 1.1(b) are the meshes of BEM and FEM at the initial designs respectively. Fig. 1.1(c) and Fig. 1.1(d) show the meshes of the final designs. It can be observed that the number of elements required in the FEM model is much larger than the BEM model, and the mesh of FEM has changed both inside the domain and along the boundary during optimization, whereas the mesh of the BEM model changes only on the boundary. In this problem only the mesh on the design boundary of the BEM model has changed.

The use of the BEM in shape optimization started from the 1980's. One of the earliest paper was written by T. Futagami (1981) [45] in which he combined the BEM with the linear programming to solve the partial differential equation. Futagami [46, 47] extended the initial linear programming to dynamic programming, and presented a coupling method of FEM and BEM. Barone and Caulk [48] optimized the position, the size and the surface temperature of circular holes inside a two-dimensional heat conductor. Meric [49, 50, 51] investigated two model problems by constructing the problems as the steady state optimal problem governed by elliptic partial differential equations.

Mota Soares, Rodrigues, Oliveira and Haug [52] proposed a model for optimal shape of solid and hollow shafts , which is based on the boundary element method and the nonlinear programming. The material derivative and the adjoint load methods were used by Mota Soares and Choi [53] to model the minimum compliance problems and the stress constraints. The determination of the optimum shape of two-dimensional structures was presented by Zochowski and Mizukami [54], with the objective of minimum area and constraints of displacements and geometries. Zhao and Adey [55] obtained the optimum shape

of fillet using BEM and the linear programming, with different design variables and design boundary modelling.

Kane [56] used the nonconforming quadratic elements to optimize the two dimensional elastic components. The sensitivity is carried out by differentiating the system matrix analytically. Defourny [57, 58] used a similar method of Kane to solve the potential problems.

Burczynsky and Adamczyk [59, 60] formulated the optimality conditions, and the nonlinear system was solved by the Newton-Raphson method. They also formulated the problems with maximum stiffness as the criterion, and extended the boundary element formulation of shape optimization to dynamic constraints. Gracia and Doblare [61] presented a formulation for the Saint-Venant torsion problems, which include homogeneous isotropic and orthotropic bodies

Eizadian and Trompette [62] , using BEM and the linear programming, developed a model for shape optimal design with objective of minimum tangential stresses. The geometry is defined by straight and circular elements. Several problems were solved by using the Lagrange multipliers method.

The coupling of FEM and BEM has been employed by Kamiya and Kita [63] which took the advantages of easier remeshing of BEM and the sparse matrix of FEM. They also presented an adaptive method for shape optimization [64]. The application of boundary element method with subregions has been developed by Kamiya, Nagai and Abe [65] for multi-regions or slender problems. Recently, Sandgren and Wu [66] employed the same idea of Nagai et al. to solve the two and three dimensional elasticity problems. The example of a hook by Sandgren demonstrated that the subregion approach can reduce the computing time significantly. Chaudouet-Miranda and Yafi applied the BEM to three-dimensional optimum design, and the modification procedure was based on the stress reduction method by Schnack [18]. The comparisons

on BEM and FEM in shape optimization have been studied by Zochowski and Mizukami [54], Hou and Sheen [68].

1.2.3 Shape Design Sensitivity Analysis

Because the design sensitivity plays a key role in shape optimization, much attention has been paid to the calculation of shape design sensitivity analysis. There are two main approaches to calculate the design sensitivity in the contents of FEM: the discretized approach (DA) and the continuum approach (CA). The DA uses a discretized model to carry out the sensitivity analysis, which includes three methods: finite difference method (FDM), analytical method (ANM) and semi-analytical method (SAM).

The FDM is to disturb the design variables one by one, and using the finite difference formula to approximate the derivatives. FDM has the advantage of being simple in concept, and easier implementation, but FDM has two serious drawbacks as indicated by [69, 70], 1) the accuracy often depends upon the perturbation step, 2) the computation cost is usually higher.

The ANM is to differentiate the system equation directly with respect to the design variables. Unfortunately the stiffness matrix is usually nonlinear with the shape design variables, therefore it is difficult to obtain the derivative of the stiffness matrix analytically. The SAM is the most used method in practical sensitivity calculation because its generality and easier implementation. This method differentiates the system equation first as in the ANM, then employs the finite difference method to calculate the derivative of the stiffness matrix. However many researches indicated that SAM could have serious accuracy problem for beam, plate and solid problems [71]-[74].

The second approach (CA) uses the material derivative method (variational method) of continuum mechanics to obtain the total derivative of structural responses. The CA derives the sensitivity formulation before dis-

cretization, so no approximation is involved in the formulation. By defining an adjoint problem, the sensitivity can be obtained from the solutions of both the initial problem and the adjoint problem. This approach was first proposed by Cea, Zolesio and Rousselet [75, 76, 77], and developed by Haug and Choi et al. [78, 79]. The general formulation of elasticity problems was presented by Haug, Choi and Komkov [79]. Dems and Mroz [32] presented a similar approach based on the variational method, which included more general boundary conditions. The same formulation of Dems was derived by R. B. Haber [80] using a mutual form of the Hu-Washizu principle.

In addition to elastostatics problems, the continuum approach has also been applied to thermoelasticity problems by Dems [81], dynamic problems by Haug [82], and the nonlinear response problems by Arora and Wu [83].

The main difficulty of using the continuum approach is how to evaluate the solution of the adjoint problem, since the adjoint loads are singular loads (i.e. concentrated point loads). Even though some local averaging method has been used to smooth the singularity [84], the accuracy is remaining an open question, especially for stress sensitivity.

As in the FEM case, there exist the same two classes of approach for shape design sensitivity by using the BEM: the discretized approach (DA) and the continuum approach (CA).

The finite difference scheme has been used by V. U. Nguyen and R. Arenicz [85] to obtain the design sensitivity in underground excavation problem. Wu [86] solved several two and three-dimensional optimum design problems by using finite difference method for sensitivity calculation.

A new finite difference based approach to shape design sensitivity calculation was presented by Zhao and Adey [87], which overcomes the two drawbacks of the finite difference method. The new approach has the advantage of finite

difference method, i.e. simple in concept and easier implementation, and can be used with either the BEM or the FEM

Kane [88] presented a formulation of direct differentiation for design sensitivity analysis, in which the system matrix was differentiated analytically after the boundary discretization. Recently Saigal, Aithal and Kane [89] developed a semi-analytical sensitivity formulation, with forward-difference approximation. Barone and Yang [90] formulated the design sensitivity by differentiating the boundary integral equation before discretization, and a rigid body integral identity was used to remove the singularity in the displacement sensitivity equation. The same concept of Barone and Yang was used by Zhang and Mukherjee [91] using a new boundary integral method [92], in which the basic unknowns were the tractions and the derivatives of the tangential displacements.

The continuum approach has been used by Mota Soares et al. [93] by introducing an adjoint system for two-dimensional solid and hollow shafts. Kwak and Choi [94, 95] have developed a general method for shape design sensitivity analysis of elliptical equations using a direct boundary integral formulation. The material derivative method was used to obtain an explicit expression for the variation of the structural response, and the formulations were applied to potential and elastostatics problems. An improved formulation of Kwak and Choi [95] was developed by Zhao and Adey [96], in which a singularity subtraction technique was employed to model the adjoint problem. Meric used the material derivative method for design sensitivity of thermoelastic solids [97].

A large amount literature on shape design sensitivity analysis and shape optimization has emerged over the last two decades. The most important conferences dedicated to structural optimization are given in [98]-[104], which provide the state of structural optimization, and can be used for further references.

1.3   References

[1] Galileo Galilei Linceo, Discorsi e dimonstrazioni matematiche, Leiden 1638.

[2] Lagrange, J. L., Sur des colonnes, Miscellanea Taurinensia (Royal Society of Turin), 1770-1773, 123.

[3] Zienkiewicz, O. C., The Finite Element Method, 3rd ed., McGraw-Hill, NewYork, 1977.

[4] Rao, S. S., The Finite Element Method in Engineering, Pergamon Press, 1982.

[5] Schmit, L. A., Structural Design by Systematic Synthesis, Proceedings of 2nd Conference on Electronic Computations, ASCE, New York, 1960, pp. 105-122.

[6] Kicher, T. P., Structural Synthesis of Integrally Stiffened Cylinders, J. of Spacecraft and Rockets, Vol. 5, 1968, pp. 62-67.

[7] Gellatly, R. A., Gallagher, R. H., A Procedure for Automated Minimum Weight Structural Design, Aero. Quart., 17, 1966, Part 1, pp. 216-230, Part 2, pp. 332-342.

[8] Schmit, L. A., Structural Synthesis 1959-1969, A Decade of Progress, Proc. Japan-US Seminar on Matrix Methods of Structural Analysis and Design, University of Alabama Press, 1971.

[9] Zienkiewicz, O. C., Campbell, J. S., Shape Optimization and Sequential Linear Programming, Optimum Structural Design (Ed. Gallagher, R. H., Zienkiewicz, O. C.), Wiley, 1973, pp 109-126.

[10] Queau, J. P., Trompette, Ph., Two Dimensional Shape Optimal Design by the Finite Element Method, Int. J. Numer. Meth. Engng., 15, 1980, pp. 1603-1612.

[11] Kristensen, E. S., Madsen, N. F., On the Optimum Shape of Fillet in Plates Subjected to Multiple In-plane Loading Cases, Int. J. Numer. Meth. Engng., Vol. 10, 1976, pp. 1007-1019.

[12] Spillers, W. R., Singh, S., Shape Optimization: Finite Element Examples, J. Struct. Div. ASCE., 107, 1981, pp. 2015-2025.

[13] Pedersen, P., Laursen, C. L., Design for Optimum Stress Concentration by Finite Element Method and Linear Programming, J. Struct. Mech., 10, 1982, pp. 375-391

[14] Botkin, M. E., Shape Optimization of Plate and Shell Structures, AIAA, Vol. 20, No. 2, 1981.

[15] Botkin, M. E., Yang, R. J., Bennett, J. A., Shape Optimization of Three-Dimensional Stamped and Solid Automotive Components, The Optimum Shape, Int. Symposium, General Motors Research Labs., Warren, Michigan, 1985.

[16] Epsing, B. J. D., A CAD Approach to Minimum Weight Design Problem, Int. J. Numer. Meth. Engng., 21, 1985, pp. 1049-1066

[17] Grandhi, R. V., Bowman, K. B., Structural Optimization for Static Aeroelastic Performance, Computer Aided Optimum Design (ed. C. A. Brebbia and S. Hernandez), CMP and Springer-Verlag, 1989.

[18] Schnack, E., An Optimization Procedure for Stress Concentration by the F.E. Technique, Int. J. Numer. Mech. Engng., Vol. 14, 1979, pp. 115-124.

[19] Tvergaard, V., On the Optimum Shape of a Fillet in a Flat Bar with Restrictions, Optimization in Structural Design (ed. A. Sawczuk and Z. Mroz), Springer-Verlag, NewYork, 1975, pp. 181-195.

[20] Oda, J., On a Technique to Obtain an Optimum Strength Shape by the Finite Element Method, Bulletin of JSME, vol. 20, 1977, pp. 160-167.

[21] Oda, J., Yamazaki, K., Pattern Transformation Method for Shape Optimization in its Application to Spoked Rotary Disks, Int. Symposium on Optimum Structural Design, Tucson, Arizona, 1981, pp. 4.29-4.35.

[22] Ramakrishnan, C. V., Francavilla, A., Structural Shape Optimization Using Penalty Function, J. Struc. Mech., vol. 3(4), 1975, pp. 403-432.

[23] Chun, Y. W., Haug, E. J., Two Dimensional Shape Optimal Design, Int. J. Numer. Meth. Engng., vol. 13(5), 1978, pp. 311-336.

[24] Rousselet, B., Haug, E. J., Design Sensitivity Analysis of Shape Variations, Optimization of Distributed Parameter Structures (Eds. Haug, E. J., Cea, J.), Sijthoff and Noordhoff, Alphen aan den Rijn, The Netherland, 1981, pp. 1397-1442.

[25] Haug, E. J., Arora, J. S., Applied optimal design, John Wiley and Sons, 1979.

[26] Prager, W., Shield, R. T., A General Theory of Optimal Plastic Design, J. Appl. Mech., Vol. 34, 1967, pp. 184-186.

[27] Berke, L., An Efficient Approach to the Minimum Weight Design of Deflection Limited Structures, Rep. of Air Force Flight Dynamics Lab. AFFDL-TM-70-4, 1970.

[28] Fleury, C., Structural Weight Optimization by Dual Method of Convex Programming, Int. J. Numer. Mech. in Engng., vol. 14, No. 12, 1979, pp. 1761-1783.

[29] Fleury, C., Braibant, V., Structural Optimization. A New Dual Method Using Mixed Variables, Int. J. Numer. Meth. Engng., 23, 1986, pp. 409-428.

[30] Dems, K., Mroz, Z., Multiparameter Structural Shape Optimization by Finite Element Method, Int. J. Numer. Meth. in Engng., vol. 13, 1978, pp. 247-263.

[31] Mroz, Z., Dems, K., On Optimal Shape Design of Elastic Structures, Optimization Method in Structural Design (eds. H. Eschenauer and N. Olhoff), 1983, pp. 224-243.

[32] Dems, K., Mroz, Z., Variational Approach by Means of Adjoint System to Structural Optimization and Sensitivity Analysis, Int. J. Solids Structures, 19, pp. 677-692, 1983. 20, pp. 527-552, 1984.

[33] Kikuchi, N., Taylor, J. E., Optimal Modification of Shape for Two-Dimensional Elastic Bodies, J. Struct. Mech., Vol. 11(1), 1983, pp. 111-135.

[34] Olhoff, N., Structural Optimization By Variational Methods, Computer Aided Optimal Design: Structural and Mechanical Systems (ed C. A. Mota Soares), Springer-Verlag, 1987, pp. 87-164.

[35] Kunar, R. R., Chan, A. S. L., A Method for the Configurational Optimization of Structures, Comput. Meth. App. Mech. Engng., Vol. 1, 7. 1976, pp. 331-350.

[36] Kodiyalam, S., Vanderplaats, G. N., Shape Optimization of Three-Dimensional Continuum Structures via Forced Approximation Technique, Int. J. Numer. Meth. Engng., 27, (9), 1989. pp. 1256-1263.

[37] Imam, M. H., Three-Dimensional Shape Optimization, Int. J. Numer. Meth. Engng., 18, 1982, pp. 661-673.

[38] Wassermann, K., Three-Dimensional Shape Optimization of Arch Dam with Prescribed Shape Functions, J. Struct. Mech., 11, 1983, pp. 465-489.

[39] Yang, R. J., Botkin, M. E., A Modular Approach for Three-Dimensional Shape Optimization of Structures, Research Pub. GMR-5216, General Motors Research Labs., 1986.

[40] Yao, T., Choi, K. K., Three-Dimensional Optimal Design and Automatic Finite Element Regrading, Int. J. Numer. Meth. Engng., Vol. 28, 1989, pp. 369-384.

[41] Brebbia, C. A., Telles, J. C. F., Wrobel, L. C., Boundary Element Technique. Theory and Application in Engineering, Springer-Verlag, Berlin, 1984.

[42] Hartmann, F., Introduction to Boundary Elements. Theory and Application, Springer-Verlag, 1989.

[43] Zhao, Z. Y., Adey, R. A., Shape Optimization - A Numerical Consideration, Proc. 11th BEM Conf., Cambridge, USA, 1989, pp. 195-208.

[44] Yang, R. J., Choi, K. K., Haug, E. J., Numerical Considerations in Structural Component Shape Optimization, ASME, 107, 1985.

[45] Futagami, T., Boundary Element and Linear Programming Method in Optimization of Partial Differential Systems, Proc. 3rd International Seminar on BEM (ed. C. A. Brebbia), Springer-Verlag, 1981, pp. 457-471.

[46] Futagami, T., Boundary Element and Dynamic Programming Method in Optimization of Transient Differential Systems, Proc. 4th International Seminar, Springer-Verlag, 1982, pp. 58-71.

[47] Futagami, T., Boundary Element Method - Finite Element Method Coupled With Linear Programming for Optimal Control of Distributed Parameter Systems, Boundary Elements (ed. C. A. Brebbia), Springer-Verlag, 1983, pp. 891-900.

[48] Barone, M. R., Caulk, D. A., Optimal Arrangement of Holes in a two-Dimensional Heat Conductor by a Special Boundary Integral Method, Int. J. Numer. Mech. Engng., 18, 1982, pp.675-685.

[49] Meric, R. A., Boundary Integral Equation and Conjugate Methods for Optimal Boundary Heating of Solids, Int. heat and mass transfer, 26, 1983, pp.261-264.

[50] Meric, R. A., Boundary Element Methods for Static Optimal Heating of Solids, ASME, J. of Heat Transfer, 106, 1984, pp. 876-880.

[51] Meric, R. A., Boundary Element methods for Optimization of Distributed Parameter Systems, Int. J. Numer. Mech. Engng., 20, 1984, pp. 1291-1306.

[52] Mota Soares, C. A., Rodrigues, H. C., Oliveira, L. M., Haug, E. J., Optimization of the Shape of Solids and Hollow Shifts Using Boundary Element Methods, Boundary Elements (ed. C. A. Brebbia), Springer-Verlag, 1983, pp. 883-889.

[53] Mota Soares, C. A., Choi, K. K., Boundary Elements in Shape Optimal Design of Structures, The Optimum Shape: Automated Structural Design (eds. J. A. Bennett, M. E. botkin), Plenum Press, 1986, pp. 199-236.

[54] Zochowski, A., Mizukami, J. S., A Comparison of BEM and FEM in Minimum Weight Design, 5th BEM Conference (ed C. A. Brebbia), Springer-Verlag, 1983, pp. 901-911.

[55] Zhao, Z. Y., Adey, R. A., Shape Optimization Using the Boundary Element Method, Computer Aided Design of Structures: Recent Advances (ed. C. A. Brebbia and S. Hernandez), CMP and Springer-Verlag, 1989, pp. 145-163.

[56] Kane, J. H., Shape Optimization Utilizing a Boundary Formulation, Proc. 2nd Boundary Element Technology Conference (eds. J. J. Connor, C. A. Brebbia), 1986.

[57] Defourny, M., Boundary Element Method and Design Optimization, Proc. 9th Conference on Boundary Elements, Stuttgart, Springer-Verlag, 1987.

[58] Defourny, M., Optimization Techniques and Boundary Element Method, Proc. 10th Conference on Boundary Elements, Southampton, Springer-Verlag, 1988.

[59] Burczynski, T., Adamczyk, T., The Boundary Element Method for Shape Design Synthesis of Elastic Structures, Proc. 7th Conference on Boundary Element Methods (ed. C. A. Brebbia), Springer-Verlag, 1985.

[60] Burczynski, T., Adamczyck, T., The Boundary Element Formulation for Multiparameter Structure Shape Optimization, Appl. Math. Modelling, 9, 1985, pp. 195-200.

[61] Gracia, L., Doblare, M., Shape Optimization By Using BEM, 10th BEM Conferences, CMP and Springer-Verlag, 1988, 491-514.

[62] Eizadian, D., Trompette, M., Shape Optimization of Bidimensional Structures by Boundary Element Method, Conference on CAD/CAM, Robotics and Automation in Design, Tucson, Arizona, 1985.

[63] Kamiya, N., Kita, E., Shape Optimization by Coupling Finite and Boundary Element Method, Proc. Boundary Elements IX (eds. C. A. Brebbia, W. L. Wendland, G. Kuhn), vol. 2, Springer-Verlag, 1987, pp. 473-484.

[64] Kamiya, N., Kita, E., Structural Optimization by an Adaptive Boundary Element Method, Boundary Element Element in Applied Mechanics (ed M. Tanaka and T. A. Cruse), Pergamon Press, 1988, pp. 393-402.

[65] Kamiya, N., Nagai, T., Abe, J., Design Boundary Elements, Boundary Element Techniques (eds. C. A. Brebbia, W. S. Venturini), Comp. Mech. Pub., 1987, pp. 221-233.

[66] Sandgren, E., Wu, S., Shape Optimization Using the Boundary Element with Substructing, Int. J. Numer. Mech. Engng., vol. 26, 1988, pp. 1913-1924.

[67] Chaudouet-Miranda, A., Yafi, F., Boundary Element Method Applied to 3D Optimum Design, IUTAM, Advanced Boundary Element Methods, Springer-Verlag, 1987, pp. 101-108.

[68] Hou, J. W., Sheen, J. S., Computational Shape Optimization: Recent Advances and Applications, Computer Aided Optimum Design of Structures (ed C. A. Brebbia and S. Hernandez), CPM and Springer-Verlag, 1989, pp. 125-134.

[69] Gill, P. E., Murray, W., Saunders, M. A., Wright, M. H., Computing Forward-Difference Intervals for Numerical Optimization, SIAM J. Sci. and Stat. Comput., Vol. 4, No. 2, 1983, pp. 310-321.

[70] Iott, J., Haftka, R. T., Adelman, H. M., Selecting Step Sizes in Sensitivity Analysis by Finite Differences, NASA TM 86382, 1985.

[71] Barthelemy, B. M., Haftka, R. T., Accuracy Analysis of the Semianalytical Method for Shape Sensitivity Calculation, Proc. AIAA/ASME/ASCE/AHS 29th Structures, Structural Dynamics and Material Conf., USA, 1988.

[72] Botkin, M. E., Shape Optimization of Plate and Shell Structures, AIAA, Vol. 20, No. 2, 1982, pp. 268-273.

[73] Braibant, V., Fleury, C., Shape Optimal Design - A Performing C.A.D. Oriented Formulation, Proc. AIAA/ASME/ASCE/AHS 25th Structures, Structural Dynamics and Materials, Palm Springs, CA., 1984.

[74] Fleury, C., Computer-Aided Optimal Design of Elastic Structures, Computer-Aided Optimal Design: Structural and Mechanical Systems (ed C.A. Mota Soares), Springer-Verlag, 1987, pp. 831-900.

[75] Cea, J., Numerical Methods of Shape Optimal Design, Optimization of Distributed Parameter Structures (eds. E. J. Haug, J. Cea), Sijthoff Noordhoff, Alphen aan den Rijn, Netherland, 1981.

[76] Zolesio, J-p., The Material Derivative Method for Shape Optimization, Optimization of Distributed Parameter Structures, Sijthoff Noordhoff, 1981, pp. 1089-1151.

[77] Rousselet, B., Implementation of Some Methods of Shape Optimal Design, Optimization of Distributed Parameter Structures, Sijthoff Noordhoff, 1981.

[78] Choi, K. K., Haug, E. J., Shape Design Sensitivity Analysis of Elastic structures, J. Struct. Mech., 11(2), 1983, pp. 231-269.

[79] Haug, E. J., Choi, K. K., Komkov, V., Design Sensitivity Analysis of Structural Systems, Academic Press, New York, 1985.

[80] Haber, B. R., A New Variational Approach to Structural Shape Design Sensitivity Analysis, Computer Aided Optimal Design: Structural and Mechanical Systems, Springer- Verlag, 1987, pp. 573-588.

[81] Dems, K., Sensitivity Analysis in Thermoelasticity Problems, Computer Aided Optimal Design: Structural and Mechanical Systems, Springer-Verlag, 1987, pp.563-572.

[82] Haug, E. J., Design Sensitivity Analysis of Dynamic Systems, Computer Aided Optimal Design: Structural and Mechanical Systems, Springer-Verlag, 1987, pp. 705-755.

[83] Arora, J. S., Wu, C. C., Design Sensitivity Analysis and Optimization of Nonlinear Structures, Computer Aided Optimal Design: Structural and Mechanical Systems, Springer-Verlag, 1987, pp. 589-604.

[84] Haug, E. J., Choi, K. K., Material Derivative Methods for Shape Design Sensitivity Analysis, The Optimum Shape: Automated Structural Design (ed: J. A. Bennett and M. E. Botkin), Plenum Press, 1986.

[85] Nguyen, V. U., Arenicz, R., Sensitivity Analysis of Underground Excavation Using Boundary Element Methods, Proc. BETECH 85 (eds. C. A. Brabbia, B. J. Noye), Springer-Verlag, 1985.

[86] Wu, S. J., Application of the Boundary Element Method for Structural Shape Optimization, PhD Thesis, The University of Missouri, Columbia, 1986.

[87] Zhao, Z. Y., Adey, R. A., A Finite Difference Based Approach to Shape Design Sensitivity Analysis, This paper will appear on Proc. of BEM12, Japan, Sept., 1990.

[88] Kane, J. H., Optimization of Continuum Structures Using a Boundary Element Formulation, PhD Thesis, The University of Connecticut, 1986.

[89] Saigal, S., Aithal, R., Kane. J. H., Semianalytical Sensitivity Formulation in Boundary Elements, AIAA Journal, Vol. 27, No. 11, 1989, pp. 1615-1621.

[90] Barone, M. R., Yang, R.-J., Boundary Integral Equations For Recovery of Design Sensitivity in Shape Optimization, AIAA Journal, Vol. 26, No. 5, 1988, pp. 589-594.

[91] Zhang, Q., Mukherjee, S., Design Sensitivity Coefficients for Linear Elasticity Problems by Boundary Element Methods, IUTAM/IACM Symposium on Discretization Methods in Structural Mechanics, Austria, 1989.

[92] Ghosh, N., Rajiyah, H., Ghosh, S., Mukherjee, S., A New Boundary Element Method Formulation for Linear Elasticity, ASME of Appli. Mech., 53, 1986.

[93] Mota Soares, C. A., Choi, K. K., Boundary Elements in Shape Optimal Design of Structures, The Optimum Shape: Automated Structural Design (ed J. A. Bennett and M. E. Botkin), Plenum, NewYork, 1986, pp. 199-231.

[94] Choi, J. H., Kwak, B. M., Boundary Integral Equation Method for Shape Optimization of Elastic Structures, Int. J. Numer. Mech. Engng., vol. 26, 1988, pp. 1579-1595.

[95] Kwak, B. M., Choi, J. H., Shape Design Sensitivity Analysis Using Boundary Integral Equation for Potential Problems, Computer Aided Optimal Design: Structural and Mechanical Systems (ed. C. A. Mota Soares), Springer-Verlag, 1987.

[96] Zhao, Z. Y., Adey, R. A., The Accuracy of the Variational Approach to Shape Design Sensitivity Analysis, Proc. EuroBEM Conf., Nice, 1990.

[97] Meric, R. A., Boundary Elements in Shape Design Sensitivity Analysis of Thermoelastic Solids, Computer Aided Optimal Design: Structural and Mechanical Systems (ed. C. A. Mota Soares), Springer-Verlag, 1987, pp. 643-652.

[98] Gallagher, R. H., Zienkiewicz, O. C. (eds), Optimum Structural Design: Theory and Application, John Wiley & Sons, 1973.

[99] Haug, E. J., Cea, J. (eds), Optimization of Distributed Parameter Structures, Sijthoff and Noordhoff, The Netherlands, 1981.

[100] Atrek, E., Gallagher, R. H., Ragsdell, K. M., Zienkiewicz, O. C. (eds), New Directions in Optimum Structural Design, John Wiley & Sons, 1984.

[101] Bennett, J. A., Botkin, M. E. (eds), The Optimum Shape: Automated Structural Design, Plenum Press, 1986.

[102] Mota Soares, C. A. (ed), Computer Aided Optimal Design: Structural and Mechanical Systems, Springer-Verlag, 1986.

[103] Eschenauer, H. A., Thierauf, G. (eds), Discretization Methods and Structural Optimization - Procedures and Applications, Springer-verlag, 1988.

[104] Brebbia, C. A., Hernandez, S (eds), Computer Aided Optimum Design of Structures, CMP and Springer-Verlag, 1989.
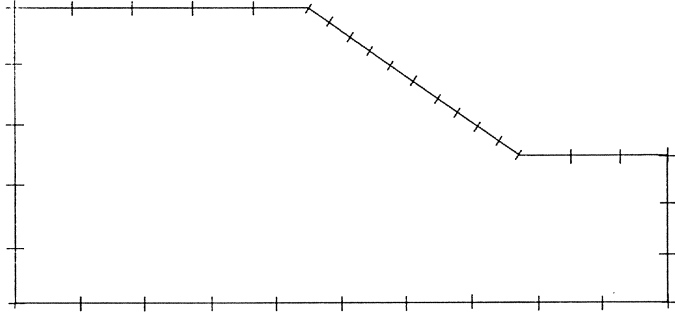
Fig. 1.1(a) The Boundary Element Model
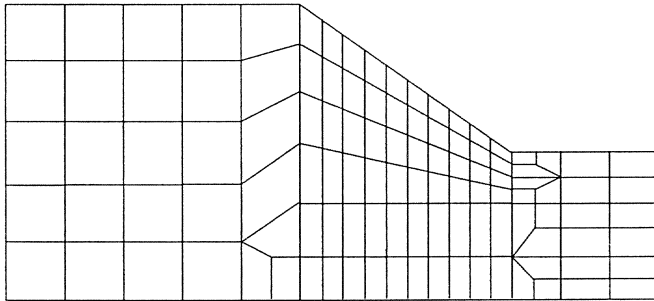
Fig. 1.1(b) The Finite Element Model
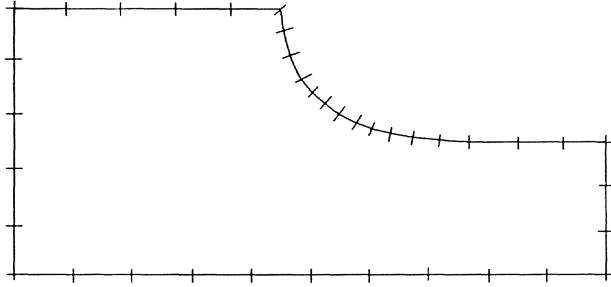
Fig. 1.1(c) The Mesh at the Final Design of the BEM Model
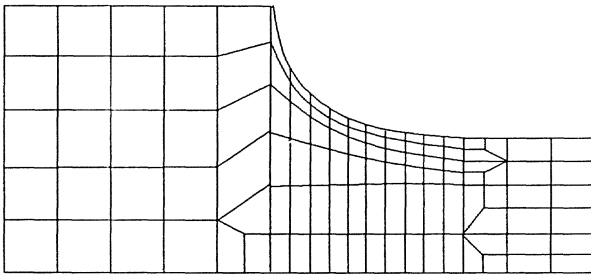
Fig. 1.1(d) The Mesh at the Final Design of the FEM Model

Chapter 2

Basic Numerical Optimization Techniques

2.1 Introduction

The aim of this chapter is to provide the basic concepts and terminology in shape optimization by the mathematical programming method, which will be used throughout the thesis. Various algorithms of the mathematical programming methods are presented to give a general view of the numerical methods available today. The information presented here is mainly from References [1]-[5], in which more details can be found.

2.2 Basic Concepts and Terminology

In general, a shape optimization problem can be formed as a minimization problem under certain constraints, which can be stated mathematically as follows:

$$\text{Minimize:} \qquad f(\mathbf{X}) \qquad\qquad (2.1)$$

Subject to:

$$g_j(\mathbf{X}) \leq 0 \qquad\qquad j = 1, M \qquad (2.2)$$

$$h_k(\mathbf{X}) = 0 \qquad\qquad k = 1, L \qquad (2.3)$$

$$x_i^l \leq x_i \leq x_i^u \qquad\qquad i = 1, N \qquad (2.4)$$

$\mathbf{X}$ are the design variables, $\mathbf{X} = [x_1, x_2, ..., x_N]^T$. $f(\mathbf{X})$ is called the objective function, which depends on the design variables $\mathbf{X}$. The objective function must be a scalar function, and its numerical value can be obtained once the design variables are fixed.

The weight of the structure is the most typical objective function in shape optimization, which can be expressed as

$$f(\mathbf{X}) = \int_\Omega \rho d\Omega \qquad (2.5)$$

where ρ is the density of the material, and the Ω is the domain occupied by the material.

In addition to the weight, the objective function can also be:

a) The maximum stress over part of the structural Ω_c, i.e.

$$f(\mathbf{X}) = Max \ \sigma(\xi) \qquad (2.6)$$

where σ is the stress, and $\xi \in \Omega_c$. The stress σ can be chosen as principle stress, Von Mises stress, etc. Such objective function is usually used for stress concentration problems.

b) Average stress over part of the structural Ω_c,

$$f(\mathbf{X}) = \int_{\Omega_c} (\frac{\sigma - \sigma_a}{\sigma_a})^2 d\Omega \qquad (2.7)$$

where σ is the maximum stress, and σ_a is the average stress. This objective can be used to formulate a fully stressed structure design.

The design variables **X** are those parameters, which are used to describe a design and can be changed freely. In shape optimization problems, **X** are the parameters which define the boundary shape. The choice of design variables for shape optimization problems and the design boundary representations will be discussed in Chapter 5.

All the restrictions on a design are called constraints. Equations (2.2) and (2.3) are inequality and equality constraints respectively, which must be satisfied for the final design. The number of equality constraints cannot exceed the number of design variables, and the number of inequality constraints can be arbitrary large.

The most common constraints in shape optimization problems are:

a) Stress constraints, for example the Von Mises stress over a structure should be less than the allowable stress
b) Displacement constraints, i.e. the displacement should not exceed the pre-scribed value.
c) Stiffness or compliance constraints
d) Stability constraints (buckling)
e) Vibration constraints (frequency)

Equation (2.4) is side constraints that are used to limit the region of search for the optimum, where x^u and x^l are upper and lower bounds of design variables respectively. The introduction of side constraints are necessary for two reasons: 1) to prevent unreasonable or meaningless designs; for example, the thicknesses of a structure should always be positive 2) considerations of the manufacturing process; for example, the cross sections of a reinforced concrete beam cannot be too thin in order to stop steel corrosion (i.e. minimum cover requirements).

A design is defined as a feasible design if all constraints are satisfied. An infeasible design implies that one or more constraints are violated. By optimum

design, we mean a design which achieves a minimum objective, at the same time satisfies all the constraints. If an objective function has the smallest value in the whole feasible design region, it will be called global minimum. If the objective has the smallest value only in part of the feasible region, we call it local minimum.

A constrained optimization problem is named as convex only if both the objective function and all the constraints are convex. A convex constrained problem has a single global minimum, and a non-convex problem may have several local minimum. Convexity can rarely be proved. Most structural optimization problems are non-convex, therefore the numerical optimization method will often lead to a local minimum.

The theoretical necessary conditions at the optimum are referred to as the Kuhn-Tucker conditions [6], which are derived from the fact that the Lagrangian function is stationary at the optimum. The Lagrangian function is defined as:

$$L(\mathbf{X}, \lambda) = f(\mathbf{X}) + \sum_{j=1}^{M} \lambda_j g_j(\mathbf{X}) + \sum_{k=M+1}^{M+L} \lambda_k h_k(\mathbf{X}) \tag{2.8}$$

where $f(\mathbf{X})$, $g_j(\mathbf{X})$ and $h_k(\mathbf{X})$ are the objective and the constraints respectively as defined in (2.1) - (2.3), λ_j and λ_k are the Lagrangian multipliers.

The following three conditions (Kuhn-Tucker conditions) are the necessary conditions for optimality:

1) $\mathbf{X}$ is feasible.

2) $\lambda_j g_j(\mathbf{X}) = 0 \qquad \lambda_j \geq 0 \qquad\qquad j = 1, M$

3) $\nabla f(\mathbf{X}) + \sum_{j=1}^{M} \lambda_j \nabla g_i(\mathbf{X}) + \sum_{k=M+1}^{M+L} \lambda_k \nabla h_k(\mathbf{X}) = 0$

These necessary conditions are also sufficient if the design space is convex. The Kuhn-Tucker conditions can be used to check the possible optimality of a design.

2.3 Mathematical Programming Methods

There are two main approaches for solving structural optimization problems, the optimality criteria (OC) method and the mathematical programming (MP) method. The OC method derives the state conditions at the optimum based on the extreme principles, and then to updated the current design toward these state conditions. On the other hand, the MP method starts with the current design, and uses the information from the current design to find how to reduce the objective function and to satisfy the constraints.

The MP method is more general than the OC method, especially for shape optimization in which the optimality conditions are difficult to formulate. Therefore the MP method is employed in the current research, and various MP methods will be discussed in the following.

For a general shape optimization problem, both the objective function and the constraints are nonlinear functions of the design variables. It is nearly impossible to solve the set of nonlinear equations (2.1)-(2.4) analytically, so numerical methods must be used instead to obtain the optimum design, or in many cases, a local optimum design. The numerical optimization methods (MP methods) usually start with an initial design $\mathbf{X}^0$, then update the improved design using following iteration process:

$$\mathbf{X}^p = \mathbf{X}^{p-1} + \alpha \mathbf{S}^p$$

where p is the iteration number, α is a scalar parameter which specifies the movement of the design variables, and vector $\mathbf{S}$ is the search directions. The above optimization process will continue until no significant change in the objective function (or no significant change in the design variables), and all the constraints are satisfied.

Various MP methods have been developed to solve the minimization problem of equations (2.1)-(2.4) with iterative procedure. In the following, some

well established methods are described with some remarks. The optimization problem can be written in matrix form as

Minimize: $\quad\quad\quad f(\mathbf{X})$ $\quad\quad\quad\quad\quad\quad\quad\quad\quad\quad$ (2.9)

Subject to:

$$\mathbf{G}(\mathbf{X}) \leq \mathbf{0} \quad\quad\quad\quad\quad\quad (2.10)$$

$$\mathbf{X}^L \leq \mathbf{X} \leq \mathbf{X}^U \quad\quad\quad\quad\quad (2.11)$$

where $\mathbf{X} = [x_1 ..... x_n]^T$, $\mathbf{G} = [g_1, g_2, ..., g_M]^T$, $\mathbf{X}^L$ and $\mathbf{X}^U$ are the lower and upper limits of the design variables. Note in the above form we omit the equality equations in order to simplify the discussions.

1) Sequential Linear Programming Method

The most simple and popular approach to solve optimization problem (2.9) - (2.11) is to approximate the objective and the constraints by linear approximation based on the Taylor expansion about $\mathbf{X}_0$, which is called the sequential linear programming (SLP) method. By using the SLP method, the optimization problem (2.9) - (2.11) becomes:

Minimize: $\quad\quad\quad f(\mathbf{X}_0) + \nabla f(\mathbf{X}_0)^T \delta\mathbf{X}$ $\quad\quad\quad\quad\quad$ (2.12)

Subject to:

$$\mathbf{G}(\mathbf{X}_0) + \nabla\mathbf{G}(\mathbf{X}_0)\,\delta\mathbf{X} \leq 0 \quad\quad j = 1, M \quad (2.13)$$

$$\delta\mathbf{X}^L \leq \delta\mathbf{X} \leq \delta\mathbf{X}^U \quad\quad\quad i = 1, N \quad (2.14)$$

where $\delta\mathbf{X}$ are the changes of the design variables, i.e.

$$\delta\mathbf{X} = [x_1 - x_1^0, ..., x_n - x_n^0]^T$$

∇f and $\nabla\mathbf{G}$ are the gradients of the objective and constraints with respect to the design variables respectively, i.e.

$$\nabla\mathbf{G}(\mathbf{X}_0) = \begin{vmatrix} \frac{\partial g_1}{\partial x_1} & , ..., & \frac{\partial g_1}{\partial x_n} \\ & .... & \\ \frac{\partial g_m}{\partial x_1} & .... & \frac{\partial g_m}{\partial x_n} \end{vmatrix}_{\mathbf{X}=\mathbf{X}_0}$$

$$\nabla f(\mathbf{X}_0) = [\frac{\partial f}{\partial x_1}, ..., \frac{\partial f}{\partial x_n}]^T |_{\mathbf{X}=\mathbf{X}_0}$$

$\delta\mathbf{X}^L$ and $\delta\mathbf{X}^U$ are the moving limits of the design variables. This linear problem can then be solved easily using the Simplex method or other standard optimization algorithms which are readily available.

Since the nonlinear functions $f(\mathbf{X})$ and $\mathbf{G}(\mathbf{X})$ are approximated by linear functions, the moving limits of the design variables must be imposed to prevent invalidation of the linear approximation. Otherwise the problem may have unbounded or oscillation solutions.

The choice of the moving limits depends upon the experiences and the problems, and a trial and error process is required to find the best one suited to the problem. Generally speaking, the moving limits should decrease as the design approaches the optimum because the linear approximation needs to be more accurate when closing the optimum. The requirement for the adjustable moving limits is considered to be the main drawback of the SLP method.

The design is converged if the following conditions are met:

$$g_j(\mathbf{X}) \leq \delta_1 \qquad j = 1, M \tag{2.15}$$

$$\delta x_i \leq \delta_2 \qquad i = 1, N \tag{2.16}$$

where δ_1 is the specified tolerance for the constraint violation, and the δ_2 is a specified small number. These two conditions imply that the iteration can be stopped when all the constraints are satisfied and there is nearly no design change any longer. Sometimes the equation (2.16) can be replaced by the convergence of the objective function, i.e.

$$\delta f(\mathbf{X}) \leq \delta_3 \tag{2.17}$$

where δf presents the change of the objective function, and δ_3 is a prescribed value.

Even though the SLP method is considered to be a poor optimization algorithm, the experience of many researchers has showed that it is often a

powerful and efficient method [8, 9]. In this thesis, the SLP method is employed to solve shape optimization problems in Chapter 5.

2) Sequential Quadratic Programming

Sequential Quadratic Programming (SQP) method is a powerful method for a wide range of optimization problems. SQP creates a quadratic approximation of objective function, and a linear approximation for constraints. The standard form of SQP is:

$$\text{Minimize:} \quad f(\mathbf{X}) = f(\mathbf{X_0}) + \nabla f(\mathbf{X_0})^T \delta \mathbf{X} + 1/2 \delta \mathbf{X}^T \mathbf{H} \, \delta \mathbf{X} \quad (2.18)$$

Subject to :

$$\mathbf{G}(\mathbf{X_0}) + \nabla \mathbf{G}(\mathbf{X_0}) \delta \mathbf{X} \leq 0 \quad (2.19)$$

where $\mathbf{H}$ is the Hessian matrix of the objective function.

SQP is usually considered to be a better method than SLP from computational accuracy and robustness viewpoints. Various modifications of the SQP can be found in [10, 11, 12].

3) Penalty Function Method

A constrained optimization problem can be transformed into an equivalent unconstrained optimization problem by introducing an external penalty function. The new function to be minimized is:

$$\text{Minimize } \phi(\mathbf{X}, r_p) = f(\mathbf{X}) + r_p \sum_j Max[g_i(\mathbf{X}), 0]^2 \quad (2.20)$$

where r_p is called the penalty parameter. The function ϕ is minimized keeping r_p constant, then r_p will increase each iteration. There are other forms of penalty function, such as the interior penalty function, the extended interior penalty function, the augmented lagrangian multiplier method, etc., more details of which can be found in [13]

4) Method of Feasible Direction

The method of feasible direction starts with a feasible design, moving to an improved feasible design by choosing a feasible direction **S**, and a small step size α. The step size α is determined to reduce the objective function as much as possible, at the same time keeping the design feasible. If the design is inside the feasible region (no active constraints), the unconstrained techniques are used to generate the direction **S**. In the case of the design at the boundary of the feasible region, the direction **S** can be obtained by solving the following sub-problem [1, 14]:

Maximize: $\qquad\qquad \beta$ $\qquad\qquad\qquad\qquad\qquad$ (2.21)

Subject to:

$$\nabla f(\mathbf{X})^T \mathbf{S} + \beta \leq 0 \qquad\qquad\qquad (2.22)$$

$$\nabla g_j^T \mathbf{S} + \theta_j \beta \leq 0 \qquad j \in J \qquad\qquad (2.23)$$

$$\mathbf{S}^T \mathbf{S} \leq 1 \qquad\qquad\qquad\qquad (2.24)$$

where J is a potential constraint set, and θ_j is called the push-off factor. θ_j presents the angle between the moving direction and the tangential direction of the jth constraint. Equation (2.24) is used to bound the solution **S**.

5) Sequential Convex Linearization Method

This method first linearizes the objective and constraints as in SLP, then reciprocal variables are used to create a conservative convex approximation. Various approaches based on convex approximation have been developed, and proved to be very efficient for a wide range of optimization problems. The theory and applications of convex approximation method can be found in [15]

Concluding Remarks

The efficiency of the above numerical optimization problem depends on the type of problem to be solved. For one particular problem, one method may

provide a faster convergence than the others, whereas in other cases it may fail to converge. Generally speaking, the choice of numerical optimization methods mainly depends on the following considerations:

1. The number of design variables

2. The properties of the objective function and the constraints, i.e. the smoothness and the order of nonlinearity.

3. The highest level of derivatives of objective function and constraints available, with reasonable accuracy and cost.

4. Robustness, efficiency, accuracy and reliability of the algorithm.

As the optimum design problems become bigger, the cost of using numerical methods increases rapidly. Which method best suits general shape optimization problems is still an open question. Since engineering problems involves more and more complex analysis, the cost of optimum design will be huge. A lot of research is still needed to improve the reliability and the efficiency of the numerical algorithms.

2.4 References

[1] Vanderplaats, G. N., Numerical Optimization Techniques for Engineering Design: With Applications, McGraw-Hill, 1984.

[2] Fletcher, R., Practical Methods of Optimization, John Wiley & Sons, 1987.

[3] Gill, P. E., Murray, W., Wright, M. H., Practical Optimization, Academic Press, 1981.

[4] Arora, J. S., Introduction to Optimum Design, McGraw-Hill, 1989.

[5] Ding, Y., Shape Optimization of Structures: A Literature Survey, Comput. and Struct., Vol. 24, No. 6, 1986, pp. 985-1004.

[6] Kuhn, H. W., Tucker, A. W., Nonlinear Programming, Proc. Second Berkeley Symposium on Math. Statis. Probabli. (ed. J. Neyman), University of California Press, 1961, pp. 481-492.

[7] Kelley, J. E., The Cutting Plane Method for Solving Convex Programs, J. SIAM, 1960, pp. 703-713.

[8] Vanderplaats, G. N., Numerical Optimization Techniques, Computer Aided Optimal Design: Structural and Mechanical Systems (ed. C. A. Mota Soares), Springer-Verlag, 1986.

[9] Pedersen, P., Laursen, C. L., Design for Minimum Stress Concentration by Finite Elements and Linear Programming, J. Struc. Meth., 10, 1982-1983, pp. 375-391.

[10] Powell, M. J. D., Algorithms for Nonlinear Constraints That Use Lagrangian Functions, Math. Prog., Vol. 14, No. 2, 1978.

[11] Han, S. P., A Globally Convergent Method for Nonlinear Programming, J. Optim. Theory appl., Vol. 22, No. 3, 1977, pp. 297-309.

[12] Gill, P. E., Murray, W., Numerical Stable Methods for Quadratic Programming, Math. Prog., 14, 1978, pp. 349-372.

[13] Fletcher, R., A Class of Methods for Nonlinear Programming With Termination and Convergence Properties, Integer and Nonlinear Programming (ed. J. Abadie), North-Holland, 1970.

[14] Zoutendijk, G., Methods for Feasible Directions, Elsevier, 1960.

[15] Fleury, C., Braibant, V., Structural Optimization. A New Dual Method Using Mixed Variables, Int. Numer. Meth. Engng., Vol. 23, 1986, pp. 409-429.

Chapter 3

The Boundary Element
Method in Elastostatics

3.1 Introduction

This chapter introduces the basic theory and numerical aspects of the boundary element method in elastostatics which will be used later on as a numerical analysis tool for shape optimization. After a historical review of the boundary element method in elastostatics, the boundary element formulation for elasticity is presented, followed by the numerical implementation. Final concluding remarks discuss the advantages and drawbacks of the boundary element method over the finite element method in the field of structural analysis, especially in the application of shape optimum design.

3.2   Review of the Boundary Element Method in Elastostatics

With the rapid developments of digital computers, many numerical techniques have been created to solve practical engineering problems. For the last two decades, one dominant numerical method is the finite element method (FEM). By discretizing the domain into small elements, and employing interpolation functions to approximate the distributions of the state variables (like displacements and stresses etc.), FEM can provide the solutions for a wide range of problems.

Recently the boundary element method (BEM) has been recognized as an attractive alternative numerical method to FEM in engineering applications. Like FEM, BEM can solve various engineering problems, such as elastostatics, heat transfer, fluid, fracture mechanics and plasticity etc. The superior feature of BEM over FEM is that it only needs to discretize the boundary, which often leads to fewer elements and easier to use.

Historically, the BEM has been developed using two different approaches: the direct formulation and the indirect formulation.

Even though the theoretical considerations of the direct integral equation had been discussed by Kupradze [1], the direct formulation in terms of engineering applications was first introduced by Rizzo in 1967 [2], which was derived from Somigliana's identity. In this formulation, the unknowns are tractions and displacements on the boundaries, and the stresses and displacements inside the domain can be obtained from the numerical integration of the boundary tractions and boundary displacements. The pioneer works have been done by Jaswon, Maiti and Symm [3] using Airy stress function for plane elastostatics, Cruse [4] for three-dimensional elastostatics, Cruse and Rizzo [5] for elasto-dynamic problems, and Lachat [6] by introducing high order elements.

The indirect method introduces fictitious unknowns in the system equation, which have no direct physical meaning. Once those fictitious unknowns have been computed, the real displacements and stresses can be obtained by boundary integration of the fictitious unknowns. The pioneer works of indirect method were due to Kupradze [1], Massonnet and Oliveira [7, 8]. Recent developments of indirect formulation can be seen in [9]-[11].

It should be mentioned that although the above two boundary element formulations are based on the same principle, i.e. representing the basic system equation by boundary variables, the solution procedures are quite different. The direct boundary element formulation has the advantage of being simple in concept, and easier for implementation, so it is the most widely used form in various applications.

In the last decade, the numerical aspects and applications of BEM have been extensively studied. In the following, four important fields of BEM in elastostatics (or other related fields) are briefly discussed, with some key references.

a) New formulations and fundamental solutions

In addition to the two basic formulations (direct and indirect formulations), many others have been proposed for special purpose applications. Quinlan et al. [12, 13] presented a BEM-like edge-function method, in which special functions were chosen to match each edge of the boundary, and the final overall solutions were obtained as a superposition from each segment. Recently a new boundary element formulation has been developed for elasticity problems by Ghost et al. [14, 15]. The basic state variables in this new formulation were the tractions and the gradients of the tangential displacements on the boundary. This formulation has the advantage of providing high accurate stresses near or on the boundary.

Another new form of boundary element formulation is the complex variable

boundary element method, which has demonstrated its high accuracy and efficiency in many applications [16, 17]. However this approach is limited to two-dimensional problems only.

The most widely used fundamental solutions in elastostatics are the Kelvin solutions. Other fundamental solutions have been used for some particular applications, which often lead to more accuracy and efficiency. For example, the semi-plane solutions (Mindlin's fundamental solutions) proposed by Telles and Brebbia [18] have been successfully used in the field of geomechanics, and the special fundamental solutions introduced by Snyder and Cruse [19] have been used for crack problems.

b) Numerical integration

Since boundary element equations are integral equations involving singular integrands (i.e. the fundamental solution becomes singular when the source point coincides with the integration point), the proper treatment of the singular integration has become essential in terms of numerical accuracy and efficiency.

As analytical solutions for those singular integrations are not available for general problems, various numerical methods have been proposed to deal with the singularity. Subdivision is the simplest technique, in which the elements near the source point are divided into small integration regions to cope with the large variations [20, 21]. Another powerful method is to transform the integral variables such that the behaviour of the singularity becomes weaker, or in some cases be eliminated completely. The details on the transformation methods can be found in [22, 23]

c) The domain integral transformation

Some domain integrals may appear in the boundary element formulation representing body forces, nonlinear effects etc. There is no difficulty in discretizing the domain into cells as in FEM, but it weakens the advantage of

BEM over FEM. Various approaches have been proposed to transform domain integrals into equivalent boundary integrals [24]-[26], so that the final boundary element equation involves only the boundary integral.

d) Coupling of BEM and FEM

For some engineering applications, coupling BEM and FEM can often produce better accuracy and efficiency. For example, BEM can be used to model infinite domains, or stress concentrations, whereas FEM can be used to model nonlinear material regions. The general approaches of such combination have been widely investigated [27]-[30] including many practical applications.

The development of BEM has led to a large quantity of publications in both academic researches and industrial applications. The boundary element reference book edited by Mackerle and Brebbia [31] covered the most important boundary element publications, as well as the software available. The basic theory and applications of BEM can be seen in the books by Brebbia [32], Banerjee and Butterfield [33], Crouch and Starfield [34], Brebbia, Telles and Wrobel [35], Brebbia and Dominguez [36], and Hartmann [37]. The recent advances on BEM can be referred to the conferences which were dedicated to the boundary element method [38]-[53].

3.3   The Boundary Element Method in Elastostatics

3.3.1   Basic Equations of Linear Elasticity

The equilibrium equations of a linear elastic body are [54]:

$$\sum_{j=1}^{3} \sigma_{ij,j} + b_i = 0 \qquad (3.1)$$

where $i = 1, 2, 3$, σ_{ij} are the components of the stress tensor and b_i are the components of the body force.

The tractions on the boundary are given by

$$t_i = \sigma_{ij} n_j \tag{3.2}$$

where n_j are the direction cosines of unit outward normal with respect to the axis x_j.

The stress tensor has the property of symmetry, so only six of the nine components are independent. The relations between strains and displacements can be expressed by:

$$\varepsilon_{ij} = \frac{1}{2}\left(\frac{\partial u_i}{\partial x_j} + \frac{\partial u_j}{\partial x_i}\right) \tag{3.3}$$

where $i = 1, 2, 3$, and $j = 1, 2, 3$. ε_{ij} and u_i are strain tensor and displacement tensor respectively.

The stress - strain relations can be expressed as:

$$\sigma_{ij} = 2\mu\varepsilon_{ij} + \lambda\varepsilon_{kk}\delta_{ij} \tag{3.4}$$

where ε_{kk} is the volumetric strain, i.e. $\varepsilon_{kk} = \varepsilon_{11} + \varepsilon_{22} + \varepsilon_{33}$, μ and λ are the Lame's constants.

δ is the Kronecher delta, and is defined as:

$$\delta_{ij} = \begin{cases} 1 & \text{if } i = j \\ 0 & \text{if } i \neq j \end{cases}$$

The Lame's constants μ and λ can be related to Young's modulus E, Poisson's ratio ν and Shear modulus G, i.e.

$$\mu = G = \frac{E}{2(1 + \nu)} \qquad\qquad \lambda = \frac{\nu E}{(1 + \nu)(1 - 2\nu)}$$

3.3.2 The Boundary Integral Formulation of Elasticity

The boundary integral formulation of elasticity can be derived by either weighted residual method, or reciprocal work theorem as shown by Brebbia [32] and Rizzo [2] respectively. In the following, the weighted residual method is used for the derivation of the basic formulation of BEM in elastostatics.

Consider an elastic body with domain Ω, and bounded by τ_1 and τ_2 as shown in Fig. 3.1. Recall the basic equilibrium equation:

$$\sum_{j=1}^{3} \sigma_{kj,j} + b_k = 0 \tag{3.5}$$

under the boundary conditions:

$$
\begin{aligned}
u_k &= \bar{u}_k & \text{on } \tau_1 \\
p_k &= \bar{p}_k & \text{on } \tau_2
\end{aligned}
\tag{3.6}
$$

Assume a weight function u^*, and let the weighted residual equals zero, we get

$$\int_{\Omega} (\sigma_{kj,j} + b_k) u_k^* d\tau = 0 \tag{3.7}$$

If we integrate the first term of equation (3.7) by parts twice, then:

$$\int_{\Omega} (\sigma_{kj,j}^* u_k + b_k u_k^*) d\Omega = - \int_{\tau} p_k u_k^* d\tau + \int_{\tau} p_k^* u_k d\tau \tag{3.8}$$

The weighting function can be any solution which satisfy the equilibrium equation. The most common weighting function used in BEM is the fundamental solution corresponding to a unit force vector acting in the infinite domain. The fundamental solutions satisfy the equation

$$\sum_{j=1}^{3} \sigma_{lj,j}^* + \Delta e_l = 0 \tag{3.9}$$

Substituting (3.9) into (3.8) and applying the property of the Dirac Delta function, finally we get the general integral equation:

$$u_l^i + \int_{\tau} p_{lk}^* u_k d\tau = \int_{\tau} u_{lk}^* p_k d\tau + \int_{\Omega} u_{lk}^* b_k d\Omega \tag{3.10}$$

where u_l^i –displacement at an internal point.

p^* , u^*–fundamental solutions

b–body force

The fundamental solutions for plane strain linear isotropic material are:

$$u_{lk}^* = \frac{1}{8\pi G(1-\nu)}[(3-4\nu)\ln(1/r)\delta_{lk} + \frac{\partial r}{\partial x_l}\frac{\partial r}{\partial x_k}] \qquad (3.11)$$

$$p_{lk}^* = -\frac{1}{4\pi G(1-\nu)r}[\frac{\partial r}{\partial n}\{(1-2\nu)\delta_{kl} + 2\frac{\partial r}{\partial x_k}\frac{\partial r}{\partial x_l}\}$$
$$- (1-2\nu)(\frac{\partial r}{\partial x_l}n_k - \frac{\partial r}{\partial x_k}n_l)] \qquad (3.12)$$

The fundamental solutions for plane stress can be obtained by the following substitution of Poisson's ratio and Young's modulus

$$E \leftrightarrow E(1 - \frac{\nu^2}{(1+\nu)^2}), \qquad \nu \leftrightarrow \frac{\nu}{1+\nu}$$

and the fundamental solutions for 3-D elasticity can be found in any standard boundary element text book (such as by Brebbia et al.[35]).

If the point is on the boundary, the equation (3.10) is modified by taking a limiting process, and the final expression is

$$c_{lk}^i u_k^i + \int_\tau p_{lk}^* u_k d\tau = \int_\tau u_{lk}^* p_k d\tau + \int_\Omega u_{lk}^* b_k d\Omega \qquad (3.13)$$

The parameter c_{lk} equals to $\delta_{lk} + d_{lk}$, where δ_{lk} is an identity matrix, and d_{lk} comes from the procedure of taking the source point of equation (3.10) into the boundary. For a smooth boundary, $d_{lk} = -1/2\delta_{lk}$. When the boundary is not smooth, such as corners, the d_{lk} can be calculated by the following formula [36]:

$$d_{lk} = \frac{-1}{8\pi(1-\nu)}\begin{bmatrix} 4(1-\nu)(\pi+\theta_2-\theta_1)+\sin 2\theta_1 - \sin 2\theta_2, \cos 2\theta_2 - \cos 2\theta_1 \\ \cos 2\theta_2 - \cos 2\theta_1, 4(1-\nu)(\pi+\theta_2-\theta_1)+\sin 2\theta_2 - \sin 2\theta_1 \end{bmatrix}$$

where the definition of θ_1 and θ_2 are shown in Fig. 3.2.

3.3.3 Numerical Implementation of the Boundary Element Method

Consider a two dimensional elastic body with K nodes on the boundary, then we can have $2K$ equations by placing the point i on each boundary node in two directions. Since each node has four degree of freedom, i.e. two tractions and two displacements, there are totally $4K$ state variables on the boundary. By specifying two of the state variavles (either traction or displacement) at each node, the remaining $2K$ unknown state variables can be computed by solving the $2K$ integral equations.

The $2K$ integral equations usually can not be solved analytically, instead a numerical method (i.e. BEM) must be used. The numerical implementation of the BEM in 2-D elasticity is presented as follows,

Step 1 Boundary Discretization

The boundary τ is divided into N elements. Within each element, the traction p and displacement u are assumed to vary according to certain interpolation functions. By introducing interpolation functions, u and p at any point of the element can be expressed by the interpolation functions and the nodal values, i.e.

$$u(\xi) = \sum_i^M \phi_i(\xi) u_i$$
$$p(\xi) = \sum_i^M \phi_i(\xi) p_i \tag{3.14}$$

where ξ is the local coordinate, M is the number of nodal points on one element, and ϕ are the interpolation functions. u_i and p_i are nodal values of displacements and tractions respectively.

The most common interpolation functions in BEM are polynomial functions of order 0,1,and 2. The zero order polynomial function generates the constant element, i.e. both traction and displacement are constant over each element.

The zero order interpolation function can be expressed as

$$\phi(1) = 1 \tag{3.15}$$

Since very rare problems have piecewise uniform displacements and tractions, the constant elements are not recommended.

The first order polynomal function generates linear elements, i.e.

$$\phi(1) = (1 - \xi)/2$$
$$\phi(2) = (1 + \xi)/2 \tag{3.16}$$

The second order polynomial functions are the most widely used interpolation functions in BEM, which are called quadratic functions, and the elements with quadratic interpolation functions are defined as quadratic elements. The quadratic interpolation functions can be written as:

$$\phi(1) \;=\; \xi(\xi - 1)/2$$
$$\phi(2) \;=\; 1 - \xi^2$$
$$\phi(3) \;=\; \xi(\xi + 1)/2 \tag{3.17}$$

Figure 3.3 shows the variations of the three different elements under the local coordinate.

The linear and quadratic elements discussed above are called continuous elements, because their external nodes are shared by adjacent elements. Another type of elements often used are the discontinuous elements, in which the external nodes are not shared by adjacent elements. The advantages of using discontinuous elements are: 1) the discontinuous elements can be used where there is a sudden change of geometry or boundary condition, whereas in the case of continuous elements, special treatments are needed (like double nodes for corners). 2) the solutions at the common node from the two adjacent discontinuous elements are usually different. This difference can be used as a

simple check to see whether the mesh is fine enough. The main drawback of the discontinuous elements is that it introduces more variables and unknowns. Fig. 3.4 shows the different discontinuous quadratic elements.

The following matrices are introduced in order to simplify the notations.

The $\mathbf{c^i}$ and the displacements at the node i

$$\mathbf{c^i} = \begin{bmatrix} c_{11} & c_{12} \\ c_{21} & c_{22} \end{bmatrix} \qquad \mathbf{u^i} = \begin{bmatrix} u_1^i \\ u_2^i \end{bmatrix} \qquad (3.18)$$

The fundamental solutions:

$$\mathbf{u^*} = \begin{bmatrix} u_{11}^* & u_{12}^* \\ u_{21}^* & u_{22}^* \end{bmatrix} \qquad \mathbf{p^*} = \begin{bmatrix} p_{11}^* & p_{12}^* \\ p_{21}^* & p_{22}^* \end{bmatrix} \qquad (3.19)$$

The vectors of displacements and tractions:

$$\mathbf{u} = \begin{Bmatrix} u_1 \\ u_2 \end{Bmatrix} \qquad \mathbf{p} = \begin{Bmatrix} p_1 \\ p_2 \end{Bmatrix} \qquad (3.20)$$

The interpolation functions (for quadratic element):

$$\mathbf{\Phi} = \begin{bmatrix} \phi(1) & 0 & \phi(2) & 0 & \phi(3) & 0 \\ 0 & \phi(1) & 0 & \phi(2) & 0 & \phi(3) \end{bmatrix} \qquad (3.21)$$

Then equation (3.13) becomes:

$$\mathbf{c^i u^i} + \int_\tau \mathbf{p^* u}\, d\tau = \int_\tau \mathbf{u^* p}\, d\tau + \int_\Omega \mathbf{u^* b}\, d\Omega \qquad (3.22)$$

Taking (3.14) into (3.22), therefore

$$\mathbf{c^i u^i} + \sum_j^N \{\int_{\tau_j} \mathbf{p^* \Phi}\, d\tau\} \mathbf{U}^j = \sum_j^N \{\int_{\tau_j} \mathbf{u^* \Phi}\, d\tau\} \mathbf{P}^j + \sum_s^M \int_{\Omega_s} \mathbf{u^* b}\, d\Omega \qquad (3.23)$$

where $\mathbf{U}^j$ denotes the nodal displacement vector, i.e. $\mathbf{U}^j = [u_1^x, u_1^y, u_2^x, u_2^y, u_3^x, u_3^y]$, and $\mathbf{P}^j$ is the nodal traction vector, $\mathbf{P}^j = [p_1^x, p_1^y, p_2^x, p_2^y, p_3^x, p_3^y]$.

Note that the integration of the body force term is carried out by dividing the domain into M small cells, in which the distribution of the body force can be approximated over each cells. In some cases, the domain integral of the body force term can be transformed to the boundary integrals as shown in [24]-[26].

The above formula presents the relations between discretized displacements and tractions when source point is at a boundary node i.

Step 2 Assembling Global Matrices

For each source point, we have two equations as shown in (3.23). Consider total K nodes on the boundary, by placing source point onto each node, there will be $2 \times K$ equations. After transforming the local coordinates into global coordinates, all the $2 \times K$ equations can be assembled into the following matrix form:

$$\mathbf{H}_{2K \times 2K} \mathbf{U}_{2K \times 1} = \mathbf{G}_{2K \times 2K} \mathbf{P}_{2K \times 1} \tag{3.24}$$

Where $\mathbf{U}$ and $\mathbf{P}$ are boundary displacement and traction vectors
$\mathbf{H}$ and $\mathbf{G}$ are influence matrices which are the integral of the fundamental solutions and interpolation functions over the boundary elements.

Step 3 Applying Boundary Conditions

At each node, there are four variables, i.e. two displacements and two tractions. After specifying the two known boundary conditions, there will be $2 \times K$ unknowns which equals to the number of equations. By rearranging matrices $\mathbf{H}$ and $\mathbf{G}$ so that all unknowns are on the left hand side, therefore the final system equation can be written in the form:

$$\mathbf{AX} = \mathbf{F} \tag{3.25}$$

Step 4 Boundary and Domain Solutions

After solving the system equation (3.25), all boundary displacements and tractions are known. The stresses on the boundary can be easily computed under local coordinates (Fig. 3.5), for plane-strain:

$$
\begin{aligned}
\sigma_{12} &= p_t \\
\sigma_{22} &= p_n \\
\sigma_{11} &= \frac{1}{1-\nu}(\nu\sigma_{22} + 2\mu\varepsilon_{11})
\end{aligned}
\tag{3.26}
$$

where p_t and p_n are components of boundary tractions along tangential and normal direction respectively. ε_{11} is the gradient of the tangential displacement, i.e. $\varepsilon_{11} = \partial u_s/\partial s$.

The internal displacements can be obtained by (3.10), i.e.

$$
\mathbf{u}^i = \sum_j^N \{\int_{\tau_j} \mathbf{u}^*\Phi d\tau\}\mathbf{P}^j - \sum_j^N \{\int_{\tau_j} \mathbf{p}^*\Phi d\tau\}\mathbf{U}^j + \sum_s^M \int_{\Omega_s} \mathbf{u}^*\mathbf{b} d\Omega
\tag{3.27}
$$

The internal stresses can be calculated by differentiating the displacement expression (3.27) and using the stress-strain relations [35], i.e.

$$
\sigma_{ij} = \int_\tau (D_{kij}p_k - S_{kij}u_k)d\tau + \int_\Omega D_{kij}b_k d\Omega
\tag{3.28}
$$

where p_k and u_k are boundary traction and displacement respectively.

For 2-D problem,

$$
D_{kij} = \frac{1}{4\pi(1-\nu)r}\{(1-2\nu)[\delta_{ki}r_{,j} + \delta_{kj}r_{,i} - \delta_{ij}r_{,k}] + 2r_{,i}r_{,j}r_{,k}\}
\tag{3.29}
$$

and

$$
\begin{aligned}
S_{kij} =\ & \frac{\mu}{2\pi(1-\nu)r^2}\{2\frac{\partial r}{\partial n}[(1-2\nu)\delta_{ij}r_{,k} + \nu(\delta_{ik}r_{,j} + \delta_{jk}r_{,i} - 4r_{,i}r_{,j}r_{,k}] \\
& + 2\nu(n_i r_{,j}r_{,k} + n_j r_{,i}r_{,k}) \\
& + (1-2\nu)(2n_k r_{,i}r_{,j} + n_j\delta_{ik} + n_i\delta_{jk} - (1-4\nu)n_k\delta_{ij}\}
\end{aligned}
\tag{3.30}
$$

where μ and ν are shear modulus and Poisson's ratio respectively, and the commas denote the derivatives.

The above 4 steps cover the basic numerical implementation of BEM. Fig. 3.6 shows a flow chart for a typical BEM analysis program.

3.4   Concluding Remarks

In engineering applications, both FEM and BEM have established their own strength and merits as numerical methods, on the other hand, both of them still possess some drawbacks. In the following, a comparision between FEM and BEM is presented, with special references for the application of shape optimization.

1) Theoretically, both FEM and BEM are based on the same kind weighted residual methods [55]. The approximation procedure of both methods are nearly the same, i.e. by introducing interpolation functions over each element to approximate the distribution of state variables. The main difference is the choice of the weighting functions.

2) As a domain method, FEM needs discretization of the whole domain, which usually leads to large number of unknowns (therefore a larger system equation). BEM needs only the discretization of the boundary, so the unknowns are far less than by FEM. This feature of BEM enables the user to use less input data, provides an easier modelling, and easier presentation for CAD. This advantage of BEM over FEM has significant importance for shape optimization, because the design variables are boundary geometry parameters which can be implemented into boundary element modelling with little cost, and also easier for remeshing during design process. On the other hand, the remeshing for FEM is very expensive, especially for three-dimensional cases.

3) The solutions by BEM, like boundary stresses, are more accurate than by FEM, especially near the place of stress concentration. This feature is very important for shape optimization in which the stresses are often used

to measure the performance of a structure, and for shape design sensitivity calculation.

4) BEM is more efficient for infinite domain problems, and FEM is more efficient for nonlinear, anisotropic materials. Generally speaking, FEM covers more engineering applications than BEM at present, but this might change with the development of BEM.

5) The final system equation of both FEM and BEM has the same form, i.e. $\mathbf{AX} = \mathbf{B}$. The left hand side matrix $\mathbf{A}$ in FEM is symmetric and sparse, whereas $\mathbf{A}$ in BEM is a fully populated nonsymmetric matrix, therefore the computation cost for solving a system of the same number unknowns in FEM is far less than in BEM. This is the one main motivation for the combination of FEM and BEM in some applications.

3.5 References

[1] Kupradze, V. D., Potential Methods in the Theory of Elasticity, Oldbourne Press, 1965.

[2] Rizzo, F. J., An Integral Equation Approach to Boundary Value Problems of Classical Elastostatics, Applied Mathematics, 25, 1967, pp. 83-95.

[3] Jaswon, M. A., Maiti, M., Symm, G. T., Numerical Biharmonic Analysis and Some Applications, Int. J. Solids Strutures, 3, 1967, pp. 309-332.

[4] Cruse, T. A., Numerical Solutions in Three Dimensional Elastostatics, Int. J. Solids Struct., 5, 1969, pp. 1259-1274.

[5] Cruse, T. A., Rizzo, F. J., A Direct Formulation and Numerical Solution of the General Transient Elasto-Dynamic Problem, J. Math. Analysis Appli., 22, 1968.

[6] Lachat, J. C., A Further Development of the Boundary Integral techniques for Elastostatics, Ph.D. Thesis, University of Southampton, 1975.

[7] Massonnet, C. E., Numerical Use of Integral Procedures, Stress Analysis (eds. O. C. Zienkiewicz and G. S. Holister), Wiley, 1965.

[8] Oliveira, E. R. A., Plane Stress Analysis by a Gerneral Integral Method, J. ASCE. Mech. Div., 1968, pp. 79-85.

[9] Beniumea, R., Sikarskie, D. L., On the Solution of Plane, Orthotropic elasticity problems by an Integral Method, J. Appl. Mech., 39, 1972, pp. 801-808.

[10] Crouch, S. L., Solution of Plane Elasticity Problems by the Displacement Discontinuity Method, Int. J. Nemer. Meth. Engng., 10, 1976, pp. 301-343.

[11] Banerjee, P. K., Integral Equation Methods for Analysis of Piece-Wise Non-Homogeneous Three-Dimensional Elastic Solids of Arbitary Shape, Int. J. Mech. Sci., 18, 1976, pp. 293-303.

[12] Quinlan, P. M., O'Callagham, M. J. A., The Edge-Function Method for Cracks, Cavities and Curved Boundaries in Elastostatics, Chapter 6, Topic in Boundary Element Research (ed. C. A. Brebbia), Vol.3, 1987.

[13] Quinlan, P. M., The Edge-Function Method with Artitary Boundaries in Fracture, Elastostatics, Viscoelasticity and Heat Conduction, Proc. ICCM-88, Springer-Veralg.

[14] Ghosh, N., Rajiyah, H., Ghosh, S., Mukherjee, S., A New Boundary Element Method Formulation for Linear Elasticity, J. Appl. Mech., Vol. 53, 1986, pp. 69-76.

[15] Ghosh, N., Mukherjee, S., A New Boundary Element Method Formulation for Three Dimensional Problems in Linear Elasticity, Acta Mechanics, 67, 1987, pp. 107-119.

[16] Hunt, B., Isaacs, L. T., Integral Equation Formulation for Ground-Water Flow, ASCE Hyd., Oct., 1981.

[17] Hromadka, T. V., Lai, C., The Complex Variable Boundary Element Method in Engnieering Analysis, Springer-Verlag, 1987.

[18] Telles, J. C. F., Brebbia, C. A., Boundary Element Solutions for Half-Plane Problems, Int. J. Solids Struct., 17, 1981, pp. 1149-1158.

[19] Snyder, M. D., Cruse, T. A., Boundary Integral Equation Analysis of Cracked Anisotropic Plates, Int. J. Frac., 11, 1975, pp. 315-328.

[20] Lachat, J. C., Watson, J. O., Effective Numerical Treatment of Boundary Integral Equations: A Formulation for Three-Dimensional Elastostatics, Int. J. Numer. Meth. Engng., 10, 1976, pp. 273-289.

[21] Jun, L., Beer, G., Meek, J. L., Efficient Evaluation of Integrals of Order $1/r$, $1/r^2$, $1/r^3$ Using Gauss Quadrature, Engineering Analysis, 2, 1985, pp. 118-123.

[22] Telles, J. C. F., A Self Adaptive Coordinate Transform for efficient Numerical Evaluaton of General Boundary Element Integrals, Int. J. Numer. Meth. Engng., 1986.

[23] Kayami, K., Brebbia, C. A., A New Coordinate Transformation Method for Singular and Nearly Singular Integrals over General Curved Boundary Elements, 9th Boundary Elements Conference (eds. C. A. Brebbia, W. L. Wendland, G. Kuhn), 1987.

[24] Nardini, D., Brebbia, C. A., A New Approach for Free Vibration Analysis Using Boundary Elements, Boundary Element Method in Engineering, Springer-Verlag, 1982.

[25] Nowak, A. J., Brebbia, C. A., The Multiple Reciprocity Method. A New Approach for Transforming BEM Domain Integrals to the Boundary, To be published in Engineering Analysis Journal.

[26] Tang, W., A Generalised Approach for Transforming Domain Integrals into Boundary Integrals in Boundary Element Methods, Ph.D Thesis, Computational Mechanics Institute, UK., 1988.

[27] Zienkiewicz, O. C., Kelly, D. W., Bettes, P., The coupling of the Finite Element Method and Boundary Solution Procedures, Int. J. Numer. Meth. Engng., 11, 1977, pp. 355-375.

[28] Brebbia, C. A., Georgiou, P., Combination of Boundary and Finite Elements in Elastostatics, Appl. Math. Modelling, 3, 1979, pp. 212-220.

[29] Kohno, K., Tsunada, T., Seto, H., Tanaka, M., Hybrid Stress Analysis of Boundary and Finite Elements by Super-Element Method, Advance in Boundary Elements, CMP and Springer-Verlag, 1989.

[30] Defigueredo, T. G. B., Brebbia, C. A., A New Hybrid Displacement Variational Formulation of BEM for Elastostatics, Advances in Boundary Elements, CMP and Springer-Verlag, 1989.

[31] Mackerle, J., Brebbia, C. A., The Boundary Element Reference Book, CPM and Springer-Veralg, 1988.

[32] Brebbia, C. A., The Boundary Element Method for Engineers, Pentech Press, 1978.

[33] Banerjee, P. K., Butterfield, R., Boundary Element Methods In Engineering Science, McGraw-Hill, 1981.

[34] Crouch, S. L., Starfield, A. M., Boundary Element Methods in Solid Mechanics, Allen and Unwin, 1983.

[35] Brebbia, C. A., Telles, J. C. F., Wrobel, L. C., Boundary Element Techniques, Theory and Applications in Engineering, Springer-Verlag, 1984.

[36] Brebbia, C. A., Dominguez, J., Boundary Elements - An Introduction Course, Computational Mechanics Pub., 1988.

[37] Hartmann, F., Introduction to Boundary Elements. Theory and Applications, Springer-Veralg, 1989.

[38] Brebbia, C. A. (ed.), Recent Advances in Boundary Element Methods, Proc. 1st Int. Conf. BEM., Southampton, Pentech Press, 1978.

[39] Brebbia, C. A. (ed.), New Development in Boundary Element Methods, Proc. 2nd Int. Seminar, CML Publications, 1980.

[40] Brebbia, C. A. (ed.), Boundary Element Methods, Proc. 3rd Int. Seminar, California, USA, CML Publications, 1981.

[41] Brebbia, C. A. (ed.), Boundary Element Methods in Engineering, Proc. 4th. Int. Seminar, Southampton, CML Publications, 1982.

[42] Brebbia, C. A., Futagami, T., Tanaka, M. (eds.), Boundary Elements, Proc. 5th Int. conf., Japan, CML Publications, 1983.

[43] Brebbia, C. A. (ed.), Boundary Elements, Proc. 6th Int. Conf., The Queen Elizabeth 2, CML Publications, 1984.

[44] Brebbia, C. A., Maier, G. (eds.), Boundary Elements, Proc. 7th Int. Conf., Italy, 1985.

[45] Tanaka, M., Brebbia, C. A. (eds.), Boundary Elements, Proc. 8th Int. Conf., Japan, CML Publication, 1986.

[46] Brebbia, C. A., Wendland, W. L., Kuhn, G. (eds.), Boundary Elements, Proc. 9th Int. Conf., Stuttgart, Germany, CML Publications, 1987.

[47] Brebbia, C. A. (ed.), Boundary Elements Proc. 10th Int. Conf., Southampton, CML Publications, 1988.

[48] Brebbia, C. A., Conner, J. J. (eds.), Boundary Elements, Proc. 11th Int. Conf., Boston, USA, CML Publications, 1989.

[49] Brebbia, C. A., Noye, B. J. (eds.), BETECH 85, Proc. 1st BETECH Conf., Adelaide, Australia, CML Publications, 1985.

[50] Conner, J. J., Brebbia, C. A. (eds.), BETECH 86, Proc. 2nd BETECH Conf., Cambridge, USA, CML Publications, 1986.

[51] Brebbia, C. A., Venturini, W. S. (eds.), Boundary Element Techniques, Proc. 3rd BETECH Conf., Brazil, CML Publications, 1987.

[52] Cruse, T. A. (ed), IUTAM Symposium on Advanced Boundary Element Method, Springer-Veralg, 1987.

[53] Brebbia, C. A., Zamana, N. G. (eds.), Boundary Element Techniques: Applications in Engineering, Proc. 5th BETECH Conf., Windsor, Canada, CML Publications, 1989.

[54] Timoshenko, S. P., Goodier, J. N., Theory of Elasticity, McGraw-Hill, 1987.

[55] Zienkiewicz, O. C., Morgan, K., Finite Elements and Approximation, John Wiley & Sons, 1983.
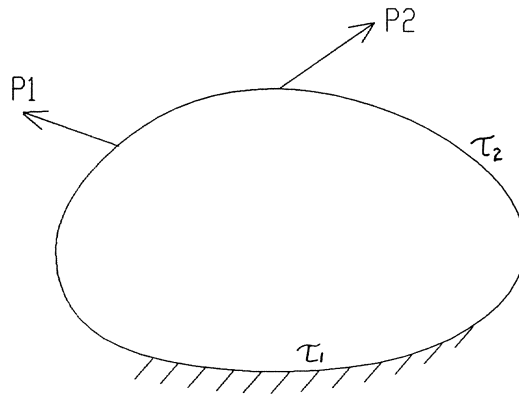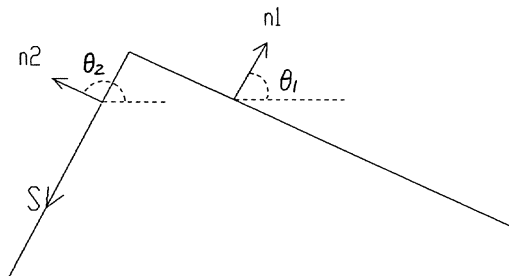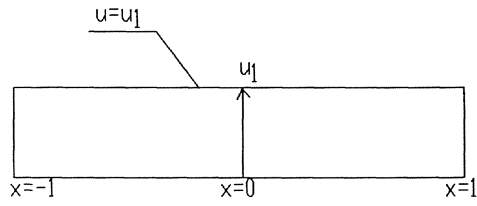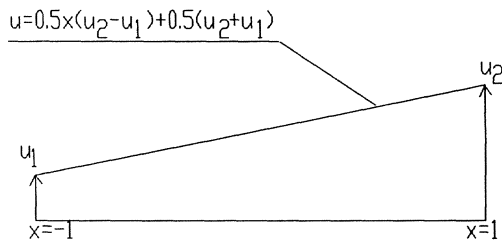
Fig. 3.1 An Equilibrium Body

Fig. 3.2 The Corner Point

Constant Element

Linear Element
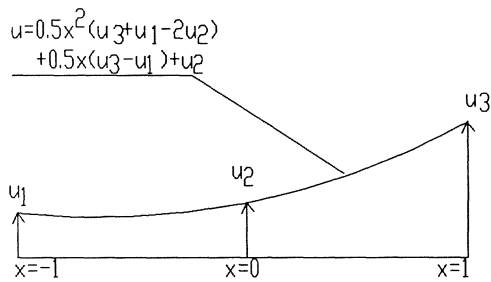
Quadratic Element

Fig 3.3 Polynomial Elements

MESH POINT

NODE POINT
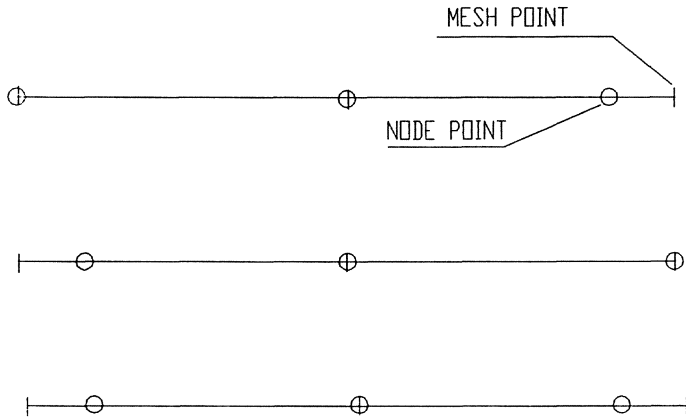
Fig. 3.4 Discontinuous Quadratic Elements

2

1

S
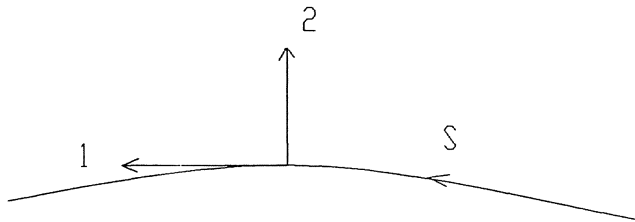
Fig. 3.5 Local Coordinates System
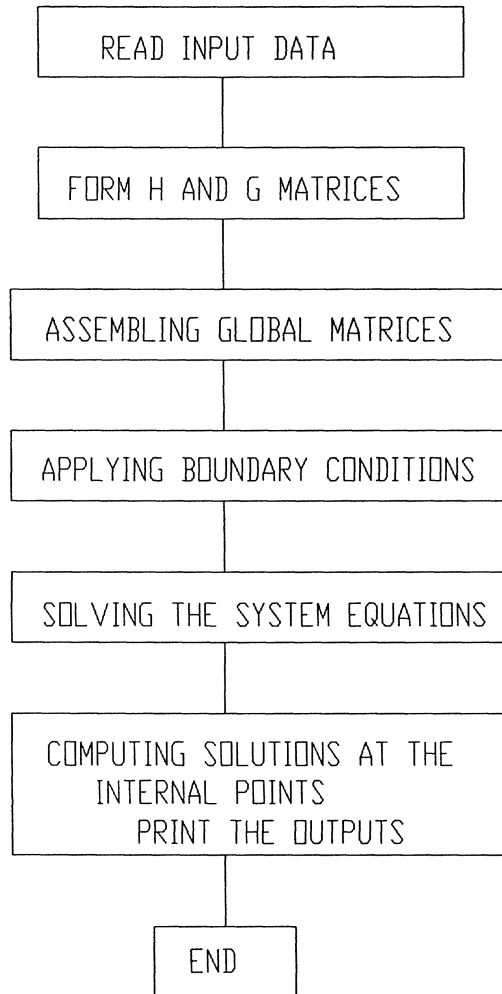
Fig. 3.6 Flow Chart of BEM Program
(2-D Elasticity)

Chapter 4

Shape Design Sensitivity Analysis using the Boundary Element Method

4.1 Introduction

The mathematical programming (MP) methods for shape optimization are iterative methods, in which the designs are modified successively until all the criteria are satisfied. A key issue during the design modification is to predict how the response of the structure changes due to the shape change of the structure. This information is called shape design sensitivity, which is defined as the rates of change of structural responses with respect to the design variables. It is essential to provide accurate design sensitivity information in order to use those MP methods discussed in Chapter 2.

The order of the sensitivity equals to the order of the derivative of the structural response. For example the first order design sensitivity of a structural response f with respect to the design variable b is defined as df/db, and the second order design sensitivity as $d^2 f/db^2$

The use of second order design sensitivity can often result in faster convergence, but most of the numerical algorithms described in chapter 2 need first order sensitivities only. This is mainly because it is far easier to compute the first order design sensitivity than the second order sensitivity. This thesis only concerns the first order shape design sensitivity, which will be simply called design sensitivity throughout the thesis except those places specially indicated.

The evaluation of the design sensitivity has become an important research topic for the last two decades since the success of MP methods for solving shape optimization problems often depends upon the way to calculate the design sensitivity, i.e. which method, how accurate and how easier (efficiency).

The main task of this chapter is to investigate different numerical approaches to design sensitivity calculation, and to develop more efficient and accurate approaches for 2-D elasticity. First the two basic approaches for design sensitivity, namely the continuum approach (CA) and the discretized approach (DA), are presented and compared. The CA is then used to derive the stress sensitivity formulation based on BEM. The main difficulty of the CA method, the appearance of the singular adjoint loads of the adjoint problem, is discussed. The term singular loads imply that the loads are concentrated forces, i.e. point forces.

Two approaches are developed to model the adjoint problem, one uses the distributed loads to replace the singular loads, and the other one employs the singularity subtraction method to remove the singular loads from the BEM equation. Both methods are proved to be more accurate than using the singular loads directly.

The total finite difference method has two drawbacks; 1) the computation cost is usually higher, 2) the accuracy of the approach often depends on the choice of the perturbation step. A new finite difference based method

is developed, which has the advantage of being simple in concept and easier implementation, and overcomes the two drawbacks of the finite difference method.

A few test examples are used to demonstrate the accuracy of the proposed formulations, and the comparisons are made with different meshes to study the influence of the mesh refinements on the accuracy of design sensitivity.

4.2 Two Basic Approaches for Design Sensitivity Analysis

4.2.1 The Discretized Approach (DA)

The various numerical methods for design sensitivity analysis can be catalogued into two classes, the discretized approach (DA) and the continuum approach (CA). In the following, the basic formulations and the numerical characteristics of these two methods are presented.

The discretized approach starts with the discretized system equation. For example if BEM is used for analysis, the final system equation can be written in matrix form

$$\mathbf{A}\mathbf{X} = \mathbf{B}\mathbf{Y} + \mathbf{P} \qquad (4.1)$$

where $\mathbf{A}$ and $\mathbf{B}$ are influence matrices, $\mathbf{X}$ is a vector containing the unknown boundary displacements and tractions, $\mathbf{Y}$ is the vector of prescribed boundary displacements and tractions, and $\mathbf{P}$ is the vector of the prescribed body force.

Differentiating equation (4.1) with respect to a design variable b_i, we have

$$\mathbf{A}\frac{\partial \mathbf{X}}{\partial b_i} = \frac{\partial \mathbf{B}}{\partial b_i}\mathbf{Y} - \frac{\partial \mathbf{A}}{\partial b_i}\mathbf{X} + \mathbf{B}\frac{\partial \mathbf{Y}}{\partial b_i} + \frac{\partial \mathbf{P}}{\partial b_i} \qquad (4.2)$$

The above formula provides the traction and displacement sensitivities on

the boundary. The stress sensitivities can be obtained by further differentiating the displacement sensitivity, and employing the stress-strain relationship as shown in [1].

It is noted that equation (4.2) has the same left hand matrix as the initial system equation (4.1), so a simple forward and back substitutions can be used for solving the equation. In order to solve equation (4.2), we must evaluate each term in right hand side of the equation. The main computation cost for this evaluation is from the first two terms because they involve the differentiation of matrices, whereas the last two terms need the differentiation of the vectors only. In practical problems the last two terms are often zero.

The first two terms in the right hand side present the differentiation of influence matrices, which will involve the differentiation of fundamental solutions. This evaluation can be performed either analytically, or numerically. The analytical differentiation will produce new kernels, which needs significant program development for those new functions as discussed by Kane [2]. The finite difference method is the most popular one, in which the design boundary is disturbed by a small quantity δ, and the derivatives of matrices $\mathbf{A}$ and $\mathbf{B}$ are calculated by finite difference formula.

Another discretized method is the total finite difference method, in which the sensitivity is obtained by direct application of the finite difference formula on the solutions of the initial structure and the disturbed structure. Assuming the initial problem has the form:

$$\mathbf{A}(b_0)\mathbf{X}(b_0) = \mathbf{C}(b_0) \tag{4.3}$$

where b_0 denotes the design variable at the initial design, which will define the initial boundary geometry, and $\mathbf{X}$ are the solutions of the initial problem.

By disturbing the initial geometry by δb, we have

$$\mathbf{A}(b_0 + \delta b)\mathbf{X}(b_0 + \delta b) = \mathbf{C}(b_0 + \delta b) \tag{4.4}$$

Solving equations of (4.3) and (4.4), and employing the finite difference formula, we can obtain the sensitivity as:

$$\frac{d\mathbf{X}}{db} \simeq \frac{\mathbf{X}(b_0 + \delta b) - \mathbf{X}(b_0)}{\delta b} \tag{4.5}$$

4.2.2 The Continuum Approach (CA)

Unlike the discretized approach, the continuum approach evaluates the design sensitivity before numerical discretization, so the formulation is exact. The basic concepts and formulations are presented as following, more details can be found in [3, 5].

Material derivative

Consider a domain Ω bounded by τ. Defining a transformation field $\mathbf{T}(\mathbf{X}, t)$, so that the point $\mathbf{X}$ pass to the point $\mathbf{X}^*$. i.e. $P \to P^*$: $\mathbf{X}^* = \mathbf{X} + \delta\mathbf{X}$. The material derivative of a smooth solution u of an elastic equation is defined as:

$$\text{Total material derivative} = \frac{Du}{Dt} = \frac{\partial u}{\partial t} + \sum_j \frac{\partial u}{\partial x_j} V_j \tag{4.6}$$

or alternatively (4.6) can be written as:

$$\dot{u} = u' + (\nabla \mathbf{u})^T \cdot \mathbf{V} \tag{4.7}$$

where $\dot{u}$ denotes the (total) material derivative of u, u' is the partial derivative of u, which presents the change of u with fixed coordinates. $\nabla\mathbf{u}$ is the gradient of u in the space, $\nabla u = [\partial u/\partial x_1 , \partial u/\partial x_2]^T$, $\mathbf{V} = [V_1, V_2]^T$, V_1 and V_2 are components of the velocity field in x_1 and x_2 directions respectively.

The material derivative operator

$$\frac{D}{Dt} = \frac{\partial}{\partial t} + \mathbf{V}^T \cdot \nabla \tag{4.8}$$

can be applied to a scalar, a vector, or a tensor function of x and t [6]. In this thesis, the notation of equation (4.7) will be used.

The material derivatives of two basic integrals are given below, the detailed derivations can be found in [3].

Consider a domain functional ϕ_1 over Ω, i.e.

$$\phi_1 = \int_\Omega f(x)d\Omega \tag{4.9}$$

The material derivative of ϕ_1 is:

$$\dot{\phi}_1 = \int_\Omega f'(x)d\Omega + \int_\tau f(x)V_n d\tau \tag{4.10}$$

where V_n is the normal component of the velocity field, i.e. $V_n = \mathbf{V}^T \cdot \mathbf{n}$.

Next, consider a functional defined as an integral over τ, i.e.

$$\phi_2 = \int_\tau f(x)d\tau \tag{4.11}$$

Then the material derivative of ϕ_2 is:

$$\dot{\phi}_2 = \int_\tau [f' + (\nabla f)^T \cdot \mathbf{V} + f(HV_n + V_{s,s})]d\tau \tag{4.12}$$

where H is the curvature of the boundary τ, and $V_{s,s}$ is the gradient of tangential velocity.

It should be mentioned here that the material derivative of a function ϕ presents the variation of ϕ, not the derivative of ϕ, i.e. $\dot{\phi} = \phi(x + \delta x, t + \delta t) - \phi(x, t)$. This can be seen clearly by the following example. Consider an area A defined as:

$$\phi = \int_A d\Omega$$

then the material derivative of ϕ can be obtained by using (4.10),

$$\dot{\phi} = \int_\tau V_n d\tau = \delta A \tag{4.13}$$

where δA is the change of area due to the boundary perturbation, not the rate of the change. But as V is the function of design variables, so the material

derivative can be parameterized into design sensitivity. In the following, we will refer the material derivative as sensitivity in a general sense, and the transformation from the material derivative to design sensitivity will be presented in 4.4.2.

The relationship between the material derivative and the design boundary perturbation

Consider an equilibrium body occupying the domain Ω which is bounded by τ. The equilibrium equations are

$$\sigma_{ij,j} + b_i = 0 \tag{4.14}$$

where σ_{ij} is the stress tensor, and the b_i is the component of the body force.

Consider another equilibrium state with solution λ as the displacement, where $\lambda = [\lambda_1, \lambda_2, \lambda_3]^T$. Multiply λ to the equation (4.14), and integrate over Ω, we have

$$\int_\Omega \sigma_{ij,j}\lambda_i d\Omega + \int_\Omega b_i\lambda_i d\Omega = 0 \tag{4.15}$$

Integrate the first term of equation (4.15) by parts, and note the boundary traction $t_i = \sigma_{ij}n_j$, we obtain the work theorem

$$\int_\Omega \sigma_{ij}(u)\varepsilon_{ij}(\lambda)d\Omega = \int_\Omega b_i\lambda_i d\Omega + \int_\tau t_i\lambda_i d\tau \tag{4.16}$$

where u_i, $\sigma_{ij}(u)$, b_i and t_i are displacement, stress, body force and boundary traction of the initial problem respectively, and λ and $\varepsilon(\lambda)$ are displacement and strain of another equilibrium state, which is named as the adjoint problem here. This adjoint problem has the same domain with the initial problem but with different boundary conditions.

Taking material derivative of equation (4.16) and using the formula (4.12), we have

$$\int_\Omega \sigma'_{ij}(u)\varepsilon_{ij}(\lambda)d\Omega \quad + \quad \int_\Omega \sigma_{ij}(u)\varepsilon'_{ij}(\lambda)d\Omega + \int_\tau \sigma_{ij}(u)\varepsilon_{ij}(\lambda)V_n d\tau$$

$$= \int_\Omega (b_i' \lambda_i + b_i \lambda_i') d\Omega + \int_\tau b_i \lambda_i V_n d\tau$$

$$+ \int_\tau [\dot{t}_i \lambda_i + t_i \dot{\lambda}_i + t_i \lambda_i (HV_n + V_{s,s})] d\tau \qquad (4.17)$$

Assuming that body force is constant, i.e. $b' = 0$. The adjoint field can be chosen such that $\dot{\lambda} = 0$. The partial derivatives of the stress and strain can be expressed as:

$$\sigma_{ij}'(u) = \sigma_{ij}(\dot{u}) - \sigma_{ij}(\mathbf{V}^T \cdot \nabla u) \qquad (4.18)$$

$$\varepsilon_{ij}'(\lambda) = \varepsilon_{ij}(\dot{\lambda}) - \varepsilon_{ij}(\mathbf{V}^T \cdot \nabla \lambda) \qquad (4.19)$$

Substituting (4.18) and (4.19) into equation (4.17). After rearrangement, we obtain:

$$\int_\Omega \sigma_{ij}(\dot{u}) \varepsilon_{ij}(\lambda) d\Omega = \int_\Omega [\sigma_{ij}(\mathbf{V}^T \cdot \nabla u) \varepsilon(\lambda) + \sigma_{ij}(u) \varepsilon_{ij}(\mathbf{V}^T \cdot \nabla \lambda)] d\Omega$$

$$- \int_\Omega b_i \mathbf{V}^T \cdot \nabla \lambda d\Omega + \int_\tau [\dot{t}_i \lambda_i + b_i \lambda_i V_n] d\tau$$

$$+ \int_\tau [t_i \lambda_i (V_n H + V_{s,s}) - \sigma_{ij}(u) \varepsilon_{ij}(\lambda) V_n] d\tau \qquad (4.20)$$

Equation (4.20) provides a general relationship between the material derivative (left hand side) and the design perturbation (right hand side), which will be used later on to derive material derivative formulations for displacement and stress sensitivities.

Material derivative of displacements

Assuming an initial boundary value problem under following boundary conditions:

$$u = 0 \qquad \text{on} \qquad \tau_1$$

$$t = p \qquad \text{on} \qquad \tau_2 \qquad (4.21)$$

Now consider a displacement constraint u at a fixed point x_0, $x_0 \in \Omega$, i.e.

$$\phi = \int_\Omega \delta(x - x_0) u d\Omega \qquad (4.22)$$

where δ is the Dirac delta function.

Taking the material derivative of equation (4.22),

$$\dot{\phi} = \int_\Omega \delta(x - x_0) u' d\Omega \tag{4.23}$$

Defining an adjoint problem under following boundary conditions:

$$u = 0 \qquad \text{on } \tau_1$$
$$t = p_a \delta(x - x_0) \quad \text{on } \tau_2 \tag{4.24}$$

where p_a is a unit force, and $p_a \delta(x - x_0)$ presents a unit force at point x_0. This adjoint problem is very simple as the only external load is the point load on x_0.

If we consider equation (4.14) for adjoint problem, and multiply the displacements of the initial problem, then the work theorem (4.16) becomes

$$\int_\Omega \sigma(\lambda)\varepsilon(u)d\Omega = \int_\Omega p_a \delta(x - x_0) u d\Omega \tag{4.25}$$

Since the equation (4.15) is true for any multiplier u, by substituting $u = u'$ and noting $\int_\Omega \sigma(u)\varepsilon(\lambda)d\Omega = \int_\Omega \sigma(\lambda)\varepsilon(u)d\Omega$, we get

$$\int_\Omega \sigma(u')\varepsilon(\lambda)d\Omega = \int_\Omega p_a \delta(x - x_0) u' d\Omega \tag{4.26}$$

Taking (4.26) into (4.23), using the relations (4.18) and noting $p_a = 1$, we have

$$\begin{aligned}
\dot{\phi} &= \int_\Omega \delta(x - x_0) u' d\Omega \\
&= \int_\Omega \sigma(u')\varepsilon(\lambda)d\Omega \\
&= \int_\Omega \sigma(\dot{u})\varepsilon(\lambda)d\Omega - \int_\Omega \sigma(\mathbf{V}^T \cdot \nabla u)\varepsilon(\lambda)d\Omega
\end{aligned} \tag{4.27}$$

Substituting (4.20) into above equation, we obtain

$$\begin{aligned}
\dot{\phi} &= \int_\Omega [\sigma_{ij}(u)\varepsilon_{ij}(\mathbf{V}^T \cdot \nabla\lambda) - b_i \mathbf{V}^T \cdot \nabla\lambda]d\Omega \\
&+ \int_\tau [t_i\lambda_i + b_i\lambda_i V_n + t_i\lambda_i(V_n H + V_{s,s}) - \sigma_{ij}(u)\varepsilon_{ij}(\lambda)V_n]d\tau \quad (4.28)
\end{aligned}$$

where $\dot{t}_i$ denotes the change of initial loads, and the other notations are the same as before.

In order to use BEM in analysis, the domain integral in above equation needs to be transformed into boundary integral. This can be done by substituting λ with $\mathbf{V}^T \cdot \nabla \lambda$ in equation (4.16), finally the material derivative of the displacement is obtained as

$$
\begin{aligned}
\dot{\phi} &= \int_\tau [t_i \mathbf{V}^T \cdot \nabla \lambda + \dot{t}_i \lambda_i + b_i \lambda_i V_n] d\tau \\
&+ \int_\tau [t_i \lambda_i (V_n H + V_{s,s}) - \sigma_{ij}(u) \varepsilon_{ij}(\lambda) V_n)] d\tau
\end{aligned}
\tag{4.29}
$$

The material derivative of stresses can be obtained in the similar way as the material derivative of displacements, which will be discussed in the next section. The numerical procedure of the continuum method is summarized as follows:

1. Solve the initial problem.

2. Formulate the adjoint problem.

3. Solve the adjoint problem. Note that the adjoint problem can be treated as a special load case of the initial problem. The left hand side matrix of the adjoint problem is the same as the initial problem, so the back substitution technique can be used to solve the adjoint equation.

4. Use the formula (4.29) to compute the material derivatives.

4.2.3   Comparisons of the Two Approaches

The following comparisons are based on general observations. In practice, which is the best method often depends on the nature of the problem itself, as well as how it is implemented.

a) The numerical implementation of the CA is relatively easier than the discretized method. This is because that the CA only involves one more extra load case for each constraint, whereas the DA needs either to disturb the design boundary or to implement some analytical formula to deal with the derivative of the matrix.

b) Theoretically, the CA is an exact formulation, which is expected to give better results than the approximation formula DA. But as the adjoint problem in the CA has concentrated adjoint loads, a unsuitable treatment of the adjoint loads will lead to poor accuracy. If finite different method is used in DA, the choice of perturbation step is crucial for the accuracy.

c) The CA requires one analysis for each constraint, whereas the DA needs one analysis for each design variable. If the active constraints are less than the design variables, then CA will require less computing time than DA.

d) The computing time for total finite difference method is often very high, due to the requirement of forming new influence matrices of $\mathbf{A}$ and $\mathbf{B}$.

4.3 The Implementation of the Material Derivative of Displacements

The displacement material derivative formula (4.29) can be written as

$$\dot{\phi} = \phi_1 + \phi_2 \tag{4.30}$$

where

$$\phi_1 = -\int_\tau \sigma_{ij}(u)\varepsilon_{ij}(\lambda)V_n)]d\tau$$
$$\phi_2 = \int_\tau [t_i\mathbf{V}^T\cdot\nabla\lambda + \dot{t}_i\lambda_i + b_i\lambda_iV_n]d\tau$$
$$+ \int_\tau [t_i\lambda_i(V_nH + V_{s,s})]$$

ϕ_1 presents the displacement change with the applied loads fixed, and ϕ_2 presents the displacement change due to the variations of the applied loads.

If we assume the design boundary is traction free, and omit the body force, the equation (4.29) becomes:

$$\dot{\phi} = \phi_1 = - \int_\tau \sigma(u)\varepsilon(\lambda)V_n d\tau \qquad (4.31)$$

For both applied loads and the adjoint loads, the conventional boundary element method can be used to calculate the stress $\sigma(u)$ and the strain $\varepsilon(\lambda)$. This calculation is very simple for the adjoint problem due to three reasons:

a) The only external load is a unit load which can be treated as a body force, there is no integral involved in the calculation of the body force term B.

b) The final adjoint equation has the same left hand side matrix with the initial applied load equation, therefore the solution of the adjoint equation can be obtained using the already factorized sets of equations of the initial problem.

c) All the constraints can be calculated in one process. For example, if m displacement material derivatives are required, all body force vectors form a new matrix $\bar{B}$, Therefore we can solve the equations as $AX = \bar{B}$.

Fig. 4.1 shows an example of a cantilever beam, and the design boundary is upper surface. Fig. 4.1(a) presents the initial problem under the applied loads, and Fig. 4.1(b) presents the adjoint problem under the adjoint loads. The corresponding displacement material derivative is the displacement at c.

The material derivative formula (4.31) is for an isolated fixed point. If we consider the point moving (such as the design boundary points), then there will be one more term which corresponds to the variation of displacement along the space. i.e.,

$$\dot{\phi} = - \int_\tau \sigma(u)\varepsilon(\lambda)V_n d\tau + \mathbf{V}^T \cdot \nabla u \qquad (4.32)$$

where $\mathbf{V} = [V_1 , V_2]^T$, V_1 and V_2 are the components of the velocity field in x_1 and x_2 directions respectively. ∇u are the gradients of the displacements, and $\nabla u = [\partial u/\partial x_1 , \partial u/\partial x_2]$.

As the boundary movement $\mathbf{V}$ is very small in the sensitivity analysis, the actual position of the boundary after moving can be treated as two steps, first moving along the normal direction of the boundary, then in the tangential direction. This can be seen from Fig. 4.2, where the design boundary τ_0 moves vertically to τ_1. The point a on the design boundary will move to b. The corresponding normal direction movement is to c. As V is so small, we can assume the point a moving to c first, then moving tangentially to b, i.e. $\mathbf{V} = \mathbf{V}_n + \mathbf{V}_s$. In the following derivation, the design perturbation will be always assumed to move in V_n and V_s directions.

Usually the point required for displacement sensitivity is on the boundary, in this case, the extra term can be expressed as:

$$\mathbf{V}^T \cdot \nabla u = u_{i,s} V_s + u_{i,n} V_n \qquad (4.33)$$

where $u_{i,s}$, $u_{i,n}$ are the gradients of the displacement u_i in tangential and normal directions respectively. s_i and n_i are the direction cosines of the tangential and the normal vectors with respect to i direction respectively.

The $u_{i,s}$ can be calculated from the boundary solutions of the initial problem, i.e.,

$$u_i = u_s s_i + u_n n_i$$

$$u_{i,s} = u_{s,s} s_i + u_{n,s} n_i \qquad (4.34)$$

where $u_{s,s}$ and $u_{n,s}$ are the tangential derivatives of the components of the displacement u_i.

The $u_{i,n}$ can be also obtained from the boundary information only [4], in

the case of plane stress, we have

$$u_{i,n} = [\frac{1-\nu^2}{E}p_n - \nu u_{s,s}]n_i + [\frac{p_s}{G} - u_{n,s}]s_i \tag{4.35}$$

where p_n and p_s denote the boundary tractions in normal and tangential directions respectively, E, G and ν are Young's modulus, shear modulus and Poisson's ratio respectively.

4.4 Stress Sensitivity Analysis by CA

4.4.1 A Simple Case

One of the most common constraints in shape optimization is the stress. For 2-D elastic problems, the maximum stress is often on the boundary, so the boundary stress sensitivity analysis is very important. In the following, the boundary stress sensitivity for a simple case is derived first, then the general formulation of stress sensitivity is developed next.

Consider a two dimensional elastic body with domain Ω and bounded by τ, $\tau = \tau_1 + \tau_2 + \tau_3 + \tau_c$, where τ_1 is the kinematically fixed boundary, τ_2 is the loading boundary, τ_c is a traction free straight boundary in which the stress constraint is required, and τ_3 is the traction free design boundary.

Consider an average stress constraint on τ_c defined as:

$$\phi = \frac{1}{l_c} \int_\tau m_c \sigma_t d\tau \tag{4.36}$$

where l_c is the length of the τ_c, m_c is a characteristic function which is one in τ_c and zero otherwise, σ_t is the Von Mises stress. For a traction free boundary, the Von Mises stress equals to the tangential stress, i.e. $\sigma_t = Du_{t,t}$, $u_{t,t}$ is the derivative of tangential displacement. $D = 2G/(1-\nu)$ for plane strain, G and ν are shear modulus and Poisson's ratio respectively.

Taking the material derivative of equation (4.36), and noting

$$\dot{\sigma}_t = \sigma'_t + \mathbf{V}^T \cdot \nabla \sigma_t \tag{4.37}$$

therefore

$$\phi' = \frac{1}{l_c} \int_\tau m_c \sigma'_t d\tau + \frac{1}{l_c} \int_\tau m_c \mathbf{V}^T \cdot \nabla \sigma d\tau \tag{4.38}$$

Because the partial derivative with respect to time can commutes with partial derivative with X, i.e.

$$\frac{\partial}{\partial t}\left(\frac{\partial u}{\partial x}\right) = \frac{\partial}{\partial x}\left(\frac{\partial u}{\partial t}\right) \tag{4.39}$$

so

$$\sigma'_t = D \frac{\partial}{\partial s}\left(\frac{\partial u}{\partial t}\right) \tag{4.40}$$

Due to the assumption that the constraint area l_c is fixed, the second term of equation (4.38) is zero, therefore

$$\phi' = \frac{1}{l_c} \int_\tau m_c D \frac{\partial}{\partial s}(u'_s) d\tau = \frac{D}{l_c}(u'_{s2} - u'_{s1}) \tag{4.41}$$

where u'_{s1} and u'_{s2} denote the material derivatives of displacements at the end of l_c in tangential directions.

Equation (4.41) shows that the material derivative of a stress function is related with the difference of the material derivatives of the tangential displacements, which is similar to the relation $\sigma = D\partial u/\partial s$.

By defining an adjoint problem, we can transform the partial derivative of the displacement by boundary information only. i.e.

$$u'_{s2} - u'_{s1} = -\int_{\tau_4} \sigma(u)\varepsilon(\lambda)V_n d\tau \tag{4.42}$$

finally:

$$\phi' = -\frac{D}{l_c} \int_{\tau_4} \sigma(u)\varepsilon(\lambda)V_n d\tau \tag{4.43}$$

The adjoint problem is governed by the following boundary conditions:

$$
\begin{aligned}
u &= 0 & &\text{on } \tau_1 \\
p &= 0 & &\text{on } \tau_2 \cup \tau_3 \\
p &= \delta(x - x_i) & &\text{on } \tau_c \quad i = 1,2
\end{aligned}
\tag{4.44}
$$

The only loads are two point loads acting at the end of τ_c along the tangential direction (opposite). Note that equation (4.42) does not include the ϕ_2 term of equation (4.30) in order to simplify the discussion. The numerical implementation of the stress sensitivity can be carried out in the same way as for displacement sensitivity discussed before, but the following points need special attention:

a) The adjoint loads are two point loads in opposite direction, which produce a stronger singular strain field near the loading area.

b) As the stress sensitivity is obtained by finite difference method, so the area l_c can not be too big in order to get accurate approximation. If l_c approaches to zero length, the sensitivity will present the sensitivity at a point.

c) The accuracy of the stress sensitivity will depend on both the initial problem and the adjoint problem. For a well posed initial problem, the solutions of the initial problem are usually accurate. As the adjoint problem involves singular loads, how to obtain good solutions of the adjoint problem is very crucial. The special techniques for dealing with the adjoint problem will be discussed in sections 4.5 and 4.6.

4.4.2 The Stress Sensitivity Formulation for the General Case

The formula (4.43) in last section is valid only for the constraint on flat undesigned boundary. In this section, a general formula is derived, which

takes account the following boundary conditions: a) all the boundary of the problem can be curved, b) the stress constraint is on the traction boundary, c) the kinematic boundary is fixed, d) no body force, e) the design boundary is traction free. The limitations of d) and e) can be left by modifying the ϕ_2 of equation (4.30).

Similar as last section, consider an average stress constraint on the boundary defined as:

$$\phi = \frac{1}{l_c} \int_\tau m_c f(\sigma) d\tau \qquad (4.45)$$

$f(\sigma)$ is a stress measure, such as the maximum stress or the Von Mises stress. For a general traction boundary, f can be expressed in terms of tangential stress σ_t, normal and tangential tractions p_n, p_s, i.e., $f = f(\sigma_t, p_n, p_s)$.

Taking the material derivative of the (4.45), we obtain

$$
\begin{aligned}
\dot{\phi} &= \frac{1}{l_c^2} \{ l_c \int_\tau m_c [\frac{\partial f}{\partial \sigma_t} \dot{\sigma}_t + \frac{\partial f}{\partial p_n} \dot{p}_n + \frac{\partial f}{\partial p_s} \dot{p}_s + f(V_n H + V_{s,s})] d\tau \\
&\quad - \int_\tau f m_c d\tau \cdot \int_\tau m_c (V_n H + V_{s,s}) d\tau \} \\
&= \frac{1}{l_c} \int_\tau m_c \{ \frac{\partial f}{\partial \sigma_t} \dot{\sigma}_t + \frac{\partial f}{\partial p_n} \dot{p}_n + \frac{\partial f}{\partial p_s} \dot{p}_s \} d\tau \\
&\quad + \int_\tau m_c (V_n H + V_{s,s}) \cdot (f - \phi) d\tau
\end{aligned}
\qquad (4.46)
$$

The variations of boundary tractions p_n and p_s can be computed once we know the nature of the loads. For example if a hydraulic load is applied on the constraint boundary, then $\dot{p}_s = 0$, and $\dot{p}_n$ is the pressure change due to the boundary variation. At present constant tractions for both normal and tangential directions are assumed, i.e. $\dot{p}_n = 0$, $\dot{p}_s = 0$.

For general curved boundaries, a convenient way to model the boundary is by the polar coordinates, thus the boundary tangential stress can be expressed as (for plane strain):

$$\sigma_t = D\varepsilon_\theta + \frac{\nu}{1-\nu} p_n = D(\frac{u_r}{r} + \frac{\partial u_s}{r\partial\theta}) + \frac{\nu}{1-\nu} p_n \qquad (4.47)$$

where u_r and u_s are normal and tangential displacements, p_n is the normal traction.

Taking material derivative of σ_t,

$$\begin{aligned}
\dot{\sigma}_t &= \sigma_t' + \sigma_{t,n} V_n + \sigma_{t,s} V_s \\
&= D[\frac{1}{r} u_r' + \frac{1}{r}\frac{\partial}{\partial\theta}(u_s')] \\
&\quad + DV_n\kappa[-\frac{u_r}{r^2} - \frac{1}{r^2}\frac{\partial u_s}{\partial\theta} + \frac{1}{r}\frac{\partial u_r}{\partial r} + \frac{1}{r}\frac{\partial^2 u_s}{\partial r\partial\theta}] \\
&\quad + \sigma_{t,n} V_n + \sigma_{t,s} V_s
\end{aligned} \tag{4.48}$$

In polar coordinates, we have the following relations (stress-strain):

$$\begin{aligned}
\frac{\partial u_r}{\partial r} &= \frac{1}{D}(p_n - \frac{\nu}{1-\nu}\sigma_t) \\
\frac{\partial u_s}{\partial r} &= \frac{p_s}{G} + \frac{u_s}{r} - \frac{\partial u_r}{r\partial\theta}
\end{aligned} \tag{4.49}$$

Substituting (4.48) into (4.46), and using (4.49), we obtain

$$\begin{aligned}
\dot{\phi} &= \frac{1}{l_c}\int_\tau m_c\frac{\partial f}{\partial\sigma_t}D[\frac{1}{r}u_r' + \frac{\partial u_s'}{r\partial\theta}]d\tau \\
&\quad + \frac{1}{l_c}\int_\tau m_c\frac{\partial f}{\partial\sigma_t}DV_n\kappa[-\frac{u_r}{r^2} + \frac{1}{rD}(p_n - \frac{\nu}{1-\nu}\sigma_t + \frac{2}{1-\nu}\frac{\partial p_s}{\partial\theta}) - \frac{1}{r^2}\frac{\partial^2 u_r}{\partial^2\theta}]d\tau \\
&\quad + \frac{1}{l_c}\int_\tau m_c\frac{\partial f}{\partial\sigma_t}[\sigma_{t,n}V_n + \sigma_{t,s}V_s]d\tau \\
&\quad + \frac{1}{l_c}\int_\tau m_c(V_n H + V_{s,s})(f - \phi)d\tau \\
&= \phi_a + \phi_b
\end{aligned} \tag{4.50}$$

where

$$\phi_a = \frac{1}{l_c}\int_\tau m_c\frac{\partial f}{\partial\sigma_t}D[\frac{1}{r}u_r' + \frac{\partial u_s'}{r\partial\theta}]d\tau$$

ϕ_b is the rest terms of equation (4.50), and $\kappa = 1$ if the boundary is convex, and equals -1 otherwise. Other notations are the same as before.

It can be seen from equation (4.50) that ϕ_b is the function of initial problem and design velocity only. Once the initial problem has been solved and the

design boundary perturbation is given, ϕ_b can be calculated directly. The contribution of ϕ_b comes from two parts: a) the movement of the constraint along space; b) the change of the constraint area. ϕ_b only appears if the constraint is on the design boundary, otherwise it equals to zero.

ϕ_a presents the stress change at the fixed area. Same as before, this can be obtained by defining an adjoint problem with displacement solution λ, then:

$$
\begin{aligned}
\phi_a &= \frac{1}{l_c}\int_\tau m_c D \frac{\partial f}{\partial \sigma_t}[\frac{1}{r}u_r' + \frac{\partial u_s'}{r\partial\theta}]d\tau \\
&= \frac{D}{l_c}\frac{\partial f}{\partial \sigma_t}\{[u_{s2}' - u_{s1}'] + \int_\tau \frac{m_c}{r}u_r' ds\} \\
&= -\frac{D}{l_c}\int_{\tau_d}\frac{\partial f}{\partial \sigma_t}\sigma(u)\varepsilon(\lambda)V_n d\tau
\end{aligned}
\tag{4.51}
$$

where τ_d denotes the design boundary. $\partial f/\partial \sigma_t$ has been assumed to be constant during the derivation.

The difference between the equation (4.51) and (4.43) is that there is one more term if the boundaries are curved. The extra term in equation (4.51) corresponds to the normal displacement sensitivity, therefore the adjoint loads include two parts: the first part is two point loads at the end of l_c along tangential opposite directions, and the second part is a uniform traction along normal direction with magnitude $1/r$. The combination of the total adjoint loads for curved boundaries is shown in Fig. 4.3(a). If the curvature of the loaded element is small, we can prove that the above adjoint loads will statically equal to the straight boundary case as shown in Fig. 4.3(b).

As can be seen from equations (4.50) and (4.51) that the material derivative is the function of the velocity field. As the velocity field is related with the changes of the design variables, the material derivative can be transformed into design sensitivity. Given a design perturbation δb, the design sensitivity of a stress constraint ϕ defined in (4.45) is

$$
\frac{d\phi}{db} = \lim_{\delta b \to 0}\frac{\dot{\phi}}{\delta b}
\tag{4.52}
$$

where $\dot{\phi}$ is the total material derivative.

The components of the velocity field V_n, V_s can be generally written as

$$V_n = f_n(\xi)\delta b$$

$$V_s = f_s(\xi)\delta b \tag{4.53}$$

where f_n and f_s are interpolation functions in normal and tangential directions respectively.

The physical meaning of f_i is the change of the design boundary in i direction due to the unit change of the design variable b. The form of f_i depends on the design boundary representation as well as the perturbation of the design variable.

By combining equations (4.50) and (4.51), and using (4.53), the design sensitivity of (4.52) is obtained as

$$
\begin{aligned}
\frac{d\phi}{db} = {} & -\frac{D}{l_c}\int_\tau \frac{\partial f}{\partial \sigma_t}\sigma(u)\varepsilon(\lambda)f_n d\tau \\
& + \frac{1}{l_c}\int_\tau m_c \frac{\partial f}{\partial \sigma_t}Df_n\kappa[-\frac{u_r}{r^2} + \frac{1}{rD}(p_n - \frac{\nu}{1-\nu}\sigma_t + \frac{2}{1-\nu}\frac{\partial p_s}{\partial \theta}) - \frac{1}{r^2}\frac{\partial^2 u_r}{\partial^2 \theta}]d\tau \\
& + \frac{1}{l_c}\int_\tau m_c \frac{\partial f}{\partial \sigma_t}[\sigma_{t,n}f_n + \sigma_{t,s}f_s]d\tau \\
& + \frac{1}{l_c}\int_\tau m_c(f_n H + f_{s,s})(f - \phi)d\tau
\end{aligned}
\tag{4.54}
$$

where

$$f_{n,s} = \frac{df_n}{ds}$$

$$f_{s,s} = \frac{df_s}{ds} \tag{4.55}$$

4.5 The Modelling of the Adjoint Problem

4.5.1 Numerical Approaches for Problems with singular Loads

One of the main concerns of the continuum method for design sensitivity analysis is the modelling of the adjoint problem because of the appearance of the singular adjoint loads. The contribution of the adjoint problem to design sensitivity formula can be written simply as

$$\dot{\phi}_a = C \int_{\tau_d} \sigma(u)\varepsilon(\lambda)V_n d\tau \qquad (4.56)$$

where C is a constant, $\sigma(u)$ and $\varepsilon(\lambda)$ are solutions of the initial problem and the adjoint problem respectively, V_n is the normal component of the velocity field, and τ_d is the design boundary.

There are two cases needed to be considered. The first case is that the adjoint loads are applied on the part of boundary which does not change shape, or inside the domain, then according to Saint Venant's principle, the unbounded strain field due to the adjoint loads is confined to a small local area, with regular strain field away from the adjoint loads (including the design boundary). Since the sensitivity analysis needs only the strain information on the design boundary as indicated by equation (4.56), the singular adjoint load will not significantly influence the distribution of the strain on the design boundary, therefore the adjoint loads can be implemented into BEM formulation directly as a body force.

The second case is when the adjoint loads are on the design boundary, in which the strain field is singular and causes problem in the formulation for sensitivity analysis. For a displacement sensitivity, the adjoint load is a unit load, therefore the strain near the load will behavior as $1/r$. Even though the use of quadratic element can not model the $1/r$ strain distribution exactly,

according to author's experience, the $\varepsilon(\lambda)$ in (4.56) can be approximated by a polynomial function. The reason for such approximation is mainly due to the facts that 1) $\varepsilon(\lambda)$ is singular at the loading point, but the final integral of (4.56) is finite since the singular term has different signs from the two sides, 2) the singular term $1/r$ dies down very quickly away from the loading point.

In the case of a stress constraint on the design boundary, the strain field becomes more singular with the order of $1/r^2$, the direct use of adjoint loads into BEM formulation will not provide satisfactory solutions. As will be shown in the examples later on, the direct implementation of two point loads in BEM formulation can only be used in a smooth boundary with uniform velocity and far away from any corners. So some treatments are required to deal with the adjoint problem for stress constraints. Four approaches have been considered in the research which are:

(1) Mesh refinement and special elements method (M1)

(2) Local singular function method (M2)

(3) Smooth load method (M3)

(4) Singularity subtraction method (M4)

In the following, each method will be discussed. The numerical procedures for M2, M3 and M4 are proposed, with full investigation of M3. The numerical implementation of M4 will be developed in section 4.6.

4.5.2 Mesh Refinement and Special Elements Methods

One common method to model singularities is to grade the mesh in the neighborhood of the singularity. The mesh refinement can minimize the area of local singularity, and can be used for weak singularity, or some corners in which the interest is the solutions away from the corners.

Another similar method is to introduce special elements such as the quarter

point elements so that the interpolation function presents some kind singularity. Both mesh refinement and special element methods can not be used to model arbitrary order singularity. As the number of constraints could be very large, so the most important feature required to formulate the adjoint problem is to keep the same mesh with the initial problem so that the factorized left hand matrix of initial problem can be used as discussed before. The mesh refinement and the special elements methods do not possess this feature, therefore they are not suitable for the modelling of the adjoint problem.

4.5.3 Local Singular Function Method

It is always possible to split the unknown displacement field into two parts near the singularity, i.e. $u = u_s + u_r$, where u_s is a singular field, and u_r is the regular field. If the analytical form of u_s can be found, then the unknown singular field u can be transformed into a unknown regular field u_r plus a known singular field u_s, such that the final system equation does not involve singular unknowns. It is called local singular function method if the splitting of displacement field is confined only locally. This approach have been used in FEM for solving crack problems [7].

This idea is used here to develop an algorithm for solving the adjoint problem by BEM, which is outlined as follows.

Consider an adjoint problem for a stress constraint on a boundary, so the adjoint loads will be two point loads on the boundary, with a small distance $2d$ between them. Fig. 4.4(a) shows an adjoint problem with domain Ω, and bounded by boundaries τ_1, and τ_2, where τ_1 is the kinematically fixed boundary, and adjoint loads are on the traction boundary τ_2. A^* is the center of the two unit loads. This adjoint problem can be split into two subproblems based on superposition as shown in Fig. 4.4(b) and 4.4(c). We denotes the adjoint problem of Fig. 4.4(a) as problem (a), the problems of Fig. 4.4(b) and Fig. 4.4(c) as problem (b) and problem (c) respectively.

Fig. 4.4(b) denotes the two point loads acting on the semi-infinite plane, and the corresponding displacements and tractions on boundary τ_1 and τ_2 are u and p respectively. The solution of the problem (b) can be easily obtained by differentiating the well known Mindlin's solutions of one point load, therefore the solutions of displacements and stresses of the problem (b) are known.

Fig. 4.4(c) presents the complementary problem (b) so that the sum of problem (b) and (c) satisfies the initial boundary conditions of the problem (a).

Such division provides us the following relation,

$$\text{solution (c)} = \text{solution (a)} - \text{solution (b)} \tag{4.57}$$

As far as the adjoint loads are not applied on the corners, the solution of problem (c) at neighborhood A^* should be regular, i.e. no singularity exists near A^*. Therefore we conclude that problem (a) and problem (b) should have the same singularity at the neighborhood of A^*. This conclusion provides such a construction of $u = u_s + u_r$ near point A^*, in which u is the singular unknown displacement field of the adjoint problem, u_s is the singular solutions of problem (b), and u_r is the remain regular solution of problem (c). This splitting process transforms the singular unknown displacement into a regular unknown displacement. In practice this splitting function could be confined in only one element where the adjoint loads are acting on the middle of the element.

Consider the adjoint loading on element k with length c, and the distance between the two point loads is 2d. The semi-infinite plate solution u_s in local coordinate ξ can be written as

$$u_s = -\frac{2}{\pi E} \log \left| \frac{\xi - A}{\xi + A} \right| \tag{4.58}$$

where

$$A = \frac{2d}{c} \tag{4.59}$$

Assuming the displacement at the load element k has the form $u_r + u_s$, with u_r having quadratic variation, i.e.

$$u = u_r + u_s = a_1\xi^2 + a_2\xi + a_3 - \frac{2}{\pi E} \log \left| \frac{\xi - A}{\xi + A} \right| \tag{4.60}$$

In order to keep the continuity with the adjacent elements, the following boundary conditions are used to obtain a_1, a_2 and a_3,

$$u_{\xi=-1} = u_1 \tag{4.61}$$

$$u_{\xi=0} = u_2 \tag{4.62}$$

$$u_{\xi=1} = u_3 \tag{4.63}$$

where u_1, u_2 and u_3 are nodal displacements.

Using boundary conditions (4.61)-(4.63), the equation (4.60) can be simplified as:

$$u = \sum_{i=1}^{3} \phi_i u_i + f(\xi, A) \tag{4.64}$$

where

$$f(\xi, A) = -\frac{2}{\pi E} [\log \left| \frac{1 + A}{1 - A} \right| \xi + \log \left| \frac{\xi - A}{\xi + A} \right|] \tag{4.65}$$

and ϕ_i are standard quadratic interpolation functions.

Note that the equation (4.65) is derived based on a flat boundary. Since the distance between the two point loads is very small, it can also be used approximately for curved boundaries.

Recall the boundary integral equation for node i,

$$c_i u_i + \sum_{j=1}^{n} \int_{\tau_j} p^* u \, d\tau = \sum_{j=1}^{n} \int_{\tau_j} u^* p \, d\tau \tag{4.66}$$

In the element k, $u = \sum \phi_m u_m + f_k(\xi, A)$, for any other elements f equals to zero, therefore we have

$$c_i u_i + \sum_{j=1}^{n} \int_{\tau_j} p^* \Phi^T d\tau U = \sum_{j=1} \int_{\tau_j} u^* \Phi^T d\tau P - \int_{\tau_k} p^* f_k(\xi, A) d\tau \qquad (4.67)$$

The final system equation in matrix form:

$$HU = GP + F \qquad (4.68)$$

where H,G are standard influence matrices,

U,P are boundary displacements and tractions respectively,

F denotes singular field term, $F_i = -\int_{\tau_k} p^* f_k(\xi, A) d\tau$.

The purpose to introduce $f_k(\xi, A)$ is to evaluate the displacement field analytically for the singular term. The solutions U of the equation (4.68) are boundary displacements except in element k, in which $u = u + f(\xi, A)$.

The difficulty related with the special shape function method is that the F in (4.68) includes high order singular integrands. For a straight boundary it is possible to compute this integral analytically. But for the general curved boundary, numerical integration is needed, therefore a proper technique for this singular integral should be used. This method has not been justified by numerical implementation, and further research is needed.

4.5.4 Smooth Loading Method

The aim to smooth the adjoint loads is to smooth the displacement field near the adjoint loads by introducing equivalent distributed loads. The equivalent loads should satisfy the following conditions.

1) Global equality

Global equality requires that statically the distributed loads should be equal to the adjoint loads both in magnitude, direction and position (center of

loads). This equality ensures that the equivalent loads have the same effects as the adjoint loads globally except the area near the loads. This is justified by Saint-Venant's.

2) Local equality

Local equality ensures that the local effects of the equivalent loads are the same as the point loads for the stress constraint. Because the adjoint loads are self-equilibrium on a small area, the strain is very small except near the loads. So it is important to evaluate the local distribution of strain accurately.

It is easier to choose the forms of loads which satisfy the global equality. The basic form of such loads are anti-symmetric distributed loads, with the center of loads coinciding with the point loads.

The requirement of local equality needs more attention. Consider a straight traction free boundary first. For quadratic element modelling, the displacements have quadratic variation in each element, the tangential stress is linear in each element. Consider a stress constraint as

$$\phi = \frac{1}{l_a} \int_{\tau_a} \sigma_s d\tau \tag{4.69}$$

here τ_a is part of the element k. As the stress is linear, the mean stress ϕ is equal to the middle point stress of the element. i.e.

$$\phi = \sigma_{sm} \tag{4.70}$$

so the stress sensitivity will be the middle point stress sensitivity of the element. The adjoint loads is shown in Fig. 4.5, where $l_a = 2a$

For a different distance a, according to the above observation, the stress sensitivity should be the same, i.e. representing the middle point stress sensitivity. By the superposition principle, the distributed loads also represents the mean stress sensitivity. So we get the following conclusion: For straight boundaries, any anti-symmetric distributed loads (including point loads) rep-

resent the adjoint loads of stress sensitivity, under the condition that loading area is small, usually within one element.

If the adjoint loads are on the curved boundary, there will be two sets of adjoint loads, one is the distributed load along normal direction, and another one is the two point loads along the tangential direction. Again the two point loads can be approximated with the same methods of straight boundary by distributed equivalent loads along the tangential direction.

The simplest distributed loads are triangle loads as shown in Fig. 4.6, which can be implemented into BEM directly as boundary traction. The distribution of the equivalent triangle loads can be calculated as following. Assuming the distributed load has the form $p = c\xi$, and the length of the element is l. In order to equivalent the distributed loads with the two point loads apart away with distance l, we have the following relation by static equivalency:

$$l \times 1 = \int_{-1}^{1} c\xi \frac{l}{2} \frac{l}{2} \xi d\xi \tag{4.71}$$

therefore

$$c = \frac{6}{l} \tag{4.72}$$

In order to further smooth the strain field, other smooth distributed loads can be chosen such as those shown in Fig. 4.7, in which the calculation of $\int u^* p d\tau$ can not be separated into $\int u^* \Phi d\tau P$. Since the distribution of p is known, the integral can be calculated directly as $\int u^* p d\tau$.

Since the adjoint loads for curved boundary can be approximated as two point loads as shown in Fig. 4.3(b), the distributed loads shown in Fig. 4.6 and Fig. 4.7 can also be employed as the adjoint loads for curved boundaries.

4.5.5   Singularity Subtraction Method

One attractive way to model the adjoint problem is to remove the singularity from the BEM equation, which is often referred as singularity subtraction method. This method has been used in many application, such as fracture mechanics [8, 9]. In the following, the basic procedure is given, the detailed development for solving the adjoint problem will be presented in the next section.

Recall the adjoint problem in matrix form:

$$\mathbf{HU} = \mathbf{GP} \tag{4.73}$$

As the adjoint loads are two point loads, so the displacement field near the adjoint loads will be singular. Assuming that the solutions of another elastic problem with the same singularity near the adjoint loads are known, noted as $\mathbf{U_s}$ and $\mathbf{P_s}$. So we have:

$$\mathbf{HU_s} = \mathbf{GP_s} \tag{4.74}$$

Subtract equation (4.73) by equation (4.74), we have

$$\mathbf{HU_r} = \mathbf{GP_r} \tag{4.75}$$

where $\mathbf{U_r} = \mathbf{U} - \mathbf{U_s}$ and $\mathbf{P_r} = \mathbf{P} - \mathbf{P_s}$.

As $\mathbf{U}$ and $\mathbf{U_s}$, $\mathbf{P}$ and $\mathbf{P_s}$ have the same singularity near the adjoint loads, therefore $\mathbf{U_r}$ and $\mathbf{P_r}$ will be regular. Since equation (4.75) involves only regular boundary conditions, it can be solved by standard BEM, and the final solutions of the adjoint problem can be obtained by adding the singular solution $\mathbf{U_s}$ and $\mathbf{P_s}$ to $\mathbf{U_r}$ and $\mathbf{P_r}$.

4.5.6 Concluding Remarks

Four approaches are investigated above for the modelling of the adjoint problem. Although the mesh refinement and special elements methods are simple in concept, the requirement for rearranging the initial mesh needs much high computation cost which makes it difficult to use in practice. All the other three methods have the same left hand side matrix with the initial problem, so the forward and back substitutions can be carried when solving the adjoint problem.

As the accuracy is concerned, the singularity subtraction method removes the singularity completely from the BEM equation, therefore better results can be expected. The smooth load method only smooth the singular field, whereas the local singular function method has the difficulty to calculate the singular integral $\mathbf{F}$ accurately.

The simplest method in term of implementation is the smooth load method in which the external load of the adjoint problem is a localized distributed load (often on one element only). The singularity subtraction method needs to compute the new regular boundary conditions ($\mathbf{U}_r$, $\mathbf{P}_r$), and the local singular function method requires the calculation of the term $\mathbf{F}$.

By considering both efficiency and the accuracy of the methods for the adjoint problem, the possible best methods are the smooth load method and the singularity subtraction method, in which the former has been fully studied above and the latter will be investigated next.

4.6 Implementation of the Singularity Subtraction Method

The singularity subtraction method (SSM) can remove the singularity completely from the BEM equation, so it is ideal for modelling the adjoint problem. In this approach the final solutions are obtained by the combination of two solutions - the regular solution and the singular solution, in which the singular solution is known analytically. This approach has been successfully applied to fracture mechanics by Aliabadi et al [8, 9], in which the exact form of the singular field is known for 2-D crack (Williams field).

The problem arises in finding a singular field with the same singularity as the adjoint problem in the vicinity of the adjoint loads. As discussed in the special shape function method, the solutions of two unit loads on the semi-infinite plane has the same singularity as the same loads acting on any smooth traction free boundary, thus they can be used as the singular field for subtraction. But as can be seen from Fig. 4.4, the relation of $\phi(a) = \phi(b) + \phi(c)$, where ϕ presents the solutions of the problem, was derived under the assumption that the domain is bounded by a closed convex boundary. This implies that no part of the domain will cross the horizontal line into the top half-plane. Fig. 4.8 shows an adjoint problem, in which part of the domain is on the other side, therefore the statement of $\phi(a) = \phi(b) + \phi(c)$ is not valid.

In order to apply SSM to arbitrary boundaries, it is necessary to built a singular field for the case of Fig. 4.8.

First, let's construct a field with two point loads acting on a semi-infinite plane. Since the analytical solutions of one point load on the semi-infinite plane are well known as the Mindlin's solutions, by differentiating the solutions along y direction, the fundamental solutions with two point loads can be found, which are given in appendix A.

Next, by using the mirror image, the above solutions can also be applied to the whole upper semi-infinite plane except the place where the two unit loads are applied (such as the case of Fig. 4.8). This can be explained as following.

Consider a domain Ω under a pair unit loads as shown in Fig. 4.9, $\Omega = \Omega_\infty + \Omega_1$, where Ω_∞ denotes the semi-infinite plane, and Ω_1 is a finite domain attached to Ω_∞. The mirror image of Ω_1 in the semi-infinite plane is denoted as Ω_2.

If the Ω_1 is removed from the Ω as shown in Fig. 4.10, then the remaining part Ω_∞ is a semi-infinite plane, so the solutions over this semi-infinite plane under the pair loads are known. These solutions are named as solutions A.

From the solutions A we can compute the displacements and tractions along the boundary of Ω_2, i.e.

$$t = t_2 \qquad u = u_2 \qquad \text{on} \quad \tau_2$$

$$t = t_{20} \qquad u = u_{20} \qquad \text{on} \quad \tau_0 \qquad (4.76)$$

where the tractions $t_i = \sigma_{ij} n_j$.

If the Ω_2 is taken from the half-plane Ω_∞, and the u_2, u_{20} or t_2, t_{20} are applied on the boundaries $\tau_2 + \tau_0$, the solutions for this boundary value problem will be exactly the same as the solutions A at domain Ω_2. Fig 4.11 shows a case where part of the boundary is subject to displacements, part to tractions. We call the solutions of Fig. 4.11 as solutions B. Obviously we have,

$$f_B(x) = f_A(x) \qquad\qquad x \in \Omega_2$$

where f_B and f_A denote the solutions B and solutions A respectively.

The elastic solutions in Ω_1 of Fig. 4.9 can be constructed as the mirror image of the solutions B, i.e. rotating the solutions B onto the domain Ω_1. The fundamental solutions for the domain Ω_1 then can be written as:

$$u_x^i = u_x$$

$$u_y^i = -u_y$$

$$\sigma_{xx}^i = \sigma_{xx}$$

$$\sigma_{yy}^i = \sigma_{yy}$$

$$\sigma_{xy}^i = -\sigma_{xy} \tag{4.77}$$

where i denotes the node in top half plane, u^i and σ^i are the displacement and stress fields in Ω_1, u and σ are the corresponding mirror image of node i in the lower half plane Ω_2, which can be obtained from the formulations of Appendix A. The boundary tractions in Ω_1 can be computed as $t_k = \sigma_{kj}^i n_j$.

The arguments for such a construction of the solutions in Ω_1 are based on the following considerations.

a) The tractions based on (4.77) along τ_0 is zero, also $u_x^i = u_x = 0$, which mean that both tractions and the displacements are continuous across the common boundary τ_0, so no discontinuity is involved in the domain Ω.

b) The Ω_2 under the boundary tractions t_2, t_{20} and displacements u_2, t_{20} forms an equilibrium state, therefore the domain Ω will still be in equilibrium.

The numerical implementation of the SSM is:

1. Form the governing equation of BEM for the adjoint problem:

$$\mathbf{HU = GP} \tag{4.78}$$

where $\mathbf{H}$,$\mathbf{G}$ are influence matrices, $\mathbf{U}$ and $\mathbf{P}$ are boundary displacements and tractions. Note the tractions are zero everywhere except two unit loads.

2. Define new boundary conditions as:

$$\mathbf{U}_r = \mathbf{U} - \mathbf{U}_s$$

$$\mathbf{P}_r = \mathbf{P} - \mathbf{P}_s \tag{4.79}$$

where $\mathbf{U}_s$ and $\mathbf{P}_s$ are the displacements and tractions given in the appendix A. If part of the boundary is on the top half plane, the equation (4.77) is used to compute the $\mathbf{U}_s$ and $\mathbf{P}_s$.

As discussed above, $\mathbf{P}$ and $\mathbf{P}_s$, $\mathbf{U}$ and $\mathbf{U}_s$ have the same singularity near the pair loads, the new variables $\mathbf{U}_r$ and $\mathbf{P}_r$ will be regular. Substituting equation (4.79) into (4.78), and noting that the $\mathbf{U}_s$ and $\mathbf{P}_s$ are the solutions of an equilibrium state, i.e. $\mathbf{HU}_s = \mathbf{GP}_s$, therefore:

$$\mathbf{HU}_r = \mathbf{GP}_r \qquad (4.80)$$

3. After solving the equation (4.80) for $\mathbf{U}_r$ and $\mathbf{P}_r$, the final solutions can be obtained by adding $\mathbf{U}_s$ and $\mathbf{P}_s$ to $\mathbf{U}_r$ and $\mathbf{P}_r$.

Unlike the point loads and element loads methods, the SSM totally removes the singularity from the BEM equation, therefore the final solutions can be expected to be more accurate, and the above procedure can be easily implemented. As we known the fundamental solutions of two point loads acting on the semi-infinite space, so this technique can be extended to three-dimensional problems.

4.7 A New Finite Difference Based Approach to Shape Design Sensitivity Analysis

Of the many approaches to design sensitivity analysis, the total finite difference method (simply noted as FDM), in which the design sensitivities are calculated by disturbing each design variable in turn, and using the finite difference formula to approximate the derivative of the constraints and the objective function, is simple in concept, and has been widely used in the past [10, 11]. However there are two serious drawbacks by using FDM; 1) the accuracy of

the design sensitivity often depends on the choice of the perturbation step, 2) the computational cost is usually higher [12].

A new finite difference based method is presented in this thesis, which overcomes the two drawbacks of FDM. By analyzing the perturbation procedure of FDM, the difference between the initial geometry and the perturbed geometry can be replaced by a perturbation load, which is a function of the stress field of the initial problem and the design boundary geometry. This new method, employing the finite difference concept and the perturbation load, will be referred as finite difference load method (FDLM).

4.7.1 A Simple Example

In order to explain the basic idea behind FDLM, a simple cantilever beam example is considered first. Fig. 4.12(a). shows a thin cantilever beam, in which the load is applied at the right end. As $l \gg b$, the beam theory can be used. The length of the beam l is chosen as the design variable, and the load is assumed to be constant during the design change.

Consider a constraint of bending moment at cross section C, with $x = \bar{x}$, thus the initial bending moment can be expressed as:

$$g(l) = M = p(l - \bar{x}) \qquad (4.81)$$

Differentiating $g(l)$ with respect the to design variable l, we obtain the design sensitivity analytically, i.e.

$$\frac{dg(l)}{dl} = p \qquad (4.82)$$

In what follows, we will use another approach to calculate the design sensitivity, i.e. using FDLM.

As the forces at any cross section of the initial beam contain two components, one is the vertical force p, another one is the bending moment M, where $M = p(l - x)$. If we cut the beam into two parts at cross section A, and apply the stresses at section A as boundary tractions, as shown in Fig. 4.12(b), where $M_a = p\delta l$ and $P_a = p$, then Fig. 4.12(a) and Fig. 4.12(b) produce the same structural responses (stress, bending moment etc.) for the remaining part of the beam, $0 \leq x \leq l - \delta l$. This means that the bending moment at C of the initial beam (Fig. 4.12(a)) has the same value of the bending moment of Fig. 4.12(b). According to the superposition principle, the loads of Fig. 4.12(b) can be separated as shown in Fig. 4.12(c) and Fig. 4.12(d), therefore the bending moment at cross section C can be expressed as

$$M = M_1 + M_2 \tag{4.83}$$

where M_1 is under the load P_a as shown in Fig. 4.12(c), and M_2 under the load M_a as shown in Fig. 4.12(d).

By definition, the design sensitivity is the change rate of g with respect to the design change. As the initial g equals to M, and the modified g after design perturbation $\delta(-l)$ is M_1, thus we have

$$\frac{dg(l)}{dl} = \lim_{\delta l \to 0} \frac{M_1 - M}{\delta(-l)} \tag{4.84}$$

where $-l$ indicates the negative change of the design variable l, which modifies the beam length from l to $l - \delta l$.

Substituting (4.83) into (4.84), we obtain

$$\frac{dg(l)}{dl} = \lim_{\delta l \to 0} \frac{M_2}{\delta l} \tag{4.85}$$

M_2 is the solution of the perturbed beam under load M_a (Fig. 4.12(d)), so $M_2 = M_a$. For a linear elastic structure, the structural response is proportional to the applied loads, so the solution $M_2/\delta l$ can be obtained by modifying the load M_a to $M_a/\delta l$. The modified load $M_a/\delta l$ is called the perturbation load

p^* in order to distinguish it with the 'adjoint load' in the continuum method, and the 'pseudo-load' in the semi-analytical finite difference method. Since $M_a = p\delta l$, the perturbation load $p^* = p$.

The solution for the perturbed beam under perturbation load p^* will give a bending moment p at cross section C, which is the same as the analytical solution by (4.82). This implies that the sensitivity of the bending moment at cross section C can be obtained by putting a perturbation load on the perturbed beam. As δl approaches zero, the perturbed beam approaches the initial beam, therefore we can apply the bending moment $p^* = p$ onto the initial beam. Fig. 4.12(e) shows the perturbation load on the initial geometry, which presents the design sensitivity respect to design variable l.

It can be clearly seen from this example that FDLM needs only the solutions of the initial structure under the perturbation loads p^*. As the sensitivity is obtained by applying the perturbation loads onto the initial structure as an extra load case, so there is neither perturbation step nor new perturbation geometry involved in the sensitivity calculation.

4.7.2 Derivation of the Finite Difference Load Method (FDLM)

Before the derivation of the finite difference load method (FDLM) for 2-D continuum structures, let us have a close look of the design boundary perturbation. Consider a smooth design boundary τ as shown in Fig. 4.13 In simplicity assuming only one design variable, the vector $\mathbf{r}$, controls the design boundary shape, with point a and b fixed.

Given an infinitely small design perturbation $\delta \mathbf{r}$, which will form a new boundary τ_1. As far as the boundary geometry is concerned, the tangential component of $\delta \mathbf{r}$ has no effect for the modification of the boundary geometry.

This indicates that only the normal component of the design perturbation $\delta\mathbf{r}$ is needed to specify the new design boundary.

The normal movement of the design boundary can be expressed as

$$V_n = f(\xi)\delta\mathbf{r}\cdot\mathbf{n} \qquad (4.86)$$

where V_n denotes the normal movement of the design boundary due to the perturbation of design variable $\mathbf{r}$, $\mathbf{n}$ is the outward normal vector, ξ presents the local coordinates. f is a shape function to interpolate the shape of the perturbation, with the values $f(a) = f(b) = 0$, $f(\mathbf{r}) = 1$. f can be any continuous functions, such as linear for the linear boundary representation, cubic for the cubic spline representation.

Now consider a general two dimensional structure as shown in Fig.4.14(a). The domain Ω are bounded by boundaries τ_1 and τ_2, where τ_1 is the kinematically fixed boundary, and τ_2 is the traction boundary. Part of boundary τ_2 is the design boundary, noted as τ_d, and the remaining part of the traction boundary is τ_t. The tractions on τ_t are $\mathbf{P}$, and tractions on τ_d have the components of T_s and T_n in tangential and normal directions. This initial boundary value problem is denoted as problem 1.

As the design boundary is controlled by the design variables, when disturbing one design variable $\mathbf{b}$ with δb, where $\delta b = |\delta\mathbf{b}|$, the design boundary will move from τ_d to τ_d'. The normal movement of the design boundary is

$$V_n(\xi) = f(\xi)\delta b n_b \qquad (4.87)$$

where n_b is the normal component of the unit vector $\delta\mathbf{b}/|\delta\mathbf{b}|$. V_n is the design boundary perturbation along normal direction, and f is the shape function for the design boundary representation.

Since V_n is very small, the stresses along contour τ_d' of the initial structure can be approximated as

$$\sigma_s^+ = \sigma_s + \frac{\partial\sigma_s}{\partial n^-}V_n$$

$$\sigma_n^+ = T_n + \frac{\partial \sigma_n}{\partial n^-} V_n$$

$$\sigma_{sn}^+ = T_s + \frac{\partial \sigma_{sn}}{\partial n^-} V_n \qquad (4.88)$$

where σ_s presents the tangential stress on the initial design boundary, σ_{ij}^+ is the stress along τ_d'. T_n and T_s are boundary tractions in normal and tangential directions respectively. V_n is the distance between τ_d and τ_d'. n^- presents the inward normal direction, as the stress does not exist outside the domain.

Cut the domain Ω along the boundary τ_d, and name the remaining domain as Ω_a bounded by $\tau_1 + \tau_t + \tau_d'$, which will be called the perturbed structure. If we apply boundary traction $\sigma_{ij}^+ n_j$ onto the boundary τ_d' of the perturbed structure, we have another boundary value problem, denoted as problem 2. Fig. 4.14(b) shows the problem 2, where p_s and p_n are the components of tractions $\sigma_{ij}^+ n_j$ along tangential and normal directions. It is obvious that the solutions of problem 1 are the same as the solutions of problem 2 for $x \in \Omega_a$.

The components p_n and p_s on the τ_d' can be obtained as follows

$$p_n = \sigma_s^+ \sin^2(\theta_n) + \sigma_n^+ \cos^2(\theta_n) + 2\sigma_{sn}^+ \sin(\theta_n) \cos(\theta_n)$$

$$p_s = \sigma_{sn}^+ (\cos^2 \theta_n - \sin^2 \theta_n) + (\sigma_s^+ - \sigma_n^+) \sin \theta_n \cos \theta_n \qquad (4.89)$$

and

$$\theta_n = \theta_n^2 - \theta_n^1 \qquad (4.90)$$

where θ_n^1 and θ_n^2 are the normal directions of boundary τ and τ' respectively.

Substituting (4.88) into (4.89), we obtain

$$p_n = \sigma_s \sin^2 \theta_n + T_n \cos^2 \theta_n + 2T_s \sin \theta_n \cos \theta_n$$
$$+ (\frac{\partial \sigma_s}{\partial n^-} \sin^2 \theta_n + \frac{\partial \sigma_n}{\partial n^-} \cos^2 \theta_n + 2\frac{\partial \sigma_{sn}}{\partial n^-} \sin \theta_n \cos \theta_n) V_n$$

$$p_s = (\sigma_s - T_n) \sin \theta_n \cos \theta_n - T_s(\sin^2 \theta_n - \cos^2 \theta_n)$$
$$+ [(\frac{\partial \sigma_s}{\partial n^-} - \frac{\partial \sigma_n}{\partial n^-}) \sin \theta_n \cos \theta_n - \frac{\partial \sigma_{sn}}{\partial n^-} (\sin^2 \theta_n - \cos^2 \theta_n)] V_n \quad (4.91)$$

The applied load T_n and T_s on the design boundary τ_d will change during the design boundary perturbation, i.e. $T_n \to T_n^a$, $T_s \to T_s^a$. Consider a structural response $g(x)$, $x \in \Omega_a$, the sensitivity due to the perturbation of design variable δb, by definition, can be written as:

$$\frac{dg}{db} = \lim_{\delta b \to 0} \frac{g_3 - g_1}{\delta b} \tag{4.92}$$

where g_1 is the response of the initial structure under loads $\mathbf{P}$, T_n and T_s. g_3 is the response of the perturbed structure under load $\mathbf{P}$, T_n^a and T_s^a, which is named as problem 3.

Because the solutions of problem 1 are the same as the solutions of the problem 2, so g_1 can be replaced by g_2, i.e. $g_2(x) = g_1(x)$, $x \in \Omega_a$. By examining equation (4.92), it is noted that the design sensitivity dg/db is the difference of solutions of problem 2 and problem 3, and divided by δb. The problem 2 and problem 3 have the same domain Ω_a, the same kinematical boundary, but with different loads, by using superposition principle and the property of elasticity (i.e. the structural response is proportional to the applied loads), we end up that the design sensitivity dg/db is the solution of the perturbed structure under certain loads, which are called perturbation loads.

The perturbation loads equal the differences of the tractions of problem 2 (i.e. $\mathbf{P}$, p_n and p_s) and problem 3 (i.e. $\mathbf{P}$, T_n^a and T_s^a), and divided by δb. As $\mathbf{P}$ is canceled out, so we have

$$
\begin{aligned}
p_n^* &= \lim_{\delta b \to 0} \frac{T_n^a - p_n}{\delta b} \\
p_s^* &= \lim_{\delta b \to 0} \frac{T_s^a - p_s}{\delta b}
\end{aligned}
\tag{4.93}
$$

where p_n^* and p_s^* are the normal and tangential components of the perturbation loads.

Noting the following approximation,

$$
\delta b \to 0 \implies
\begin{cases}
\theta_n \to 0 \\
\cos \theta_n \to 1 \\
\sin \theta_n \to 0
\end{cases}
\tag{4.94}
$$

Substitute (4.91) into (4.93). After lengthy algebra derivation, finally we have

$$
\begin{aligned}
p_n^* &= -\frac{\partial \sigma_n}{\partial n^-} f(\xi) n_b - 2T_s c_i + \frac{\partial T_n}{\partial b} \\
p_s^* &= -\frac{\partial \sigma_{sn}}{\partial n^-} f(\xi) n_b - (\sigma_s - T_n) c_i + \frac{\partial T_s}{\partial b}
\end{aligned}
\tag{4.95}
$$

where $\partial T_n / \partial b$ and $\partial T_s / \partial b$ is the change rate of the external load on the design boundary with respect to the design variable b, and $c_i = \sin \theta_n / \delta b$ which depends on the design boundary modelling.

It can be seen from the above procedure that once the perturbation loads are known, the design sensitivities can be obtained by solving the boundary value problem of the perturbed structure under perturbation load p^* as shown in Fig. 4.14(c). Since the limiting process $\delta b \to 0$ leads the perturbed structure approaching to the initial structure (i.e. $\Omega_a \to \Omega$), so the perturbation loads can be applied on the initial structure to calculate the design sensitivity. We name the problem of the initial structure under the perturbation loads as the perturbation problem, therefore the design sensitivities are the solutions of the perturbation problem.

4.7.3 Further Discussions of FDLM

The perturbation loads given by (4.95) are obtained assuming that V_n is positive moving towards the domain Ω (i.e. n^- direction). In order to keep the conventional notation that V_n is positive in n^+ direction, we can simply change the sign of p_n^* and p_s^* in (4.95). The geometry change from towards

the domain to outward the domain will also change the sign of c_i, $\partial T_n/\partial b$ and $\partial T_s/\partial b$, so (4.95) becomes,

$$p_n^* = \frac{\partial \sigma_n}{\partial n^-}f(\xi)n_b - 2T_s c_i + \frac{\partial T_n}{\partial b}$$

$$p_s^* = \frac{\partial \sigma_{sn}}{\partial n^-}f(\xi)n_b - (\sigma_s - T_n)c_i + \frac{\partial T_s}{\partial b} \tag{4.96}$$

where n^- denotes the normal towards domain. $f(\xi)$ is the shape function of the design perturbation, which is positive outward domain. Fig. 4.15 shows a case of design boundary perturbation, in which $f(a) = f(b) = 0$, $f(c) = 1$.

In order to clarify the meanings of c_i, n_b, $\partial T_s/\partial b$, $\partial T_n/\partial b$, an example of a concrete wall subject to water pressure shown in Fig. 4.16 is used for demonstration. The design boundary is ad, z is the angle of the slope ad, and the design variable is b. Given a design perturbation δb, we have

$$n_b = \sin(z)$$

$$c_i(x) = -\frac{1}{h}\sin^2(z)$$

$$f(x) = \frac{x}{h}\sin(z)$$

$$\frac{\partial T_s(x)}{\partial b} = 0$$

$$\frac{\partial T_n(x)}{\partial b} = \frac{x}{h}\sin^2(z)\cos(z) \tag{4.97}$$

It can be seen form (4.97) that n_b depends on the direction of δb only, $f(x)$ is the function of position x, and c_i, $\partial T_s/\partial b$, $\partial T_n/\partial b$ are functions of x, n_b and $f(x)$.

From (4.96), it is clear that we need to evaluate the derivatives of stresses σ_n and σ_{sn} along normal directions in order to obtain the perturbation loads. By considering the equilibrium equation of a small block along the boundary, these two terms can be obtained by boundary information only, which has been used in the continuum approach without proof. Since the polar coordinates are very convenient coordinates for general 2-D boundary modelling and include

the case of $X - Y$ coordinates, the polar coordinates will be used for the derivations of the derivatives. The detail derivation can be found in appendix B, and the results are given as following:

$$\frac{\partial \sigma_n}{\partial n^-} = k(\frac{\partial \sigma_{r\theta}}{r\partial \theta} + \frac{\sigma_r - \sigma_\theta}{r} + X_r)$$

$$\frac{\partial \sigma_{sn}}{\partial n^-} = k(\frac{\partial \sigma_\theta}{r\partial \theta} + \frac{2}{r}\sigma_{r\theta} + X_s) \qquad (4.98)$$

where $\sigma_{r\theta}$, σ_r and σ_θ are the tangential boundary traction, normal boundary traction and tangential stress respectively. $k = 1$ if r^+ is in the n^+ direction, otherwise $k = -1$. X_r and X_s are the components of the body force in radial and tangential direction respectively.

The solutions of the displacements and stresses of the perturbation problem present the displacement and stress sensitivities at a fixed point, i.e. $\partial u/\partial b$, $\partial \sigma/\partial b$. If the constraint is an integral at a fixed area,

$$g = \int_\tau h(\sigma, u)d\tau \qquad (4.99)$$

then the sensitivity can be written as

$$\frac{\partial g}{\partial b} = \int_\tau [\frac{\partial h}{\partial \sigma}\frac{\partial \sigma}{\partial b} + \frac{\partial h}{\partial u}\frac{\partial u}{\partial b}]d\tau \qquad (4.100)$$

where h is a general function of the displacement and the stress. $\partial u/\partial b$, $\partial \sigma/\partial b$ are the solutions from FDLM, $\partial g/\partial b$ denotes the design sensitivity at a fixed area.

The structural response $g(x)$ discussed above is in a fixed area. If the constraint is defined on the design boundary, the constraint area will move as the design boundary moves. For such case the design sensitivity obtained above can be modified by using the material derivative method.

According to the material derivative concept, the total change of a function g can be separated into two parts as stated in equation (4.50),

$$\frac{Dg}{Dt} = \delta g_t + \delta g_x \qquad (4.101)$$

where Dg/Dt presents the total change of the function g, δg_t is the change of g at a fixed area (the ϕ_a in equation (4.50)), i.e. $\delta g_t = g(x, t + \delta t) - g(x, t)$, δg_x presents the contribution due to the movement of the constraint area (ϕ_b of (4.50)), i.e. $\delta g_x = g(x + \delta x, t) - g(x, t)$.

Since the sensitivity is the change rate of g with respect to the design variable b, by dividing (4.101) by δb, and let $\delta b \to 0$, we obtain the design sensitivity

$$\frac{dg}{db} = \lim_{\delta b \to 0} \frac{1}{\delta b}(\delta g_t + \delta g_x) = \frac{\partial g_t}{\partial b} + \frac{\partial g_x}{\partial b} \qquad (4.102)$$

where dg/db is the final design sensitivity, $\partial g_t/\partial b$ is the design sensitivity at a fixed area which can be obtained from the solutions of FDLM. The second term is due to the movement of the constraint.

(4.102) is the general formulation for shape design sensitivity. The calculation for $\partial g_x/\partial b$ depends upon the type of constraints. If a constraint is defined at one point of the design boundary, then [13]

$$\delta g_x = g_{,s}V_s + g_{,n}V_n \qquad (4.103)$$

$g_{,s}$ and $g_{,n}$ present the gradients of g in tangential and normal directions respectively, V_s and V_n is the movement of the constraint along tangential and normal directions respectively.

Note $V_s = f(\xi)\delta b s_b$ and $V_n = f(\xi)\delta b n_b$, so

$$\frac{\partial g_x}{\partial b} = g_{,s}f(\xi)s_b + g_{,n}f(\xi)n_b \qquad (4.104)$$

where s_b and n_b are the components of unit vector $\delta \mathbf{b}/|b|$ in tangential and normal directions respectively.

For other case of g, the expressions of $\partial g_x/\partial b$ can be derived in a similar way.

The numerical implementation of the FDLM for design sensitivity calculation can be summarized as following:

1. Solve the initial problem under the applied loads.

2. Calculate the perturbation loads given by formula (4.96).

3. Apply the perturbation loads to the initial structure, and the design sensitivities can be obtained from the solutions of FDLM. The perturbation problem can be solved using the already factorized system equation of the initial problem.

4. If the constraint is on the design boundary, add $\partial g_x/\partial b$ to the above solutions.

4.7.4 Concluding Remarks

The FDLM formulation is based on the continuum model, no discretization approximations are involved during the derivation of the perturbation loads. As the perturbation loads of FDLM are acting on the initial geometry, thus the solution under this load can be solved efficiently by using already factorized matrices for the initial problem analysis. Subsequently it is very easy to implement using the existing analysis programs

Although the formula for perturbation loads has been derived for 2-D elastic problems, It can be easily extended to 3-D problems using the same concepts. FDLM can be coupled with either FEM or BEM for design sensitivity analysis.

4.8 Numerical Examples

As presented in previous sections that four different approaches have been developed to obtain stress sensitivity, which are:

1. the continuum method by applying point loads as the adjoint loads (PLM).

2. The continuum method by applying distributed element loads as the adjoint loads (ELM).

3. The continuum method by using singularity subtraction method for the adjoint problem (SSM).

4. The new finite difference load methods (FDLM).

In the following, four test examples are used to study the accuracy of these four methods. The influences of the mesh refinement are also investigated. The examples are:

1. A cantilever beam.

2. A circular plate under internal pressure.

3. A fillet.

4. An elastic ring under a concentrated load.

The stress constraint of these examples is the average stress over part of the boundary, i.e.

$$\phi = \frac{1}{l_c} \int_\tau m_c \sigma d\tau \qquad (4.105)$$

where l_c is the element length of the stress constraint.

In all the examples, continuous elements are used in BEM analysis, and the computations are carried out on a VAX 11/750 of C.M.I.

4.8.1   A Cantilever Beam

The first example is a cantilever beam as shown in Fig. 4.17. The dimensions of the beam are: b=2 and L=10. The material properties are: Young's modulus $E = 1.0 \times 10^7$, and Poisson's ratio $\nu = 0.3$. The loads are applied at the right end parabolically with p=4/3. The depth of the beam is chosen as the design variable. As this is a thin beam, so the beam theory can be used as the analytical solutions.

Let us first examine the stress sensitivities along the lower surface of the beam under a given mesh as shown in Fig. 4.18. The sensitivity results at fixed elements along the lower surface are listed in Table 4.1, and are plotted in Fig. 4.19., in which FDM is the finite difference results by disturbing the design variable by 0.01%. PLM, ELM, SSM and FDLM are sensitivities obtained numerically. The relative error is defined as:

$$\delta = |\frac{\sigma_{nu} - \sigma_{FDM}}{\sigma_{FDM}}| \qquad (4.106)$$

where σ_{nu} and σ_{FDM} are the numerical solutions and finite difference solutions respectively.

It can be seen from the results that all the four methods agree with the finite difference method well except at element 10, which is near the tip of the beam. ELM, SSM and FDLM give better results than PLM in general. The poor accuracy at element 10 may be due to the following reasons: a) the stress level at element 10 is very small; b) the stress sensitivity level of element 10 is also small; c) the influence of the corner which often causes poor BEM results. It is noted that the FDM results are nearly the same with the analytical solutions of beam theory (within 0.5%).

The mesh refinement method is used next to investigate the relationship between the stress sensitivity and the boundary mesh. The mesh arrangement is shown in Fig. 4.20, where N_1 denotes the element's number on the upper

surface and the bottom surface, and N_2 for the elements on the two ends. The design boundary is the top surface of the beam, and the design variable is the depth of the beam. The stress constraint is at the middle point A of the lower surface of the beam. A finite difference method with very fine mesh and 1×10^{-4} perturbation gives a stress sensitivity value of 10 at A, which will be served as the exact solution.

The numerical results are given in Table 4.2 and plotted in Fig. 4.21. The first column of the Table 4.2 is the boundary element mesh, column 2 and 3 are stresses by BEM and related error compared with beam theory solutions. The next 8 column are stress sensitivities and their relative errors compared with FDM solution at A (i.e. 10). From these results it can be observed that the accuracy of the stress obtained by BEM is higher than the stress sensitivity. This is probably because stress sensitivity is a function of stresses of the initial problem, therefore the stress sensitivity can not be expected to have better accuracy as stress itself.

As the number of elements are increased, the numerical sensitivities approach the exact solution. All the four methods provide good accuracy with a reasonable fine mesh. Again the accuracy of PLM is relatively poor than the others.

4.8.2   A Circular Plate Under Internal Pressure

The reason for choosing this problem is that we know the analytical solutions for both stresses and the stress sensitivities, which makes it possible to evaluate the exact errors of the numerical sensitivities.

Due to symmetry, only quarter of the ring is modelled as shown in Fig. 4.22. The design boundary is the outer ring surface, and the design variable is the outer ring radius b. As the analytical solutions for this problem are

available [14], we will use the analytical solutions to derive the perturbation loads for FDLM, and by solving the perturbation problem analytically, we can prove that the FDLM will give the exact solution.

The tangential and normal stresses of the out ring surface are:

$$\sigma_s = \frac{a^2}{b^2 - a^2}(1 + \frac{b^2}{r^2}) \qquad r = b$$

$$\sigma_n = 0 \qquad\qquad (4.107)$$

By using the formula (4.96), the perturbation loads on the outer ring surface can be obtained:

$$p_n^* = -\frac{2a^2}{b(b^2 - a^2)}$$

$$p_s^* = 0 \qquad\qquad (4.108)$$

The solutions for an elastic ring under external uniform load p^* can be obtained analytically, which are (for stresses) :

$$\sigma_s = -\frac{2ba^2}{(b^2 - a^2)^2}(1 + \frac{a^2}{r^2})$$

$$\sigma_n = -\frac{2ba^2}{(b^2 - a^2)^2}(1 - \frac{a^2}{r^2}) \qquad (4.109)$$

These solutions are the same the with the derivatives of the initial stress (4.107) with respect to the design variable b. Thus we proved that the solutions of FDLM are exact for this example.

Next, we will exam the accuracy of the stress sensitivity of PLM, ELM, SSM, and FDLM respectively with the mesh refinements. Note the perturbation loads for FDLM will be obtained numerically by using (4.96). The material properties are: $E = 1.0 \times 10^7$, and $\nu = 0.3$. N_1 and N_2 are the elements number, and the density of the pressure is 1. The radii are: a=4, b=6. The constraint is the point A on the inner ring surface.

In the same way as last example, the stress sensitivities obtained with different approaches and meshes are listed in Table 3 and plotted in Fig. 4.23. It can be observed that ELM, SSM and FDLM converge very fast, PLM also provides a good result with a fine mesh. Again as in the beam example, the error of the stress sensitivity is always greater than the error of the stress.

4.8.3   A Fillet Example

The dimensions and the boundary element modelling are shown in Fig. 4.24. Young's modulus and Poisson's ratio are 30.0×10^6 and 0.293 respectively. The external loads is 100, and 45 continuous quadratic elements are used for the analysis.

The design boundary τ is denoted by ab (from element 24 to element 33). The design boundary movement is given by $V_n = b \times \mathbf{c}$, where the vector $\mathbf{c} = [0, 1, 1, 1, 1, 1, 1, 1, 1, 0]$ as shown in Figure 4.25.

The stress sensitivity results for the design boundary elements are shown in Table 4.4, and plotted in Fig. 4.26. The finite difference (FDM) results are obtained by disturbing the design variable by 1×10^{-4}.

The agreements between FDM and PLM,ELM, SSM and FDLM are very good except for element 24, which is near the corner. The reason for the poor results on element 24 may be due to the fact that stresses are singular near the corner, so the evaluation for stress sensitivity by either FDM or other methods may not be reliable. The results indicate ELM, SSM, and FDLM give better results than PLM in general.

4.8.4   An Elastic Ring under a Concentrated Load

This example is used to demonstrate the accuracy of the various approaches for more complex example. The problem is shown in Fig. 4.27. Due to symmetry, only quarter of the ring is modelled as shown in Fig. 4.28. The design boundary is the outer ring surface, and the constraints are the inner ring surface stresses. 32 quadratic elements are used, $N_1 = 10$, $N_2 = 6$. The material properties are: $E = 1.0 \times 10^7$, $\nu = 0.3$, and the geometry data are: a=1.5, b=2.25.

A uniform velocity field is assumed first, i.e. $V_n = 1$, The stress sensitivities at each element of the inner ring are listed in Table 4.5, and plotted in Fig. 4.29. The finite different results (FDM) are obtained by disturbing the outer ring surface with $\delta = 1 \times 10^{-4}$. As can be seen from the results that all the numerical methods provide excellent agreements with finite difference results, whereas the PLM gives relatively poor results especially near the corners.

Another velocity field is used next to check the influence of the velocity field, with $V_n = b * sin(2x)$, where b is the design variable, and x is the angle as shown in Fig. 4.28. The sensitivity results are listed in Table 4.6. Generally the results are not as accurate as in uniform velocity case, but the agreements are still good. The worst results by PLM appear near the corners, which may be due to the fact that the BEM solutions by using point load is approximately correct only in the sense of integral, not the distribution. When this integral is multiplied by a nonlinear velocity field, the results become worse.

It should be mentioned here that the c_i term in equation (4.96) is zero for the uniform velocity case, but it is non-zero for the $sin(2x)$ velocity in which $c_i = -2/r \times cos(2x)$.

4.9   Concluding Remarks

Based on the theoretical consideration discussed in this chapter, and the justification of the numerical examples presented in last section, we conclude the following observations on the accuracy and the limitations of the four numerical methods for design sensitivity analysis.

1. The four methods are developed base on 2-D elastic problem, but all of them can be extended to 3-D problem with the same procedure.

2. The accuracy of the stress sensitivity is better in the case of smooth design boundary than the non-smooth boundary, and poor accuracy occurs when the constraint is near a corner.

3. In general, ELM, SSM and FDLM give better results than PLM.

4. The sensitivity results can be deteriorate when the constraint is on an area with small stress and stress sensitivity.

5. The accuracy of stress sensitivity usually are not as good as stress itself.

6. The stress and the displacement constraints using FDLM can be on either a traction boundary or a kinematical boundary, whereas the continuum approaches (PLM, ELM and SSM) are developed for the traction boundary only. The extension of the continuum approaches to kinematical boundary is straightforward in concept, but further research is needed to investigate the numerical accuracy.

Element's No.	1	2	3	4	5
σ	-19.44	-17.29	-15.33	-13.18	-11.14
FDM	29.71	26.62	23.31	20.14	16.98
PLM	28.03	24.35	21.56	18.67	15.77
$\delta\%$	5.6	8.5	7.5	7.3	7.1
ELM	29.59	25.29	22.46	19.46	16.45
$\delta\%$	4.4	5.0	3.6	3.4	3.1
SSM	29.00	26.07	22.85	19.74	16.65
$\delta\%$	2.4	2.1	2.0	2.0	1.9
FDLM	29.18	25.96	22.87	19.80	16.74
$\delta\%$	1.8	2.5	1.9	1.7	1.4
Element's No.	6	7	8	9	10
σ	-9.10	-7.07	-5.44	-3.02	-1.01
FDM	13.85	10.74	7.65	4.57	1.53
PLM	12.85	9.89	6.84	3.46	-1.31
$\delta\%$	7.2	7.9	10.6	24.2	*
ELM	13.44	10.42	7.38	4.24	6.96
$\delta\%$	3.0	3.0	3.5	7.2	354.9
SSM	13.58	10.51	7.45	4.53	4.55
$\delta\%$	1.9	2.1	2.6	0.9	197.7
FDLM	13.68	10.64	7.59	4.56	1.86
$\delta\%$	1.2	0.9	0.8	0.2	21.5

Table 4.1 Low Surface Stress Sensitivities of the Beam

* indicates the numerical results having the opposite sign compared with the FDM method.

Mesh	Stress	δ	PLM	δ	ELM	δ	SSM	δ	FDLM	δ
$n_1 \times n_2$	σ	%	σ'_p	%	σ'_e	%	σ'_s	%	σ'_f	%
3×1	-9.864	1.4	9.147	8.5	9.456	5.4	13.839	38.4	9.471	5.3
5×1	-10.085	0.9	8.728	12.7	9.695	3.1	10.420	4.2	10.231	2.3
7×2	-10.134	1.3	9.048	9.5	9.834	1.7	9.745	2.6	10.308	3.1
9×2	-10.076	0.8	9.215	7.9	9.837	1.6	10.065	0.7	10.189	1.9
11×3	-10.072	0.7	9.377	6.2	9.887	1.1	10.069	0.7	10.183	1.8
Exact	-10.000		10.000							

Table 4.2 Stress Sensitivity of the Cantilever Beam

Mesh	Stress	δ	PLM	δ	ELM	δ	SSM	δ	FDLM	δ
$n_1 \times n_2$	σ	%	σ'_p	%	σ'_e	%	σ'_s	%	σ_f	%
1×1	2.587	0.5	-0.686	28.5	-0.768	20.0	-0.761	20.7	-0.510	46.9
3×1	2.601	0.1	-0.910	5.2	-0.98	2.1	-0.931	3.0	-0.930	3.0
5×2	2.600	0.0	-0.927	3.4	-0.950	1.0	-0.957	0.3	-0.960	0.0
7×3	2.600	0.0	-0.936	2.5	-0.953	0.7	-0.960	0.0	-0.960	0.0
11×3	2.600	0.0	-0.941	2.0	-0.955	0.5	-0.960	0.0	-0.960	0.0
Exact	2.600		-0.960							

Table 4.3 Stress Sensitivity of the Circular Plate

Element	24	25	26	27	28
σ	150.0	88.8	70.9	59.7	50.7
FDM	-103.80	-134.40	-44.78	-27.77	-20.64
$PLM\ \sigma_p'$	-83.25	-115.36	-46.56	-28.71	-21.15
$\delta\%$	19.0	13.9	4.0	3.4	2.5
$ELM\ \sigma_e'\ \%$	-96.42	-128.96	-44.97	-27.95	-20.77
$\delta\%$	6.4	3.8	0.4	0.6	0.6
$SSM\ \sigma_s'$	-214.13	-116.52	-46.89	-28.73	-21.15
$\delta\%$	108.0	13.0	4.7	3.4	2.5
$FDLM\ \sigma_f'$	-113.01	-120.10	-43.52	-27.68	-20.59
$\delta\%$	9.7	10.6	2.8	0.3	0.2
	29	30	31	32	33
σ	42.9	35.7	28.3	20.2	9.4
FDM	-17.24	-15.79	-16.00	-22.58	6.29
$PLM\ \sigma_p'$	-17.44	-15.73	-15.55	-18.94	1.67
$\delta\%$	1.2	0.4	2.8	16.1	73.44
$ELM\ \sigma_e'$	-17.30	-15.79	-15.88	-22.11	2.77
δ	0.3	0.0	0.8	2.1	55.96
$SSM\ \sigma_s'$	-17.44	-15.73	-15.63	-19.25	-6.17
$\delta\%$	1.2	0.4	2.3	14.7	*
$FDLM\ \sigma_f'$	-17.22	-15.80	-15.88	-23.02	4.57
$\delta\%$	0.1	0.1	0.8	1.9	27.3

Table 4.4 Stress Sensitivity of the Fillet Example

Element's No.	1	2	3	4	5
σ	135.5	92.2	51.6	16.3	-15.2
FDM	-285.34	-211.11	-126.87	-51.97	15.63
PLM	-313.79	-214.04	-129.99	-54.82	13.04
$\delta\%$	10.0	1.4	2.4	5.5	16.5
ELM	-281.70	-212.09	-128.25	-52.68	15.56
$\delta\%$	1.3	0.5	1.1	1.4	0.5
SSM	-289.96	-211.12	-126.09	-51.04	16.64
$\delta\%$	1.6	0.5	0.6	1.8	6.4
FDLM	-287.29	-212.81	-127.91	-52.48	15.59
$\delta\%$	0.7	0.8	0.8	1.0	0.3
Element's No.	6	7	8	9	10
σ	-42.68	-65.51	-83.16	-95.17	-101.26
FDM	75.07	124.59	163.04	189.28	202.78
PLM	73.02	123.74	164.60	197.13	253.04
$\delta\%$	2.7	0.7	1.0	4.1	24.8
ELM	75.64	125.90	165.18	192.76	198.61
$\delta\%$	0.8	1.0	1.3	1.8	2.1
SSM	76.11	125.67	164.10	190.70	206.13
$\delta \%$	1.4	0.9	0.7	0.8	1.7
FDLM	75.51	125.53	164.29	190.89	204.80
$\delta\%$	0.6	0.8	0.8	0.8	1.0

Table 4.5 Stress Sensitivities of the Elastic Ring

Element's No.	1	2	3	4	5
σ	135.5	92.2	51.6	16.3	-15.2
FDM	-60.42	-87.74	-93.73	-62.73	-9.30
PLM	-81.20	-89.14	-90.79	-60.47	-10.00
$\delta\%$	34.4	1.6	3.1	3.6	7.5
ELM	-58.70	-88.93	-94.05	-62.97	-10.03
$\delta\%$	2.9	1.4	0.4	0.4	7.8
SSM	-61.34	-89.25	-95.14	-63.68	-9.72
$\delta\%$	1.5	1.7	1.5	1.5	4.5
FDLM	-59.46	-86.97	-93.12	-62.33	-9.18
$\delta\%$	1.6	0.9	0.7	0.6	1.3
Element's No.	6	7	8	9	10
σ	-42.68	-65.51	-83.16	-95.17	-101.26
FDM	44.98	81.63	89.95	69.81	41.50
PLM	41.36	76.92	86.96	72.88	65.95
$\delta\%$	8.0	5.8	3.3	4.4	59.0
ELM	43.77	80.52	89.51	70.97	39.65
$\delta\%$	2.7	1.4	0.5	1.7	4.5
SSM	44.59	81.61	90.21	70.30	42.56
$\delta\ \%$	0.9	0.1	0.3	0.7	2.6
FDLM	44.81	81.31	89.35	69.07	40.80
$\delta\%$	0.4	0.4	0.7	1.1	1.7

Table 4.6 Stress Sensitivities of the Elastic Ring

(under $V_n = sin(2x)b$)

4.10 References

[1] Kane, J. H., Optimization of Continuum Structures Using a Boundary Element Formulation, PhD Thesis, The University of Missouri, Columbia, 1986.

[2] Saisal, S., Aithal, R., Kane, J. H., Semianalytical Sensitivity Formulation in Boundary Elements, AIAA Journal, Vol. 27, No. 11, 1989, pp. 1615-1621.

[3] Haug, E. J., Choi, K. K., Komkov, V., Design Sensitivity analysis of structural Systems, Academic Press, New York, 1985.

[4] Choi, J. H., Kwak, B. M., Boundary Integral Equation Method for Shape Optimization of Elastic Structures, Int. J. Numer. Meth. Engng., 26, 1988, pp. 1579-1595.

[5] Dems, K., Mroz, Z., Variational Approach by Means of Adjoint System to Structural Optimization and Sensitivity Analysis, int. J. Solids Structures, 19, pp. 677-692, 1983. 20, pp. 527-552, 1984.

[6] Malvern, L. E., Introduction to the Mechanics of a Continuous Medium, Prentice-Hall, New Jersey, 1969.

[7] Benzley, S. E., Representation of Singularities with Isoparametric Finite Elements, Int. Numer. Meth. Engng., Vol. 8, 1974, pp. 537-545.

[8] Aliabadi, M. H., An Enhanced Boundary Element Method for Determining Fracture Parameters, Proc. 4th Conf. Numer. Meth. in Fracture Mechanics, Texas, 1987, pp.27-39.

[9] Portela, A., Aliabadi, M. H., Rooke, D. P., Boundary Element Analysis of V-Notched Plates, Conf. of 4th BEM, 1989, pp. 147-156.

[10] Wang, S. Y., Sun, Y., Gallagher, R. H., Sensitivity Analysis in Shape Optimization of Continuum Structures, Comput. Struct., 20, 1985.

[11] Haftka, R. T., Malkus, D. S., Calculation of Sensitivity Derivatives in Thermal Problems by Finite Differences, Int. Numer. Meth. Engng., 17, 1981, pp. 1811-1821.

[12] Camarda, C. J., Adelman, H. M., Static and Dynamic Structural Sensitivity Derivative Calculations in the Finite Element Based Engineering Analysis Language (EAL) System, NASA TM-85743, 1984.

[13] Zhao, Z. Y., Adey, R. A., Shape Optimization Using the Boundary Element Method, Computer Aided Optimum Design: Recent Advance, CMP and Springer-Verlag, Southampton, 1989.

[14] Timoshenko, S. P., Goodier, J. N., Theory of Elasticity, McGraw Hill, 1982.

[15] Jaswon, M. A., City University, London, Personal Communication.
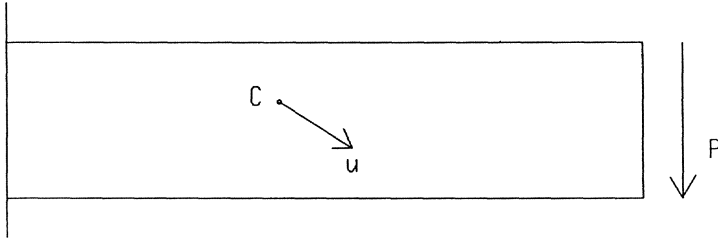
Fig. 4.1(a) The Initial Problem of the Beam
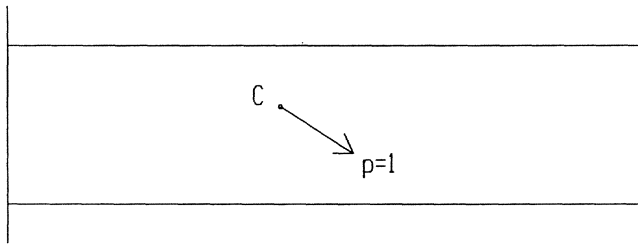
Fig. 4.1(b) The Adjoint Problem for Displacement Sensitivity
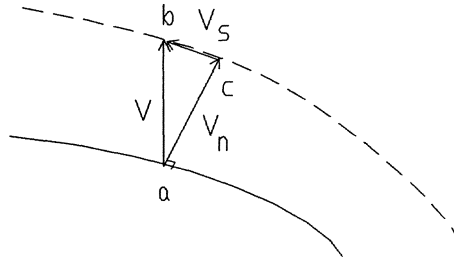
Fig. 4.2 Velocity Field on the Design Boundary
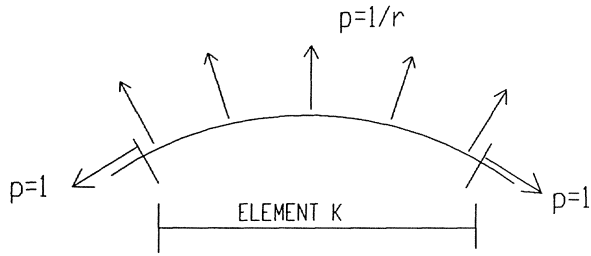
Fig. 4.3(a) Adjoint Loads on Curved Boundaries
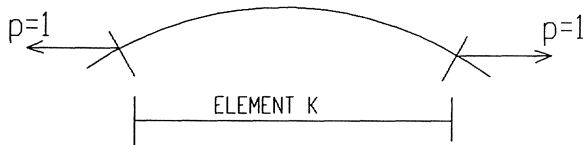
Fig. 4.3(b) Equivalent Adjoint Loads
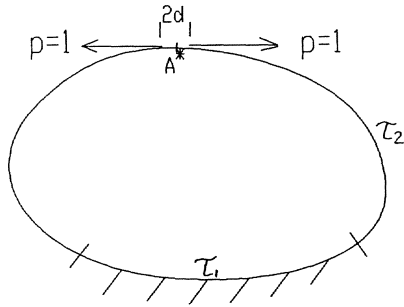
Fig. 4.4(a) The Initial Problem
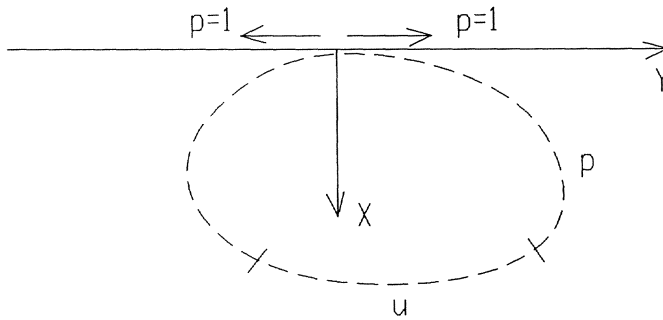
Fig. 4.4(b) Semi-Infinite Plane Solutions
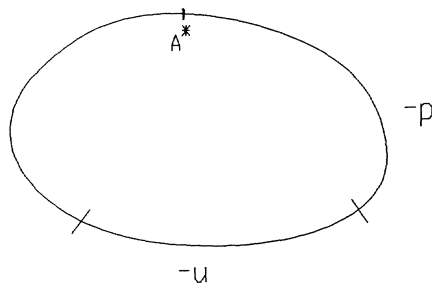
Fig. 4.4(c) Regular Field Problem
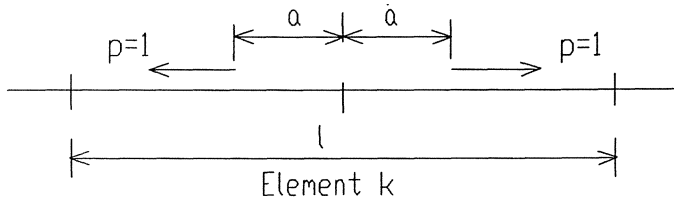
Fig. 4.5 Point Adjoint Loads
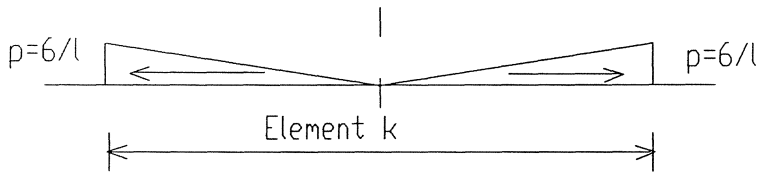
Fig. 4.6 Distributed Adjoint Loads
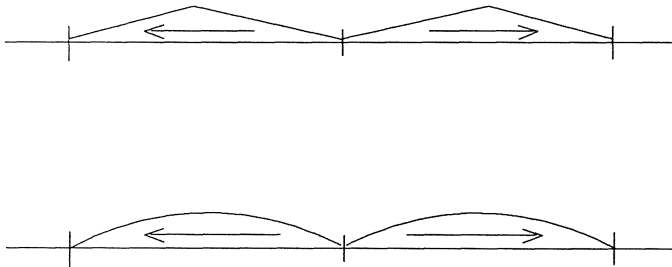
Fig. 4.7 Smooth Distributed Loads
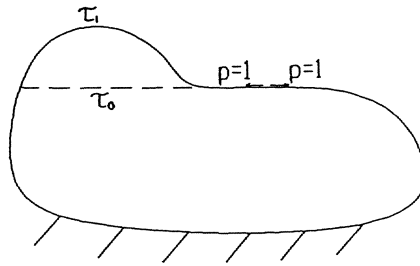
Fig. 4.8 An Adjoint Problem
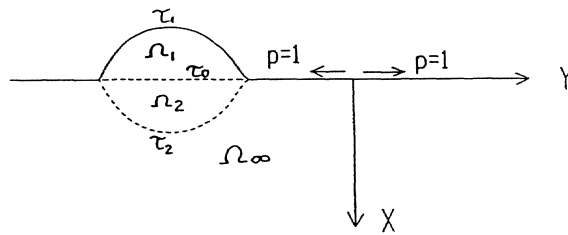
Fig. 4.9 A Semi-Infinite Plane with an Extra Part
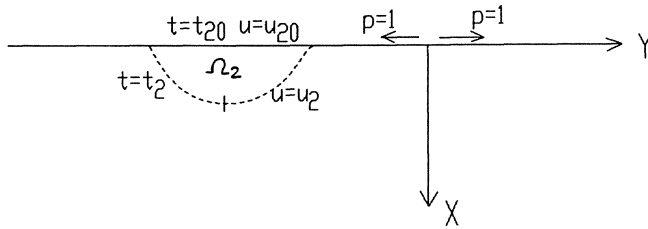
Fig. 4.10 The Semi-Infinite Plane
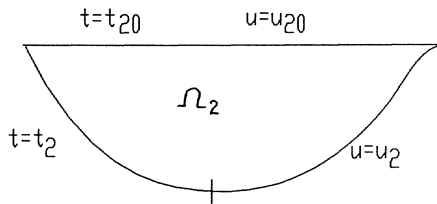
Fig. 4.11 An Equilibrium State
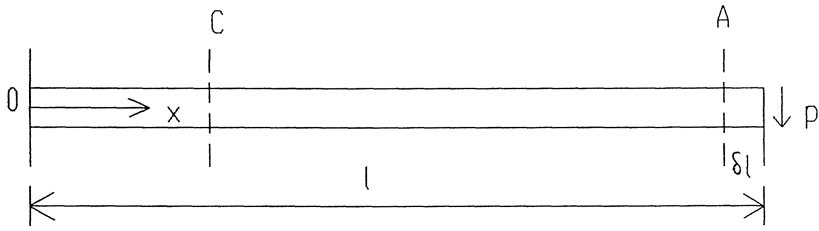
4.12(a)
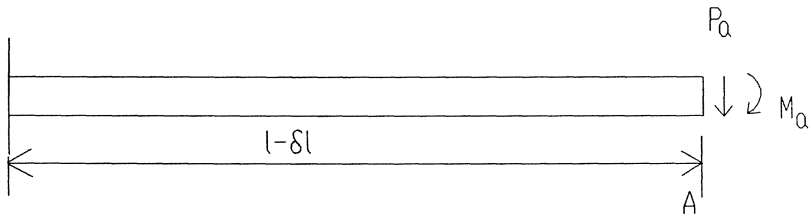
4.12(b)
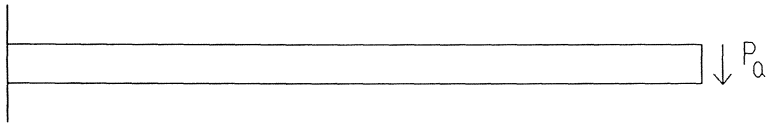
4.12(c)
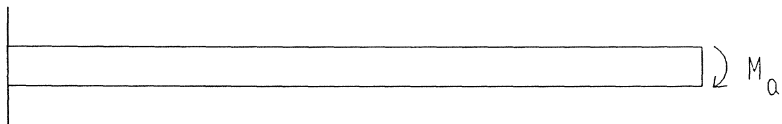
4.12(d)
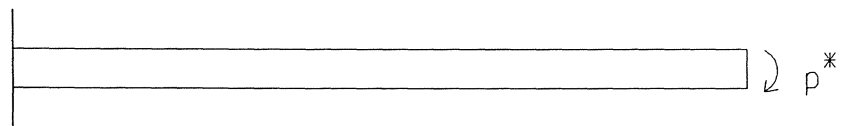
4.12(e)

Fig. 4.12 A Thin Cantilever Beam
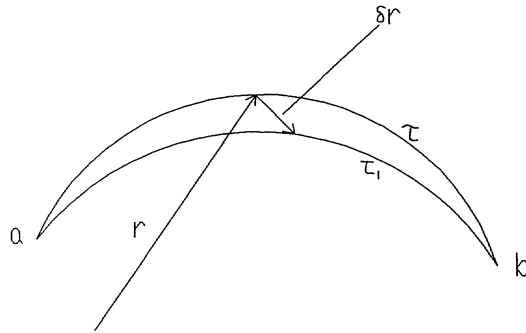
Fig. 4.13 Design Boundary Perturbation
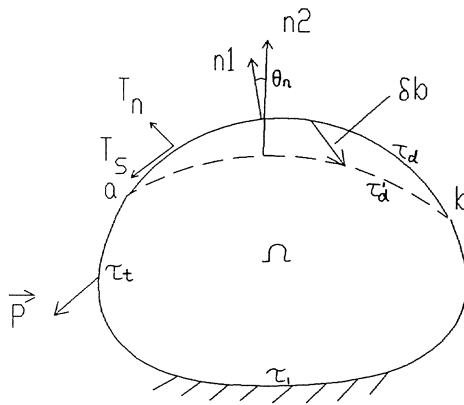
Fig. 4.14(a) Problem 1
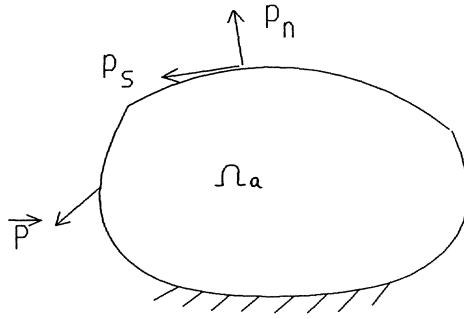
Fig. 4.14(b) Problem 2
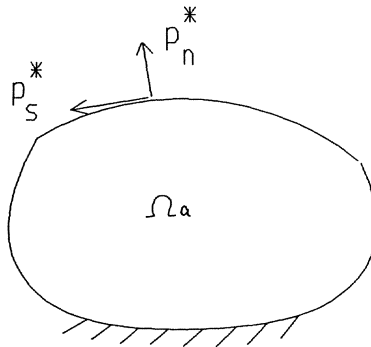
Fig. 4.14(c) The Perturbation Loads
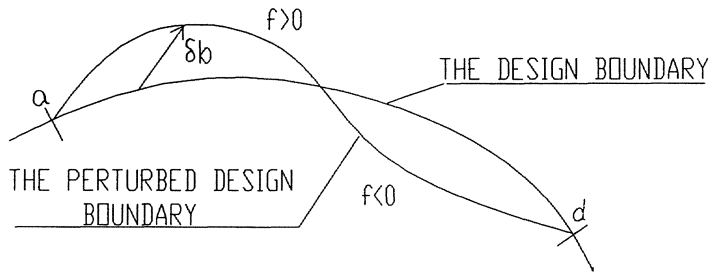
Fig. 4.15 The Definition of Function f
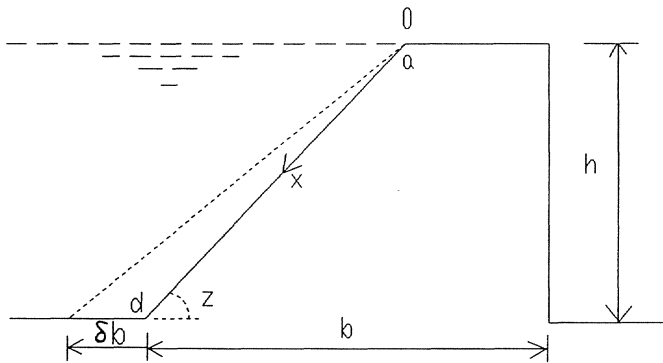
Fig. 4.16 An Explanation Example
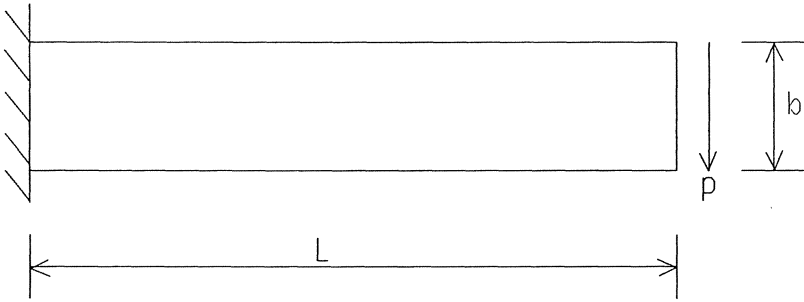
Fig. 4.17 A Cantilever Beam
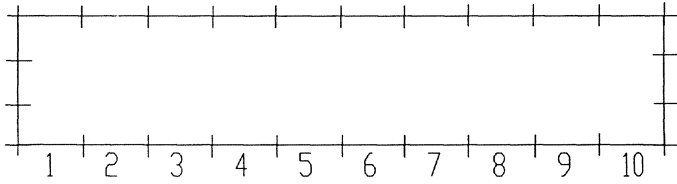
Fig. 4.18 Boundary Modelling

ww
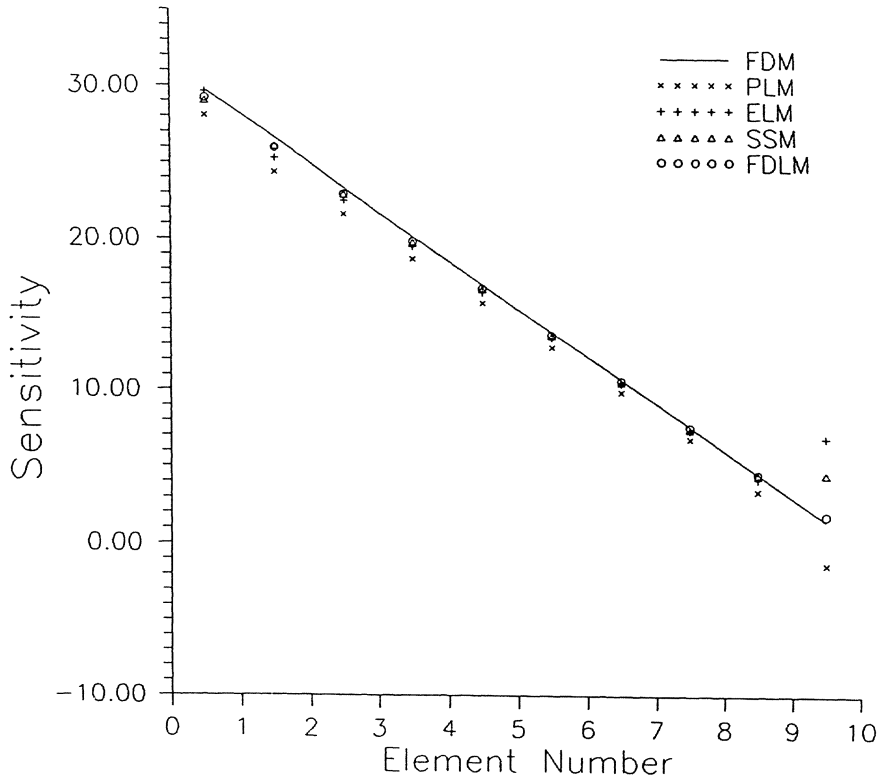
Fig. 4.19 Design Sensitivities of the Lower Surface of the Beam
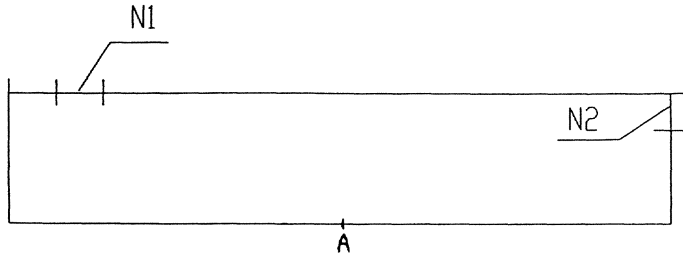
Fig. 4.20 The Arrangement of the Meshes
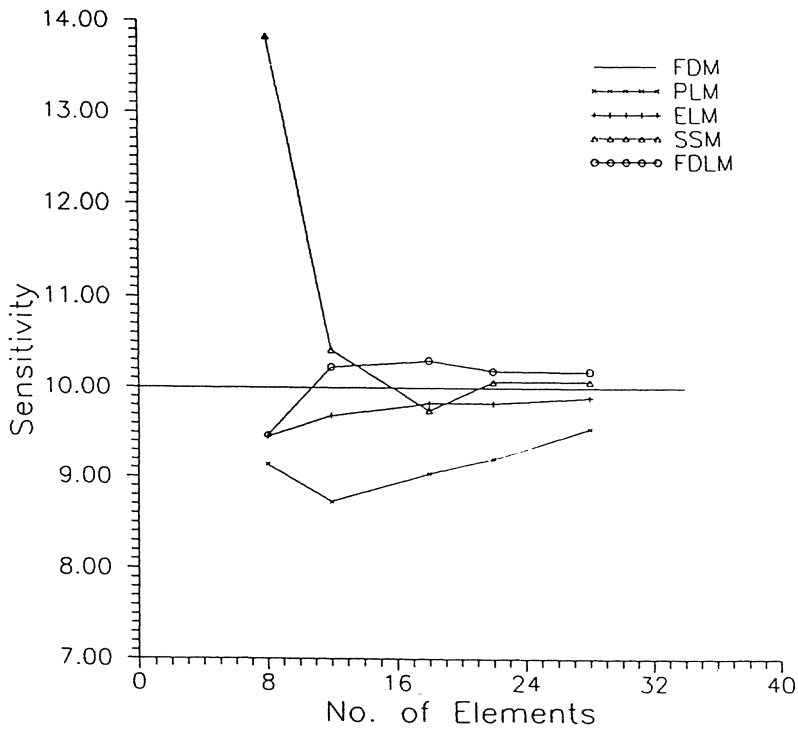
Fig. 4.21 Design Sensitivities of the Beam With Mesh
Refinement
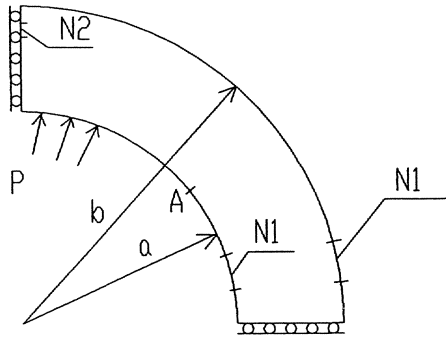
Fig. 4.22 A Circular Plate Example
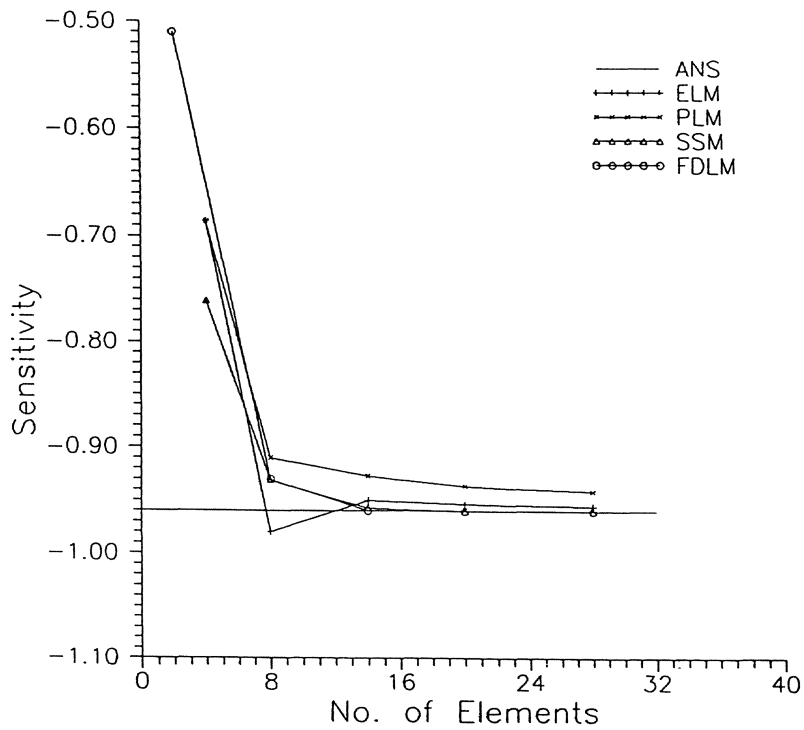
Fig. 4.23 Design Sensitivities of the Circular Plate
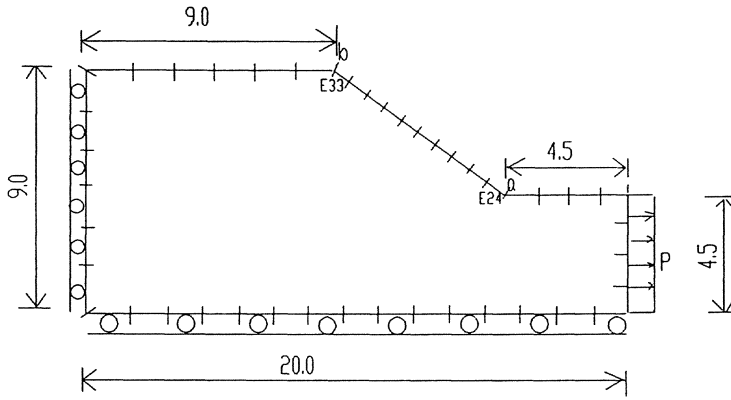
Fig. 4.24 Fillet Example
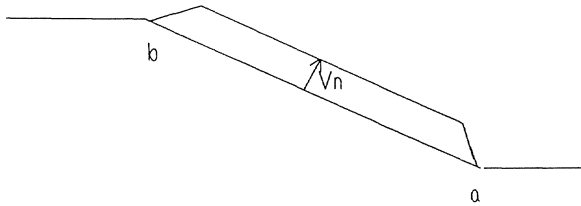
Fig. 4.25 Design Boundary Perturbation
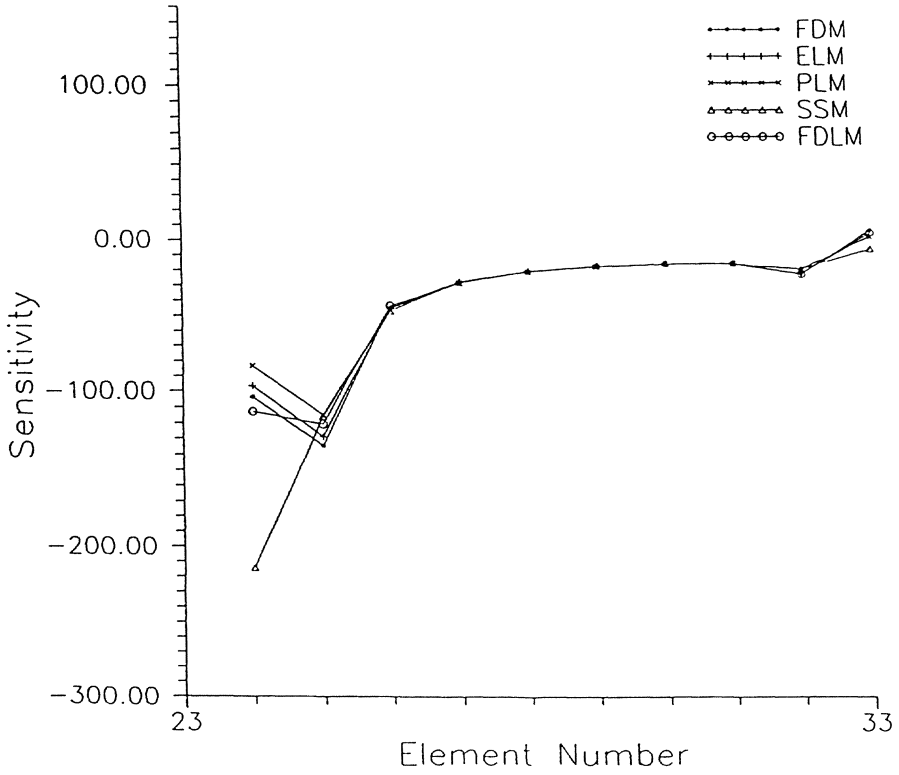
Fig. 4.26 Design Sensitivities of the Fillet
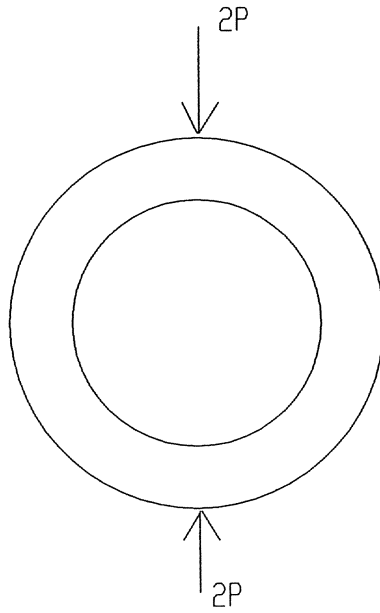
Fig. 4.27 An Elastic Ring Example
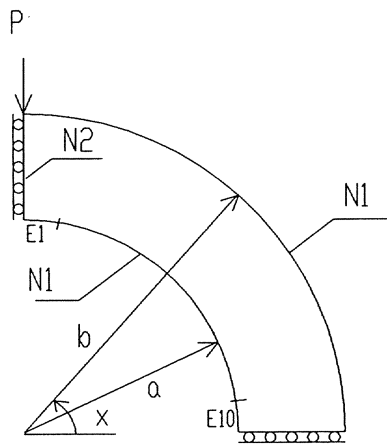
Fig. 4.28 BEM Modelling
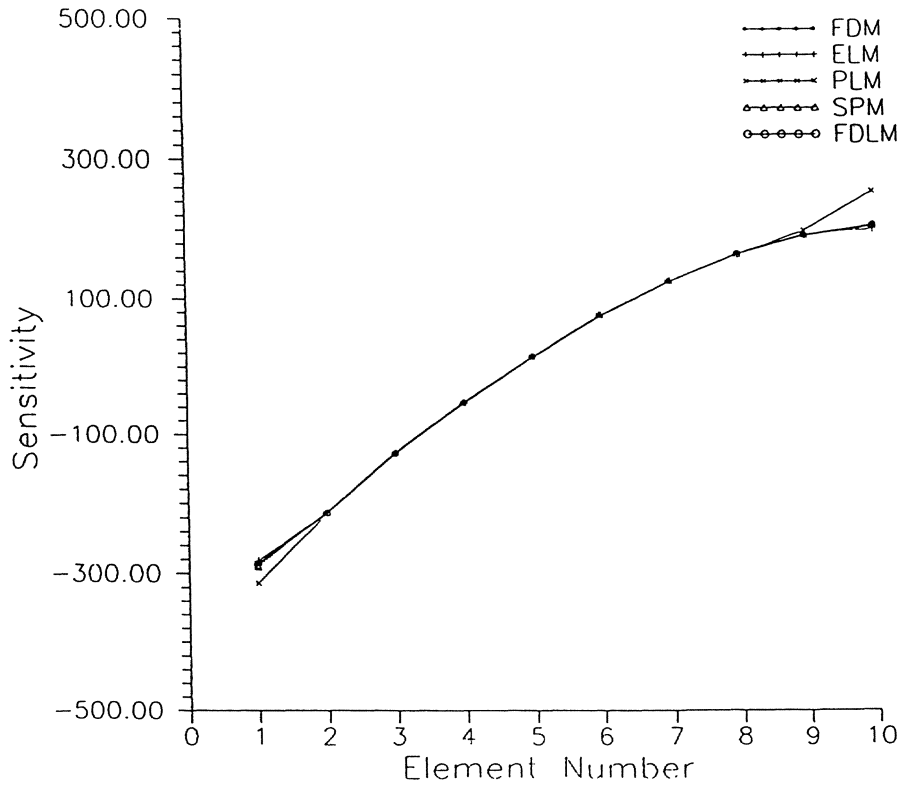
Fig. 4.29 Design Sensitivities of the Elastic Ring

Chapter 5

Shape Optimization Using the Boundary Element Method

5.1 Introduction

In the previous chapters, different elements of shape optimization are discussed, including mathematical programming methods, the boundary element method and shape design sensitivity analysis. An integrated shape optimization system contains a number of subproblems which must be treated properly in order to obtain a satisfied optimum design. The five main subproblems of a shape optimization system are described as following:

1) Structural Analysis

Structural analysis provides the response of a structure under certain loads. The responses, e.g. displacements and stresses, are used to measure the structural performance, and used in optimization for the evaluations of objective function, constraints, and design sensitivities, so an accurate structural analysis package is very important in shape optimization system.

2) Optimum Problem Formulation

Transforming an engineering design into an optimization problem needs both experience of the engineering design as well as numerical shape optimization techniques in order to select the design variables, the objective function, and the constraints. For example, we want to design an elastic component with the minimum cost for the production and the minimum stress concentration. The designer may choose either a multiple objective formulation where both the cost and the stress concentration are to be minimized, or to choose the cost as the objective whereas the maximum stress concentration as a constraint. When considering the cost of production, he should take into account both the cost of the material and the manufacturing cost (labours and machines). The different choice of the objective function, the design variables and the constraints will influence the use of the optimization algorithms.

3) Design Sensitivity Analysis

Design sensitivity analyses provide the gradients of the objective function and constraints with respect to the design variables. The capability to obtain the design sensitivity in an accurate and efficient manner is essential for all shape optimization system.

4) Optimization Algorithms

Various mathematical programming techniques have been developed to solve numerical optimization problems. Unfortunately there does not exist a universal algorithm which works well for all problems, this is because that the convergence and the efficiency of a particular algorithm is dependent on the problem to be solved. A general shape optimization system should contain wide range of algorithms so that users can have many choices according to their problems.

5) Design Modeling

As shape optimization is an iterative process, each iteration will form a new boundary. The task for design boundary representation, the boundary node relocation, the adaptive remeshing, and the error estimation, all have a strong influence on the final design.

In addition to the five basic elements, an advanced shape optimization system should also include many other facilities, such as interactive computer graphics for pre- and post-processing and intermediate result displays, expert system to provide a design data base etc.

The five basic elements mentioned above are connected to each other as a whole to form a shape optimization system. During shape optimization, any one element fails to perform properly, the whole system could collapse. Therefore a throughout understanding of each element and careful implementation are crucial for a shape optimization system. Element 1,3 and 4 have been discussed in chapter 2, 4 and 3 respectively. In the remaining sections of this chapter, we will discuss some issues of the design modelling and numerical implementation of shape optimization system, and present some numerical examples to justify those discussions and observations.

5.2   The Design Model and the Analysis Model

In a shape optimization system, there exist two distinct models: the design model and the analysis model. The design model is used to describe the geometry of a design, in which the design boundary is controlled by the design variables, whereas the analysis model is employed for the numerical analysis. Generally speaking, the design model is created first which has few master control points, and the analysis model is imposed on the design model which usually has many more nodes where the geometry is defined. Fig. 5.1 shows a fillet example with 5 design variables located on the design boundary ab. Fig.

5.1(a) is a design model, and Fig. 5.1(b) is an analysis model. It should be noted that both the design model and the analysis model are the approximation of the geometry of the real problem.

5.2.1   The Design Model

The main concern of the design modelling is: How to choose the design variables, or in other word how to model the design boundary.

One simple choice of the design variables is to select all the nodes of the analysis model on the design boundary as design variables. However this will often yield huge number of design variables, and the continuity between elements can not be guaranteed.

The most widely used method for design variables is to choose some master nodes. By defining a few master nodes (also called key nodes, control nodes) as the design variables, the design boundary can be represented as some kinds of fitting of these master nodes. Various fitting techniques have been used in the literature, such as polynomial representation [1, 2, 3], cubic spline [4, 5, 6], Bezier and B-spline [10]

The main advantage of spline fitting over the polynomial fitting is that high order polynomial is not stable, and can result in oscillatory design boundary, whereas a spline is composed by low order polynomial with continuity between adjacent pieces. Fig. 5.2 shows an example of the same master nodes with different fitting methods. It can be seen that different fitting will produce different curve, and the cubic spline and B-spline have a better smoothness than the polynomial forms.

Another way to model the design boundary is to use the concepts of design elements. This method basically subdivides the boundary into a number of de-

sign elements, with each element controlled by one to a few design parameters (design variables). The further details can be found in reference [7, 8, 9]

The choice of the design variables also depends on the nature of the geometry of the design boundary. For example if the design boundary is a circle, and the design requires the shape of the design boundary remaining as a circle, then the obvious choices of the design variables are the position of the center point of the circle and the radius of the circle.

5.2.2   The Analysis Model - Remeshing Problem

The structural response can be solved by numerical analysis method, such as FEM and BEM. One special problem occurs for shape optimization problem due to the modification of the design boundary, therefore it is necessary to either relocate the nodes or totally regenerate the mesh on the design boundary. One main advantage of BEM over FEM in shape optimization problem is the attractive feature of BEM in which there is no need for domain remeshing.

Even though boundary element discretization is relatively easier than FEM, it still needs an automatic mesh generator to prevent mesh distortion and odd distribution. Various error indicators and refinement methods have been developed for BEM which have been proved to have better accuracy and efficiency than FEM [11, 12, 13]

As the shape optimization system involves many iterations, so the minimum refinements of the mesh at each iteration can save a lot computing cost. For some problems, it will be not necessary for the adaptive mesh if we can put the first mesh right. A simple scheme is proposed for the mesh generation as follows:

Step 0 A new design boundary is obtained at iteration i.

Step 1 The first mesh on the design boundary will be generated based on the following three criteria.

1. The element length is proportional to $1/k$, where k is the curvature of the boundary. Since large k will usually produce high stress variation, therefore this will put more elements near big stress variation.

2. The maximum ratio of two adjacent elements should within recommended range, expressed as $1/c \leq l_i/l_{i+1} \leq c$, c can be taken as 3 for smooth boundaries, 2 for corners. This is used to assure the H and G matrix having a good conditions.

3. The maximum length of the elements should not be bigger than the maximum length in the previous iteration to prevent too coarse mesh.

Step 2 Carry out the structural analysis based on the mesh given by step 1.

Step 3 Two basic checks after the analysis of step 2.

1. Global equilibrium, i.e.

$$R_1 = \int_\tau t_i d\tau + \int_\Omega b_i d\Omega \tag{5.1}$$

where t_i and b_i are boundary traction and body force respectively, and R_1 is the residual. R_1 is mainly from the discretization error when the prescribed boundary conditions are displacements, in which the distribution of the unknown tractions are approximated by the interpolation functions.

2. Strain Compatibility at the common nodes which belong to two adjacent elements,

$$R_2 = |\varepsilon_1 - \varepsilon_2| \tag{5.2}$$

where ε_1 and ε_2 are the strain measure at the common node i from two different elements 1 and 2 as shown in Fig. 5.3, and R_2 is the difference of these two measure. R_2 presents the discontinuity of the strain.

If either R_1 or R_2 is greater than the specified value, then a mesh refinement is needed. Go back to step 2 after the mesh refinement. Continue this process until both R_1 and R_2 satisfy the conditions.

The mesh refinements can be carried out by two ways, the h method and the p method. The h method refines the mesh by decreasing the mesh size h, and keeps the order p of the piecewise polynomials fixed. In the p method, the mesh size h is fixed, and the order p of the polynomials is increased. Both methods and their combinations ($h - p$ method) have been widely used in BEM.

The first generated mesh by step 2 provides an easier and efficient method, which, in many 2-D cases, will create a well distributed mesh with no further adaptive mesh needed. Fig. 5.4 shows an application of such mesh generator, Fig. 5.4(a) represents the final mesh of a circle at the iteration i, and Fig. 5.4(b) represents the first new mesh at iteration $i + 1$. It can be seen that the new mesh is well distributed.

5.3 Shape Optimization Implementation

5.3.1 Introduction

The structure design is usually carried out by 'trial and error' method, which can be illustrated by Fig. 5.5. Starting with an initial design, the structural responses of the design can be evaluated by structural analysis such as FEM and BEM. If the analysis results do not satisfy the criteria set by engineers, then a new design will be proposed, which in many ways depends on the designer's experience and intuition. After remodelling the design, the structural analysis will be carried out again. Repeating this process until the analysis results satisfy all the criteria.

The analysis itself gives no indication of how to improve the design, especially for a complex structure with multiple load cases. Thus it is very difficult for designers to modify the current designs manually.

Optimal structural design, on the other hand, takes into account these criteria in a systematical way so that the modified design will move toward the optimal design. Fig. 5.6 shows a typical shape optimization system, which contains the 5 basic elements discussed in 5.1.

The optimal design starts the optimization formulation, in which the design criteria are implemented into the optimization formulation in terms of objective function, constraints and the design variables. After the structural analysis, an improved design will be obtained by minimizing the objective, and keeping constraints to be satisfied. If the new design satisfies the convergence test, then the possible 'best design' is obtained. Otherwise the new design will be remeshed, and repeat the loop starting structural analysis until the satisfied design is obtained. As the whole design loop is done by computer, with the designer's interface, the design process will be more economical and reliable compared with the manual design.

5.3.2   SOP - A Shape Optimization Program

A shape optimization program - SOP (Shape Optimization Program) has been developed for research purpose by the author. The computer code in Fortran includes one main program SOP, and five main Subroutines SOP1 - SOP5, which is used for 2-D elastic optimum structure design. The flow diagram of SOP is shown in Fig. 5.7. In what follows we will describe the functions of the main subroutines, and discuss some numerical considerations during implementation.

SOP - The main program

The functions of SOP are to call other subroutines, and to control the overall flow of the program.

SOP1 - Input data of BEM and optimization parameters

The optimization parameters contains: number of design variables, number of constrains, the objective function, and the initial parameters for optimizer ADS.

SOP2 - Boundary element analysis

This subroutine solves the 2-D elastic problem using quadratic boundary elements. The element types can be either continuous or discontinuous, as shown in Fig. 5.8.

In addition to the normal boundary conditions (tractions and displacements), SOP2 can also handle the point loads. The point loads are treated as body forces, and the system equation can be written as

$$\mathbf{HU} = \mathbf{GP} + \mathbf{B} \tag{5.3}$$

where $\mathbf{H}$ $\mathbf{G}$ are influence matrices, and $\mathbf{U}$ and $\mathbf{P}$ are vectors of displacements and tractions respectively. The body force term $\mathbf{B}$ with point loads b_1, b_2, ... and b_n can be obtained as:

$$B_i = \sum_j^n \int_{\Omega \to 0} b_j u^* d\Omega = \sum_j^n b_j u^*(P_j, Q_i) \tag{5.4}$$

where $u^*(P, Q)$ denotes the fundamental solutions with source point at j, and the integration point at i.

The LU decomposition method is employed to solve the BEM equation. The procedure of LU decomposition is as following, which is mainly from [14].

Consider a linear equation,

$$\mathbf{AX} = \mathbf{F} \tag{5.5}$$

The matrix **A** can be decomposed as a product of two matrices, i.e.

$$\mathbf{A} = \mathbf{LU} \tag{5.6}$$

where **L** is the lower triangular, and **U** is upper triangular, therefore,

$$\mathbf{AX} = \mathbf{L(UX)} = \mathbf{LY} = \mathbf{F} \tag{5.7}$$

and

$$\mathbf{UX} = \mathbf{Y} \tag{5.8}$$

As **L** is triangular, so the equation 5.7 can be solved for **Y** by simple forward substitution. After **Y** is known, the real unknown **X** can be obtained by solving equation 5.8, in which the back substitution will take place.

The advantage of splitting one linear system equation into two successive ones is that it is more efficient to solve linear equation with different right hand **F**. After decomposition **A** into **LU**, the solutions for any right hand **F** can be obtained by one forward substitution and one back substitution. This feature will be useful for solving adjoint problems during sensitivity analysis, in which each adjoint load will be treated as one extra load case.

SOP3 - Sensitivity analysis

The continuum method using the adjoint loads is used for sensitivity analysis. The adjoint load for displacement sensitivity is a point load (treated as body force), and the adjoint loads for stress sensitivity are the triangular element loads. The adjoint problems will be solved by using the already factorized **LU** method as discussed in SOP2.

SOP4 - Optimizer ADS

ADS is a general purpose numerical optimization programming containing a wide variety of algorithms, which have been widely used in optimization system [15]. Numerous options are provided by ADS for solving both unconstrained

functions and constrained functions. ADS is called by the main program SOP as a subroutine.

SOP5 - Mesh Generator

A simple mesh generator for design boundary modelling is implemented according to the step 2 of 5.2.3. Two types of design boundary representations are used, one is the linear boundary representation, and the other is the cubic spline representation.

The linear representation links the master nodes by straight lines. Fig. 5.9 shows an example of design boundary ab controlled by n master nodes b_1, b_2, ... , b_n. In the case of the design variables b_i presenting the y coordinates of the boundary ab, and x_i is the x coordinate of b_i, then the design boundary can be expressed as,

$$f(x) = \frac{x^{i+1} - x}{x^{i+1} - x^i}b_{i+1} + \frac{x - x^i}{x^{i+1} - x^i}b_i \quad , x^i \le x \le x^{i+1} \tag{5.9}$$

The variation of the design boundary is,

$$\delta f(x) = \frac{x^{i+1} - x}{x^{i+1} - x^i}\delta b_{i+1} + \frac{x - x^i}{x^{i+1} - x^i}\delta b_i \tag{5.10}$$

δf will be used to calculate the velocities in normal and tangential directions (i.e. V_n and V_s).

A cubic spline is constructed by piece-wise third-order polynomials arranged such that adjacent elements are forced to join together with continuous first and second derivatives. Therefore cubic splines do not have the wiggle problem associated with high-order polynomials [16].

Consider n master nodes with coordinates (x^1, y^1), (x^2, y^2), ..., (x^n, y^n) as shown in Fig. 5.10, and the y coordinates are the design variables. So the design boundary on interval x^i and x^{i+1} has the form [14],

$$f(x) = Ay_i + By_{i+1} + C\ddot{y}_i + D\ddot{y}_{i+1} \tag{5.11}$$

where $\ddot{y}_i$ denotes the second derivative of the curve, and

$$A = \frac{x^{i+1} - x}{x^{i+1} - x^i}$$

$$B = \frac{x - x^i}{x^{i+1} - x^i}$$

$$C = \frac{1}{6}(A^3 - A)(x^{i+1} - x^i)^2$$

$$D = \frac{1}{6}(B^3 - B)(x^{i+1} - x^i)^2 \qquad (5.12)$$

let $x^{i+1} - x^i = h$, and substituting 5.12 into 5.11,

$$f(x) = \frac{x^{i+1} - x}{h}y_i + \frac{x - x^i}{h}y_{i+1} + \frac{x^{i+1} - x}{6h}[(x^{i+1} - x)^2 - h^2]\ddot{y}_i$$
$$+ \frac{x - x^i}{6h}[(x - x^i)^2 - h^2]\ddot{y}_{i+1} \qquad (5.13)$$

where $y_i = b_i$, $y_{i+1} = b_{i+1}$. $\ddot{y}$ can be obtained by considering the continuity of the second derivative at every node, and by specifying the boundary conditions at x^1 and x^n [17].

The variation f due to the change of the design variable b_i can be derived as

$$\delta f(x) = \frac{x^{i+1} - x}{h}\delta y_i + \frac{x - x^i}{h}\delta y_{i+1} + \frac{x^{i+1} - x}{6h}[(x^{i+1} - x)^2 - h^2]\delta \ddot{y}_i$$
$$+ \frac{x - x^i}{6h}[(x - x^i)^2 - h^2]\delta \ddot{y}_{i+1} \qquad (5.14)$$

note that each time only one design variable is nonzero, i.e. only one δy_i is nonzero. The evaluaton of $\delta \ddot{y}$ can be carried out by the finite difference method.

5.4   Numerical Examples

The program SOP is used here for shape optimal design problems. Some of the examples are solved by modified version of SOP - called SOP1, in which

BEASYG and BEASY[1] are used for the preprocessor and structural analyses. Numerical examples are presented to justify the theory implemented in SOP, and to investigate the different features of shape optimization. The four examples are:

1) A beam example
2) A fillet example
3) An infinite plate with a hole
4) A connecting rod

The objective function for all these examples is the area of the component, which can be calculated by transforming the domain integral into boundary integral using Greens theorem, i.e.

$$F(x) = \int_\Omega dx\,dy = \oint_\tau y n_y d\tau = \sum_i^n \int_{\tau_i} y_i n_y d\tau \qquad (5.15)$$

where n is the boundary element number, n_y is the y component of normal vector, and y_i is the y coordinate of element i.

The constraint is the Von Mises stresses,

$$G(x) = \frac{\sigma}{\sigma_a} - 1 \qquad (5.16)$$

where σ_a is the allowable stress, and σ is the Von Mises stress which can be expressed as

$$\sigma = \sqrt{\sigma_{xx}^2 + \sigma_{yy}^2 + 3\sigma_{xy}^2 - \sigma_{xx}\sigma_{yy}}$$

The stress sensitivities are carried out by using the continuum method, in which the adjoint loads are the distributed triangular loads. The design variables are the master nodes on the design boundary. The design boundary is modelled by either linear or cubic spline representation.

---

[1]BEASYG and BEASY are the commercial programs of Computational Mechanics Institute

5.4.1 A Beam Example

The first example is the optimum design of a cantilever beam. The beam is subject to a uniform vertical traction at its right end with $p = 10N/m$, and the total force $P = 40N$ will remain constant during optimization. The initial shape and the boundary discretization of the beam are shown in Fig. 5.11, where $b = 4m$, $l = 10m$.

The problem is considered as a plane stress problem. The material properties are: Young's modulus $E = 1.0 \times 10^7 psi$, Poission's ratio $\nu = 0.3$. The allowable stress is taken arbitrarily as $\sigma_a = 130 N/m^2$.

The design model is shown in Fig. 5.12, in which 5 master nodes are chosen as the design variables, which can move in y direction only. Due to the symmetry, the master nodes on the top surface of the beam can be linked with the design variables as

$$y_{i+5} = 2c - y_i \qquad , i = ,1,2,3,4,5 \qquad (5.17)$$

where c is the y coordinate of the central axis. The design boundary is formed by piecewise straight line connecting the master nodes.

The initial value of the objective function is 40.000, and the maximum stress violation is 6.3×10^{-2}. The final deign is obtained after 7 iterations, the objective function is reduced to 29.066, and the maximum stress violation as 0.42×10^{-2} which is within the required limits of maximum stress violation 1.0×10^{-2}. The term 'final design (sometimes called optimum design)' is used here to indicate the final design after the convergence test, in which the objective reaches a local minimum, and all the constraints are satisfied.

The modification history and the history of the objective function of the beam are shown in Fig. 5.13 and Fig. 5.14 respectively. It is noted that the shape at iteration 3 is nearly the same as the final shape. This also can be seen from the history of the objective, in which it decreases rapidly in the first

3 iterations, and then keeps almost constant.

The stress distribution of the beam at the initial design and the final design are shown in Fig. 5.15, which indicate that the stress level over the design surface has increased significantly. The big variation of the Von Mises stress along the design boundary are due to two reasons, 1) the mesh is very coarse, 2) the design boundary is piecewise linear, which will produce sudden change of the geometry at the master nodes.

A refined mesh is used next as shown in Fig. 5.16, with 7 master nodes y_1, ..., y_7. The optimum design is obtained after 7 iterations as shown in Fig. 5.17, which is nearly identical to the previous design. The stress distribution of this design is far smoother as can be seen from Fig. 5.18. This shows that even with similar shape, the stress distribution by BEM can differ a lot with different meshes, therefore it is advisable to avoid using a too coarse mesh in shape optimization problems.

In order to prevent the appearance of the nonsmooth boundary, a cubic spline boundary representation is employed. 7 design variables are used with the initial mesh as in Fig. 5.16. During optimization, the automatic remeshing is carried out to put more elements near the tip such that the load effects can be confined in a small area. The design converges at iteration 8, and the final design and the mesh distribution are shown in Fig. 5.19. The stress distribution of the final design are shown in Fig. 20. It can be seen that the stresses are more smoother than the linear case (Fig. 5.18).

5.4.2 A Fillet Example

The fillet example has been widely used to test optimization system, since it presents a large number of optimization problems with stress concentrations [18, 19]. The initial geometry of the fillet is shown in Fig. 5.21, where *ab* is

the design boundary with a and b fixed. The external load p at the right hand end is 100 psi. The material properties are: $E = 1.0 \times 10^7$ psi, $\nu = 0.3$. The allowable stress is assumed as 120 psi.

Piecewise linear design boundary

The y coordinates of 9 points on the design boundary are chosen as design variables as shown in Figure 5.22. The initial value of the objective function is 145.125, and the maximum stress violation is 0.244. The final design is obtained after 9 iterations, the objective function reduces to 134.420, and the maximum stress violation is 2.13×10^{-2}. The initial design variables are

$$4.950, 5.400, 5.850, 6.300, 6.750, 7.200, 7.650, 8.100, 8.550$$

and the final values are

$$4.500, 4.501, 4.586, 5.650, 4.789, 4.922, 5.143, 5.384, 5.806$$

The final shape is shown in Figure 5.23.

If only 4 design variables are used, i.e. y_2, y_4, y_6 and y_8, then the design converge after 6 iterations, the objective function becomes 138.046, and there is no stress violation. The final design is shown in Fig. 5.23. It can be observed that the linear boundary representation produce a nonsmooth boundary, especially for the case of less design variables.

Cubic spline boundary

The 9 design variables are the same as in piecewise linear boundary shown in Figure 5.22. The final design is obtained after 8 iterations, the objective function reduces to 134.284, and the maximum stress violation is 4.9×10^{-3}. The design variables at the final shape are

$$4.504, 4.504, 4.571, 4.636, 4.766, 4.896, 5.101, 5.311, 6.069$$

The final boundary shape is shown in Figure 5.24.

Figure 5.25 shows the change of the objective function and the maximum stress constraint during the optimization process. It can be seen that the objective function reaches the minimum for the first few iterations, the maximum stress constraint does not converge at this stage. Then both the objective function and the maximum stress constraint converge to the final optimal values as the iteration proceeds.

If only 4 design variables are used, after the same number of the iterations, the objective function is 137.294, and the maximum stress violation is 7.6×10^{-3}. The final design is shown in Figure 5.24.

New design variable system using the cubic spline

It is noted that the left hand design boundary of the final design (Fig. 5.24) is nearly vertical, therefore this part of the design boundary is not efficiently controlled by the master nodes. A new set of design variables is chosen as shown in Fig. 5.26 which takes into account this consideration. The design variables are equally spaced along $\bar{x}$, and can move in $\bar{y}$ direction only.

Different number of design variables (NDV) are used, and the final shapes are shown in Fig. 5.27. If no remeshing is carried out during the optimization, the final design has a wiggling design boundary as shown in Fig. 5.27(a), whereas the remeshed final design of Fig. 5.27(b) is smooth. The final designs are almost the same for NDV = 5,7,9, which have a similar shape with FEM results [18]. But further decrease NDV from 5 to 3 will cause a nonsmooth boundary and a big increase of the objective function. The further increase NDV from 9 to 11 will result in a wiggling boundary. Therefore we have the observation: if the master nodes are used as design variables, the number of design variables should be within a range in order to get a smooth boundary. According to author's experiences, the remeshing of the design boundary is easier for small NDV than big NDV. The wiggling shape for large NDV also appears in using FEM for the optimum design of the fillet [18].

5.4.3 A Plate With a Hole

A square plate with a central hole is shown in Fig. 5.28, subject to the in-plane tensile loads. The objective is to reduce the stress concentration along the hole. It has been proved that the best shape of the hole in an infinite plate for minimum stress concentration is an elliptic, with the ratio of the axes being equal to the ratio of the applied tensile loads, i.e.

$$\frac{a}{b} = \frac{\sigma_x}{\sigma_y} = v \tag{5.18}$$

where a and b present the axes of the elliptic in x and y direction respectively, v is the ratio of the applied stresses in x and y directions.

Since the size of the hole is far smaller than the size of the plate, therefore the plate can be treated as an infinite plate, so the optimum shape of the hole can be taken as an elliptic with $a/b = v$.

Due to symmetry, only quarter of the plate is considered, and the design model is shown in Fig. 5.29. 7 design variables are used, which present the distance of the boundary master nodes to the central point o. The design boundary is represented by a cubic spline passing through the 7 master nodes. The mesh at the initial shape is also shown in Fig. 5.29. 6 elements are used to describe the quarter of the hole.

Case 1, $v = 1$

(The analytical solution is a circle)

The final design is obtained after just 4 iterations as shown in Fig. 5.30, which is almost a circle. The maximum error of the geometry is 0.5%, and the maximum stress error is 2.1%. The geometry error is defined as

$$\delta_g = |\frac{r_{nu} - r_{an}}{r_{an}}| \tag{5.19}$$

where r_{nu} and r_{an} are the numerical value and the analytical value respectively.

The stress error is defined as

$$\delta_s = |\frac{\sigma_{nu} - \sigma_{an}}{\sigma_{an}}| \tag{5.20}$$

where σ_{nu} and σ_{an} are the numerical stress and the analytical stress respectively. The analytical stress along an elliptic in an infinite plate is $\sigma_{an} = \sigma_x + \sigma_y$.

Case 2, $v = 2$

(The analytical solution is an elliptic with $a/b = 2$.

The final design is reached in 6 iterations, which is shown in Fig. 5.31. The maximum geometry error is 1.9%, and the maximum stress error is 4.9%. It should be mentioned here that the cubic spline can never model an elliptic exactly, so further reducing the geometry error is nearly impossible.

5.4.4   A Connecting Rod

This example is taken from Abe et al. [20] as shown in Fig. 5.32. The load p is 200 psi, and the allowable stress is 400 psi. The right quarter circle is subject to normal displacement constraints.

The design boundary is ab with a and b fixed. The geometry constraints are introduced such that the minimum dimensions of the fillet are not less than the left side width in order to prevent buckling. It is assumed that the stress constraints are on the design boundary only.

Let us consider the linear boundary representation first, in which 7 master nodes on the design boundary are chosen as the design variables. The final design is obtained after 8 iterations as shown in Fig. 5.33. The area of the connecting rod is reduced from 701.487 at the initial design to 463.762 at the final design. This result is similar with the result by Abe et al. [20].

In order to obtain a more smooth boundary, a cubic spline is used with 6 master nodes on the design boundary. The final design is obtained after 7

iterations, and the area is reduced to 463.135. The final shape is shown in Fig. 5.34.

It is found from the final designs of both linear case and the cubic spline case that there is no stress violation all over the boundary except the stress near the point A on the top of the half circle, in which the stress violation is 40% for the linear case and 35% for the cubic case. This is because that the stress at A of the initial design is 380 psi, which is quite close to the allowable stress. Any deep cut along the fillet boundary will increase the stress at A significantly. If the stress constraints are imposed on all the boundary, then the final design using the cubic spline is obtained after 12 iterations. The area is reduced to 570.721, and there is no stress violation. The final design is shown in Fig. 5.35.

5.5 References

[1] Bhavikatti, S. S., Ramakrishnan, C. V., Optimum Shape Design of Rotating Disks, Comput. Struct., 11, 1980, pp. 397-401.

[2] Imam, M. H., Three-Dimensional Shape Optimization, Int. J. Numer. Meth. Engng., 18, 1982, pp. 661-673.

[3] Botkin, M. E., Shape Optimization of Plate and Shell Structures, AIAA, 20, 1982, pp. 268-273.

[4] Weck, M., Steinke, P., An Efficient Technique in Shape Optimization, J. Struct. Mech., 11, 1983, pp. 433-449.

[5] Luchi, M. L., Poggialini, A., Persiani, F., An Interactive Optimization Procedure Applied to the Design of Gas Turbine Discs, Comput. Struct., 11, 1980, pp. 629-637.

[6] Zhzo, Z. Y., Adey, R. A., Shape Optimization, A Numerical Consideration, Proc. BEM11, CMP and Springer-Verlag, Boston, August, 1989, pp.195-210.

[7] Fleury, C., Computer Aided Optimal Design of Elastic Structures, Prof. Computer Aided Optimal Design: Structural And Mechanical Systems, Springer-Verlag, 1987.

[8] Rasmussen, J., Interactive Shape Optimization with Design Elements, Proc. GAMM Seminar, FRG, Springer-verlag, 1988.

[9] Kane, J. H., Optimization of Continuum Structures Using A Boundary Element Formulation, PhD thesis, University of Connecticut, USA, 1986.

[10] Braibant, V., Fleury, C., Shape Optimal Design Using B-Spline, Comput. Meth. Appli. Mech. Engng., 44, 1984, pp. 247-267.

[11] Mota Soares, C. A., Leal, R. P., Choi, K. K., Boundary Elements in Shift Optimal Design of Structural Components, Computer Aided Design: Structural and Mechanical Systems, Springer-Verlag, 1987, pp. 605-632.

[12] Gonzalez, A., Alarcon, E., adaptive Refinements in Boundary Elements, Proc. First World Congress on Computational Mechanics, Austin, Texas, 1986.

[13] Rencis, J. J., Muellen, R. L., A Self-Adaptive Mesh Refinement Technique for Boundary Element Solution of the Laplace Equation,Comput. Meth. Appl. Mech. Engng., 1986.

[14] Press, W. H., Flannery, B. P., Teukolsky, S. A., Vetterling, W. T., Numerical Recipes, Cambridge University Press, Cambridge, 1987.

[15] Vanderplaats, G. N., ADS - A Fortran Program For Automated Design Synthesis, Engineering Design Optimization Inc., USA, 1987.

[16] Rogers, D. F., Adams, J. A., Mathematical Elements for Computer Graphics, McGraw-Hill Book Company, New York, 1967.

[17] Mortenson, M. E., Geometric Modeling, John Wiley & Sons, 1985.

[18] Yang, R. J., Choi, K. K., Haug, E. J., Numerical Considerations in Structural Component Shape Optimization, ASME, 107, 1985, pp. 334-339.

[19] Choi, J. H., Kwak, B. M., Boundary Integral Method for Shape Optimization of Elastic Structures, Int. J. Numer. Meth. Engng., 26, 1988, pp. 1579-1595.

[20] Abe, J., Nagai, T., Kamiya, N., Minimum Weight Design by Boundary Element Method, Computer Aided Optimum Design: Recent Advances, CMP and Springer-Verlag, Southampton, UK., 1989.
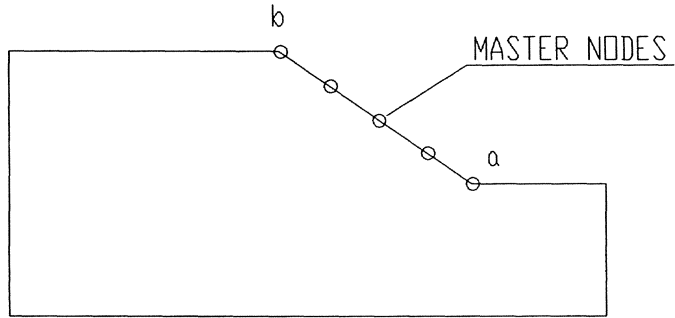
Fig. 5.1(a) The Design Model
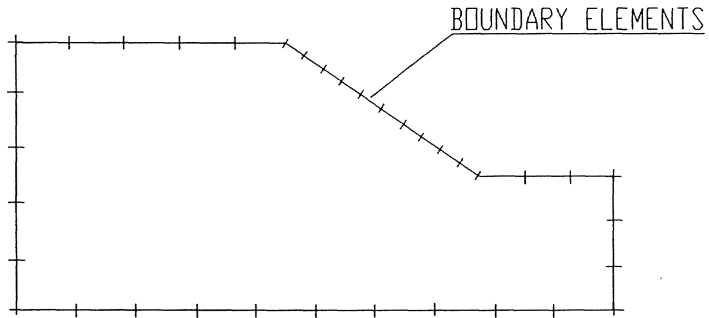
Fig. 5.1(b) The Analysis Model
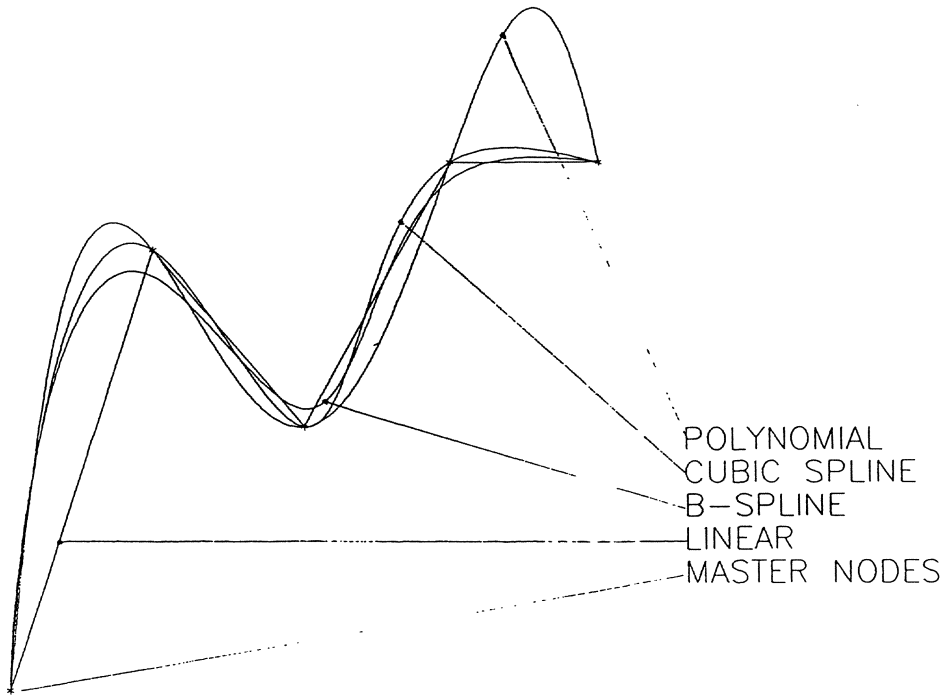
Fig. 5.2 The Comparison of the Different Curves

POLYNOMIAL
CUBIC SPLINE
B—SPLINE
LINEAR
MASTER NODES

COMMON NODE i

ELEMENT 1   ELEMENT 2
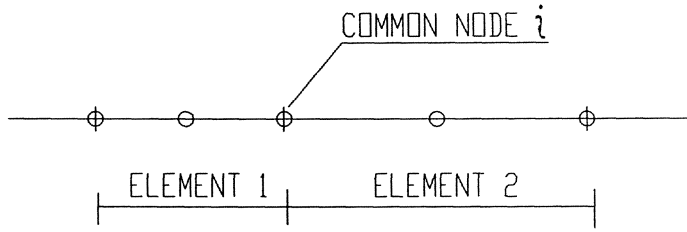
Fig. 5.3 The Common Node on a Smooth Boundary
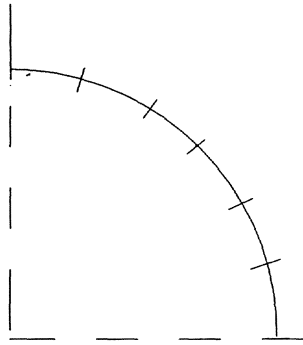
Fig. 5.4(a) Modelling of a Quarter Circle
(iteration i)
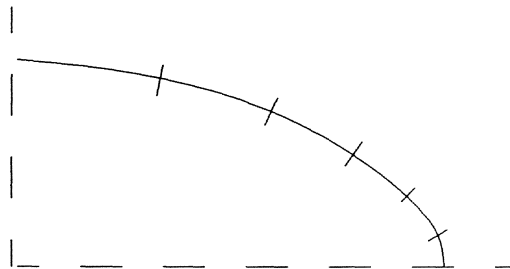
Fig. 5.4(b) Modelling of a Quarter Elliptic
(Iteration i+1)
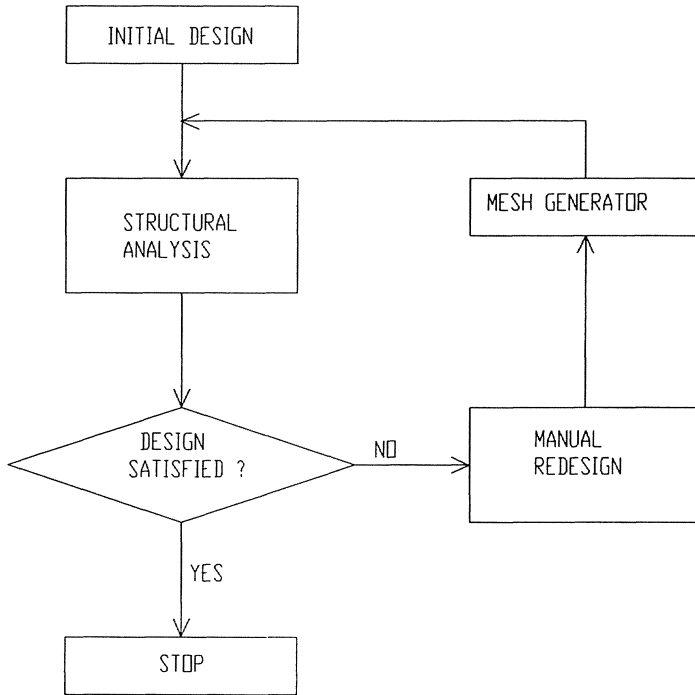
Fig. 5.5 Manual Design Process
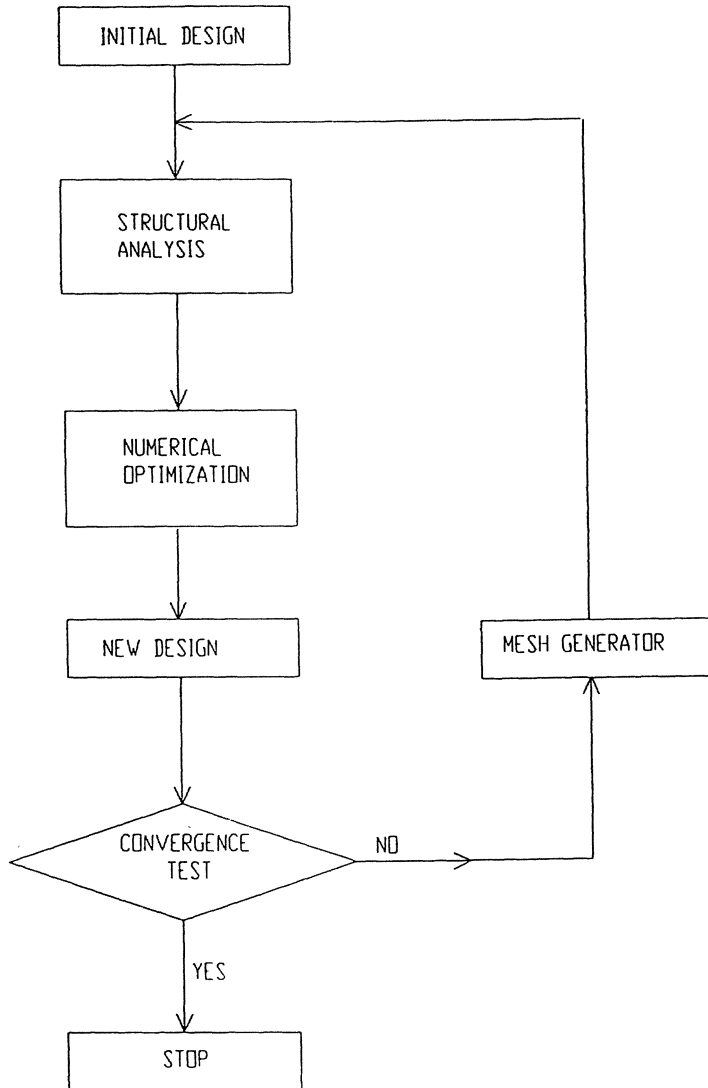
Fig. 5.6 Automatic Design Process
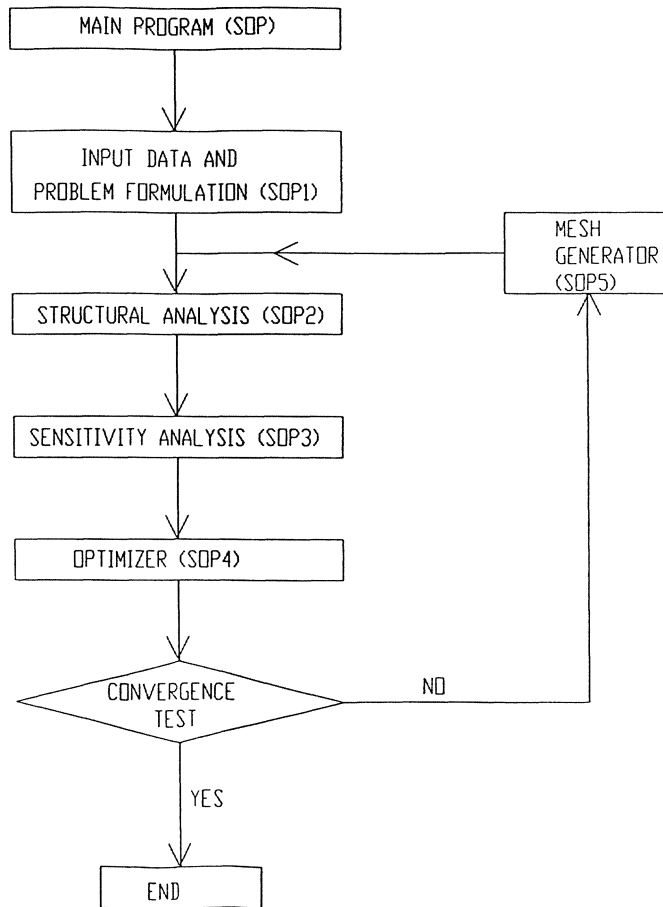
Fig. 5.7 The Flow Chart of SOP
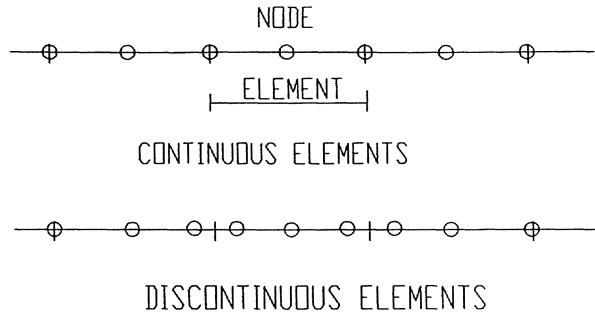
Fig. 5.8 The Element Types
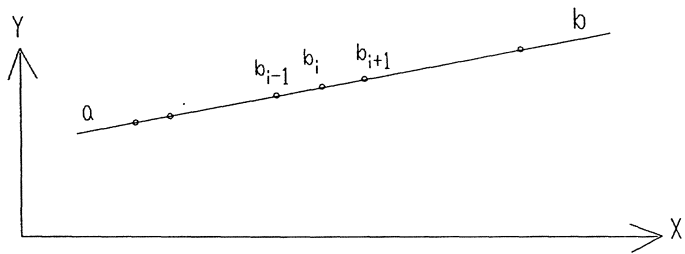
Fig. 5.9 The Linear Boundary Representation
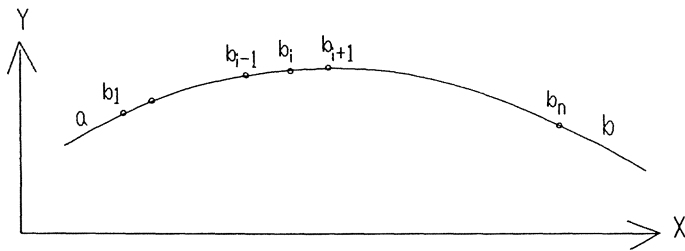
Fig. 5.10 The Cubic Spline Boundary Representation
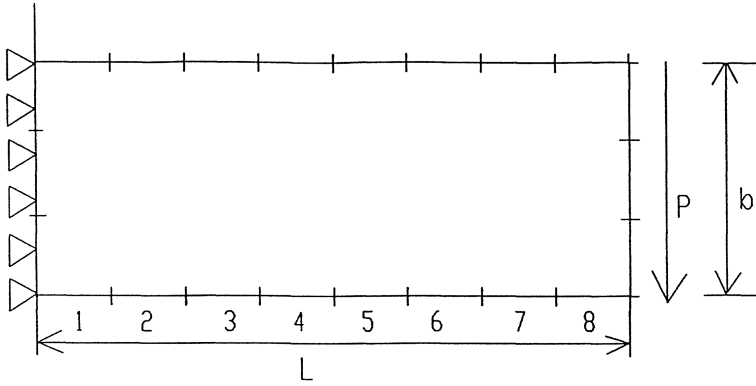
Fig. 5.11 The Beam Example
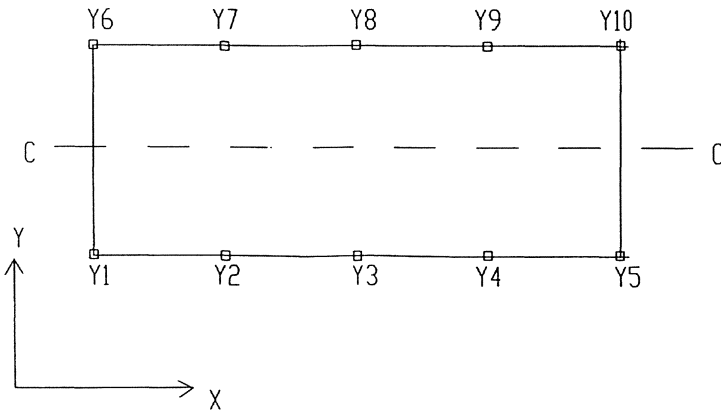
Fig. 5.12 The Design Model
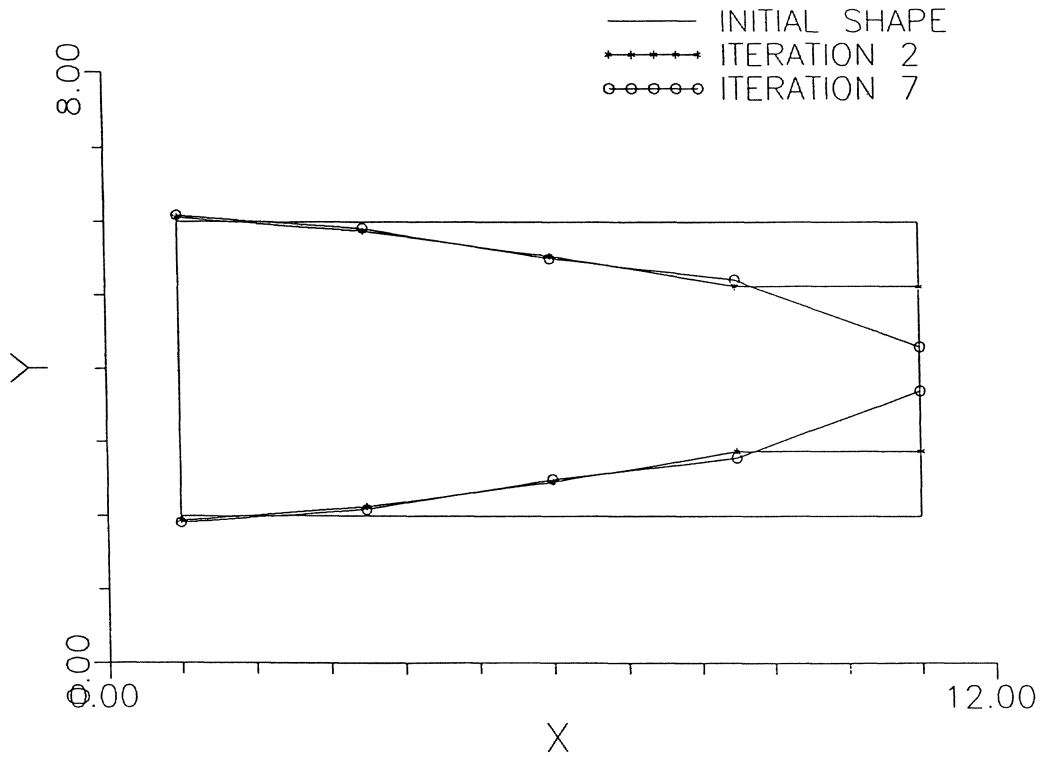
Fig. 5.13 Modifications of the Beam
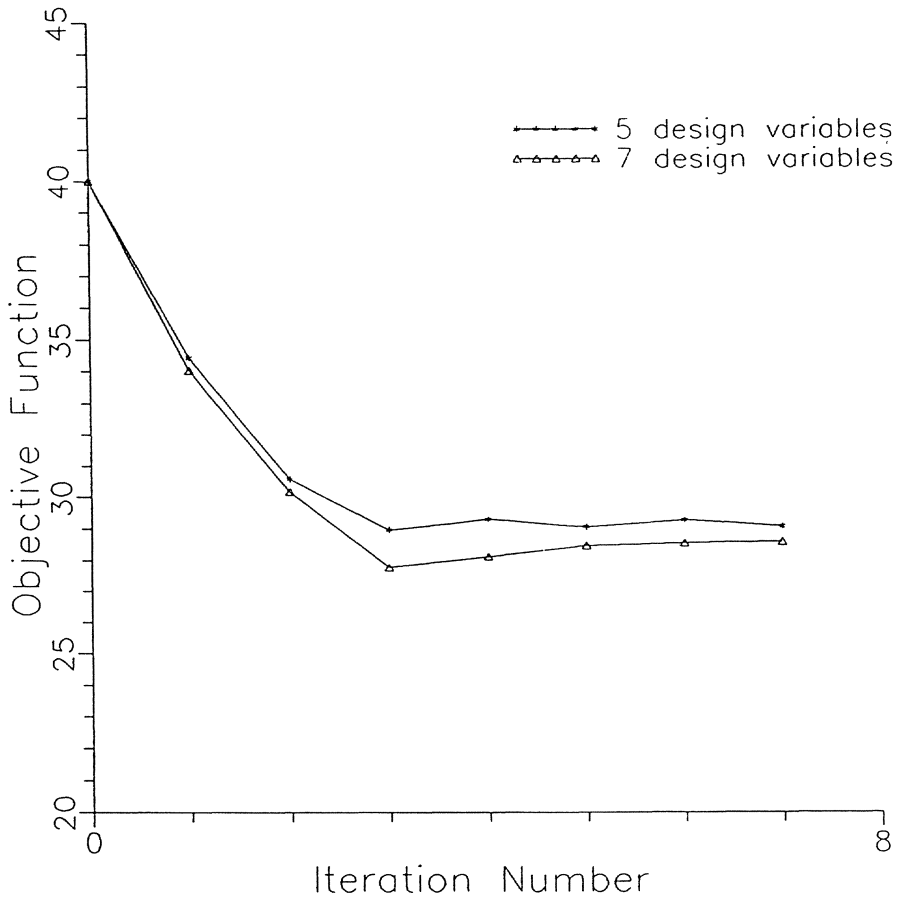
Fig. 5.14 History of the Objective Function
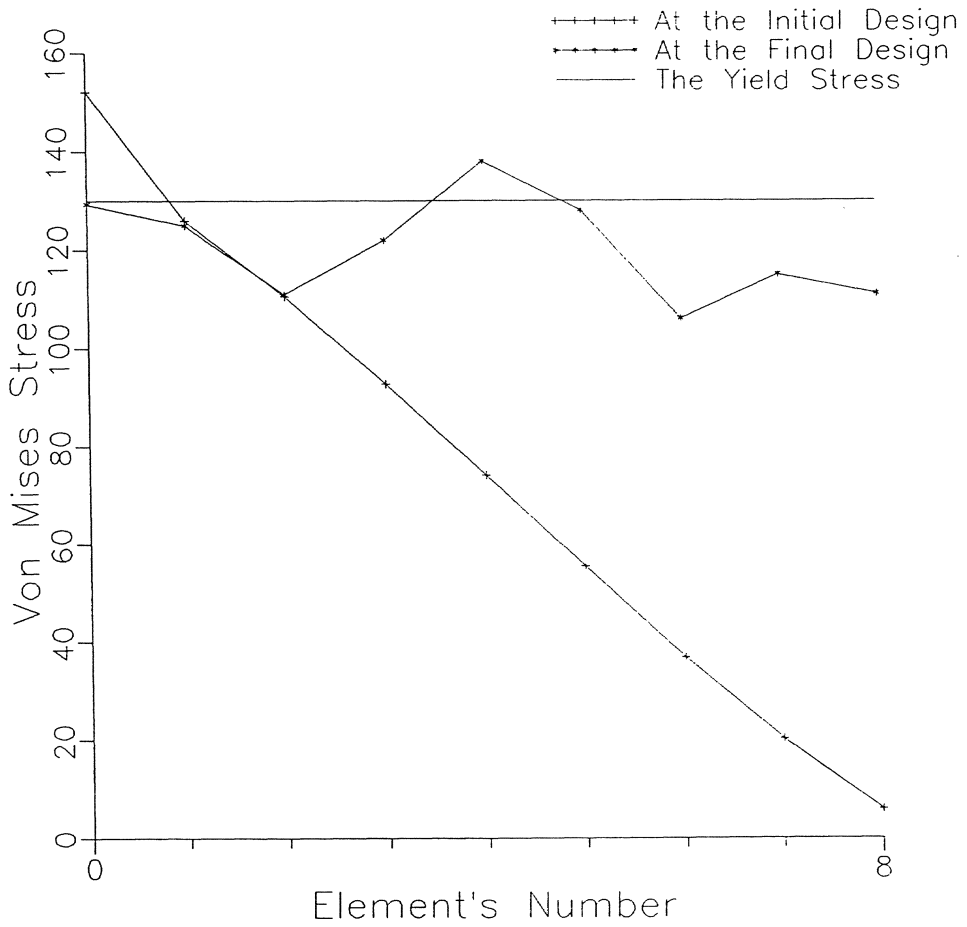
Fig. 5.15 The Stress Distribution of the Beam
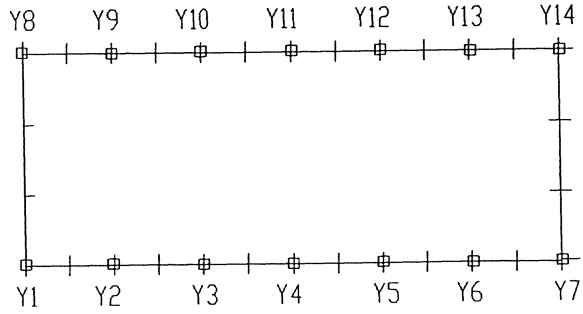
Fig. 5.16 The Design Model
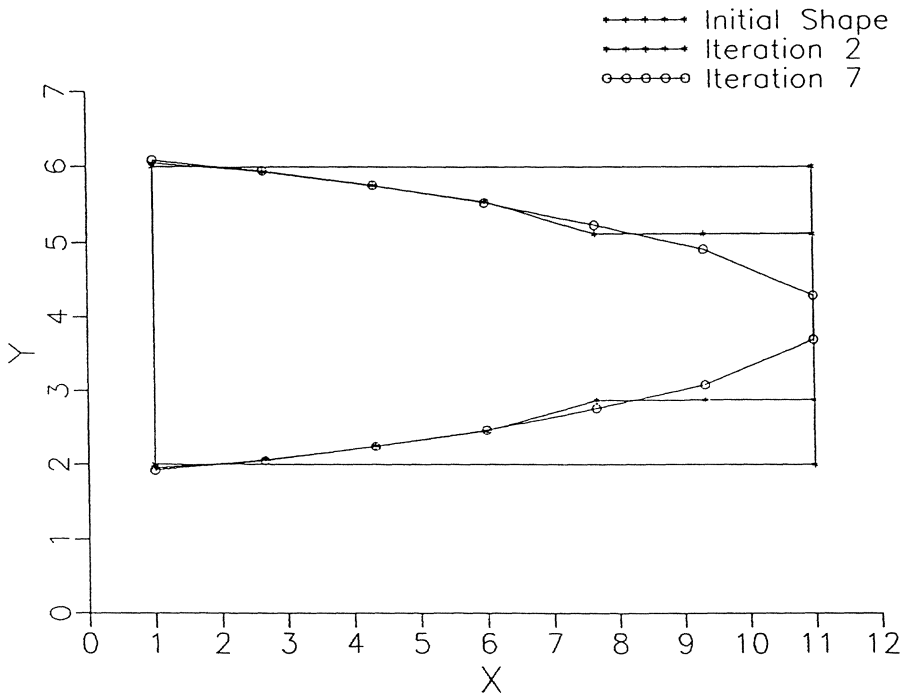
Fig. 5.17 Modifications of the Beam
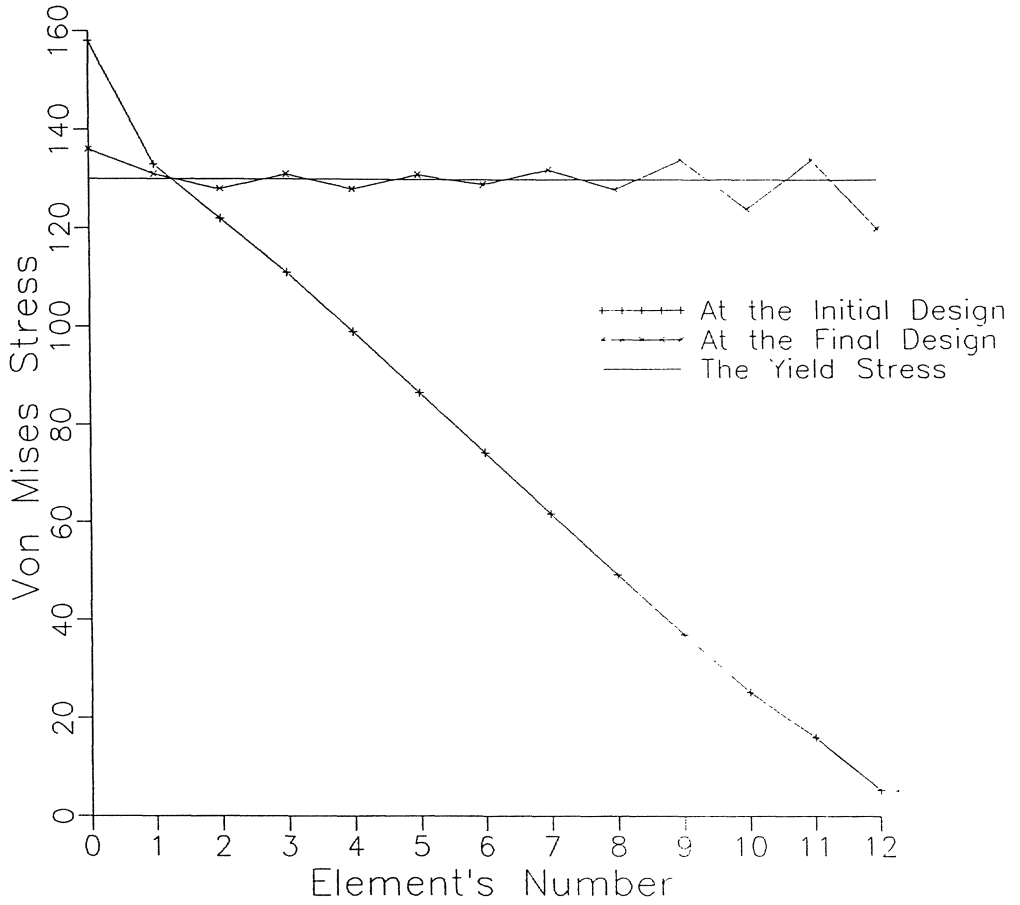
Fig. 5.18 Stress Distribution of the Beam
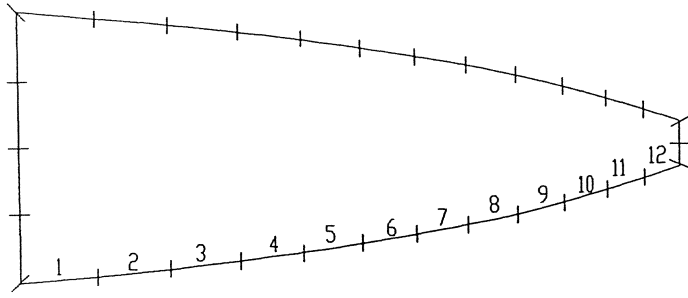
Fig. 5.19 The Mesh at the Final Design
(Cubic Spline)
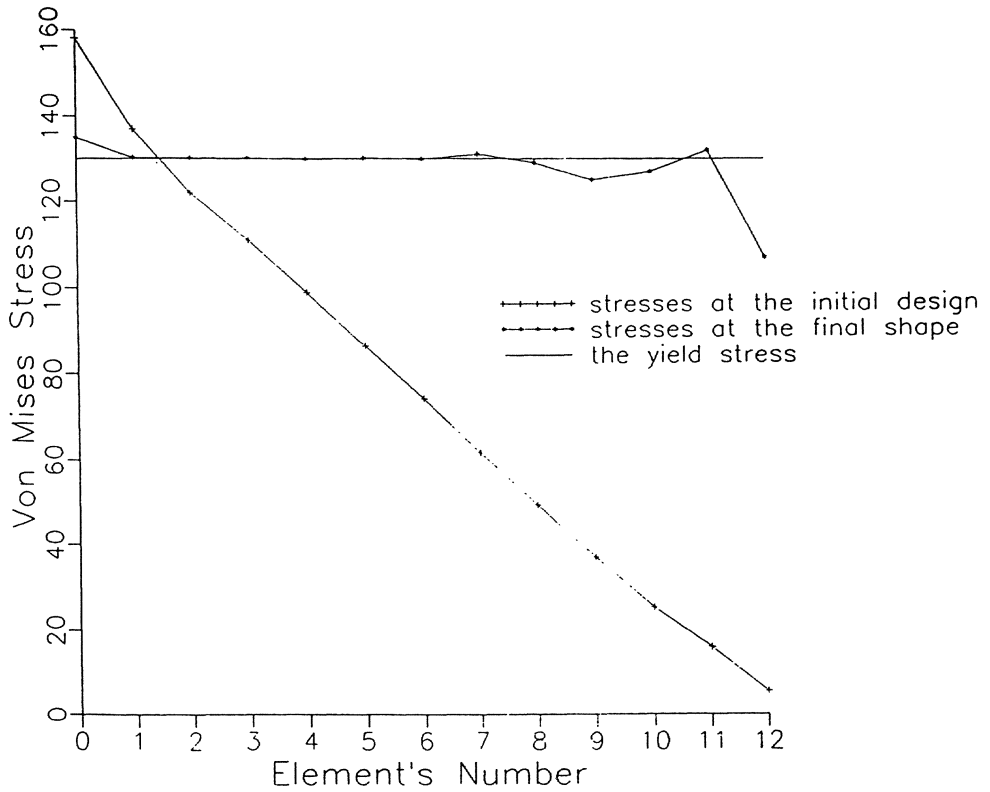
Fig. 5.20 Stress Distribution of the Beam
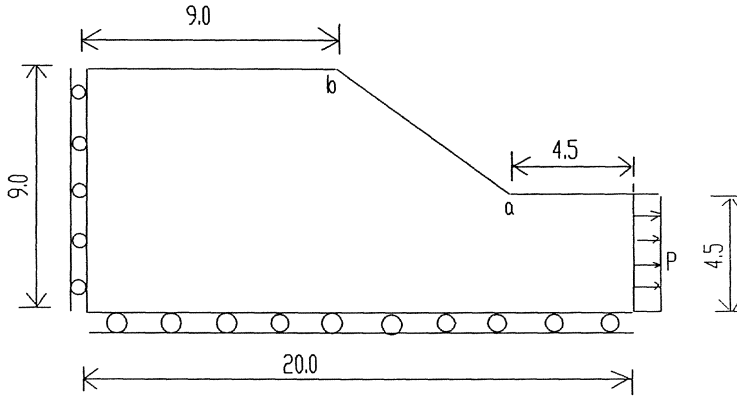
Fig. 5.21 The Fillet Example
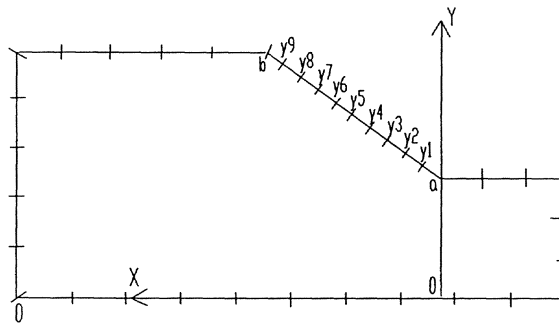
Fig. 5.22 The Analysis Model and the Design Variables
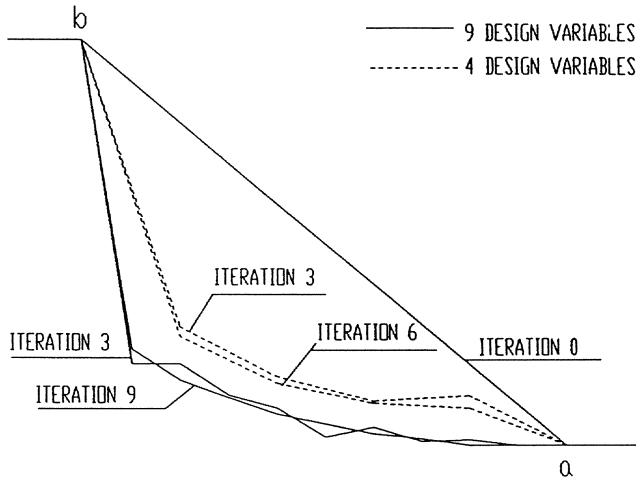
Fig. 5.23 Iteration History
(Linear Case)
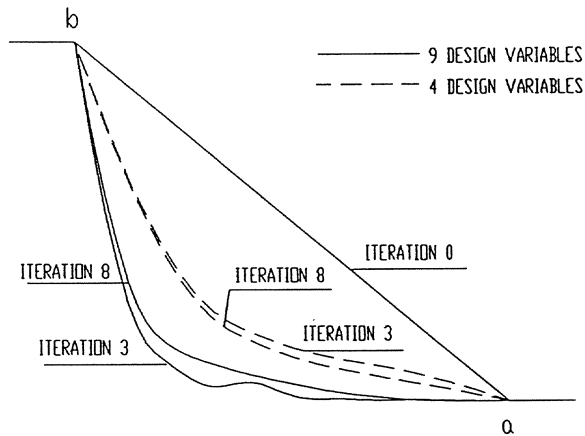
Fig. 5.24 Iteration History
(Cubic Spline)
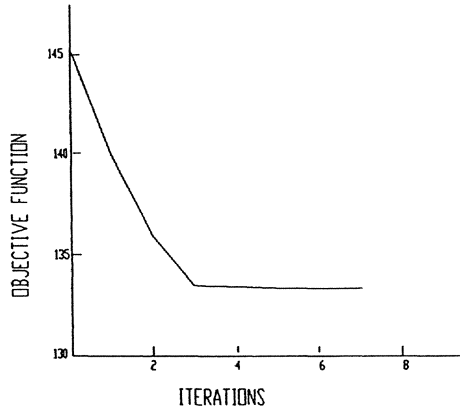
Fig. 5.25(a) History of the Objective Function
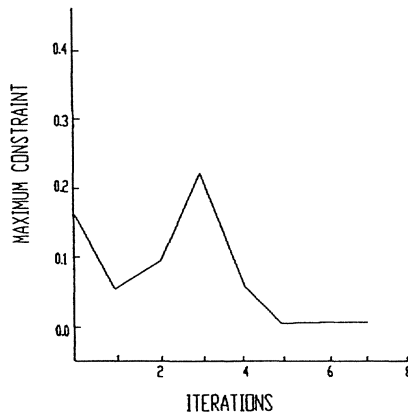
Fig. 5.25(b) History of the Maximum Constraints
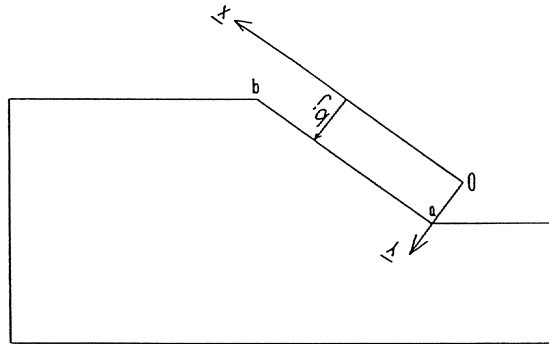
Fig. 5.26 New Design Variable System
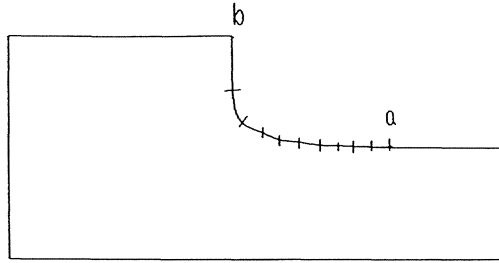
```
NO OF DESIGN VARIABLES = 9
NO OF ITERATIONS      = 9
TOTAL AREA            = 132.262
NO OF ELEMENTS ON
THE DESIGN BOUNDARY   = 10
```

Fig. 5.27(a) The Final Design without Remeshing
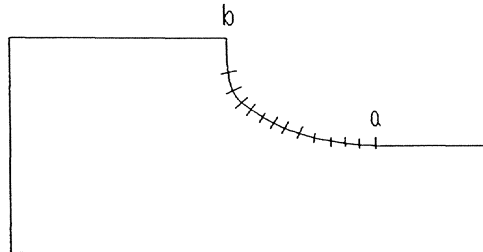

```
NO OF DESIGN VARIABLES = 9
NO OF ITERATIONS      = 6
TOTAL AREA            = 134.906
NO OF ELEMENTS ON
THE DESIGN BOUNDARY   = 13
```

Fig. 5.27(b) The Final Design with Remeshing
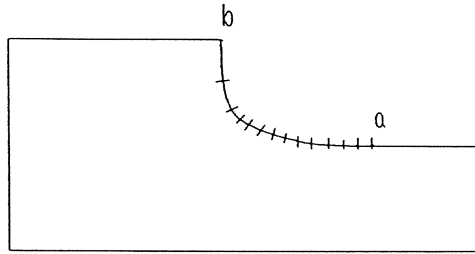
NO OF DESIGN VARIABLES = 7
NO OF ITERATIONS   = 7
TOTAL AREA   = 133.188
NO OF ELEMENTS ON
THE DESIGN BOUNDARY   = 12

Fig. 5.27(c) The Final Design of the Fillet
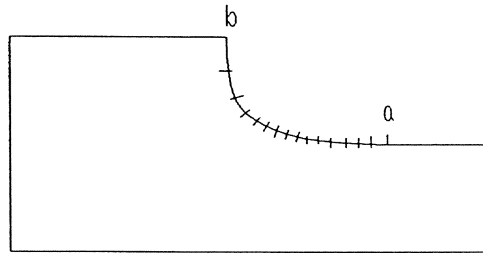
NO OF DESIGN VARIABLES = 5
NO OF ITERATIONS   = 9
TOTAL AREA   = 133.328
NO OF ELEMENTS ON
THE DESIGN BOUNDARY   = 15

Fig. 5.27(d) The Final Design Of the Fillet
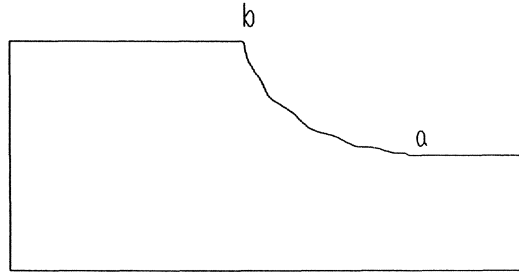
Fig. 5.27(e) The Final Design of the Fillet
(NDV=9)
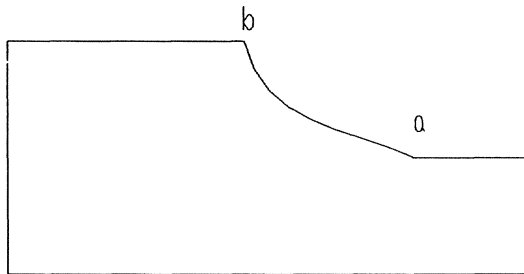
Fig. 5.27(f) The Final Design of the Fillet
(NDV=3)
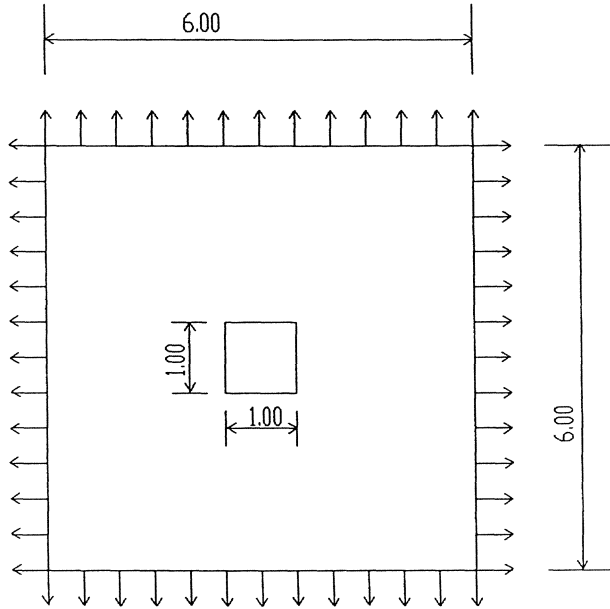
Fig. 5.28 A Plate with a Hole
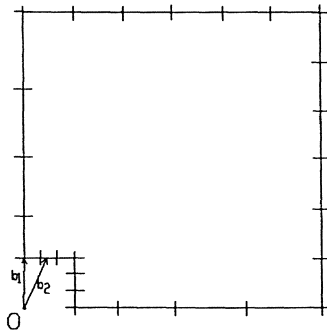
Fig. 5.29 The Design Model and the Analysis Model
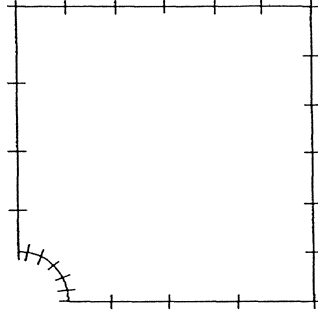
Fig. 5.30 The Final Design ($\nu = 1$)
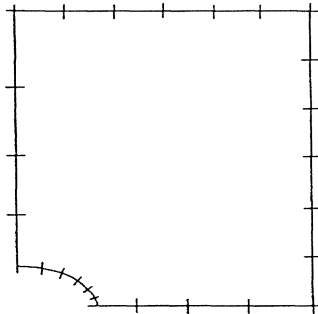
Fig. 5.31 The Final Design ($\nu = 2$)
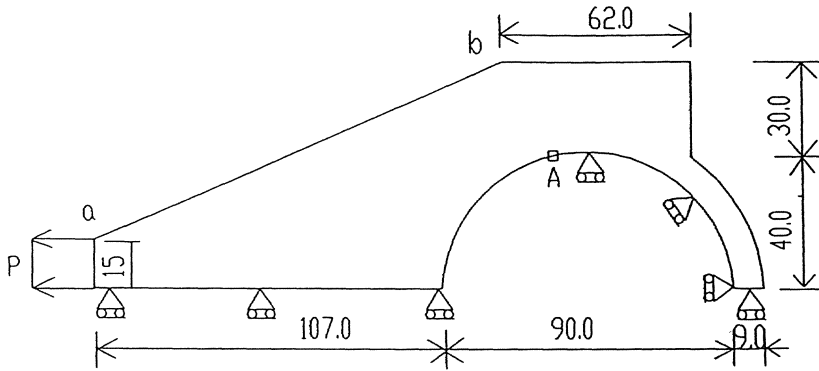
Fig. 5.32 A Connecting Rod
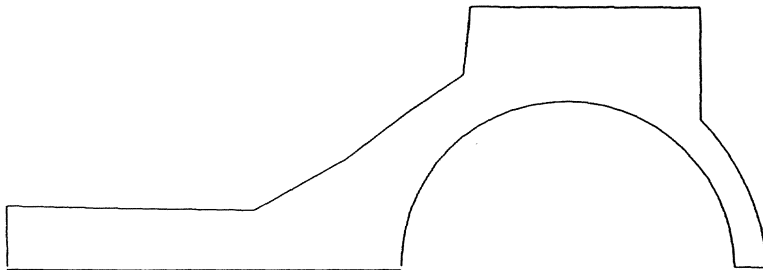
Fig. 5.33 The Final Design (Linear Case)
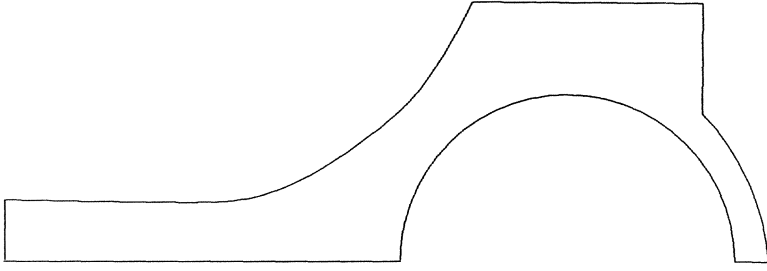
Fig. 5.34 The Final Design (Cubic Spline)
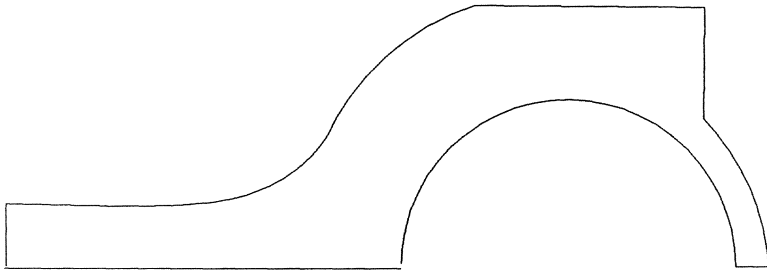
Fig. 5.35 The Final Design (Cubic Spline)

Appendix A

Fundamental Solutions of the Semi-infinite Plane

For a semi-infinite plane under a unit load as shown in Fig. A-1, the Mindlin's solutions are (plane strain):

Stresses:

$$\sigma_{xx} = -\frac{2}{\pi}\frac{x^2 y}{r^4} \tag{A.1}$$

$$\sigma_{xy} = -\frac{2}{\pi}\frac{y^2 x}{r^4} \tag{A.2}$$

$$\sigma_{yy} = -\frac{2}{\pi}\frac{y^3}{r^4} \tag{A.3}$$

Displacements:

$$u_x = -k_d\{-(1-2\nu)\theta - \frac{xy}{r^2}\} \tag{A.4}$$

$$u_y = -k_d\{2(1-\nu)\ln(r) - \frac{y^2}{r^2} \tag{A.5}$$

where $k_d = 1/2\pi G$, and G is the shear modulus.

For a semi-infinite plane under one pair unit loads along the tangential direction as shown in Fig. A-2, the solutions can be obtained by differentiating

the Mindlin's solutions in y direction, the solutions are given below for plane strain.

Stresses:

$$\sigma_{xx} = \frac{2}{\pi}\frac{x^2(x^2 - 3y^2)}{r^6}\delta y \tag{A.6}$$

$$\sigma_{xy} = \frac{2}{\pi}\frac{2xy(x^2 - y^2)}{r^6}\delta y \tag{A.7}$$

$$\sigma_{yy} = \frac{2}{\pi}\frac{y^2(3x^2 - y^2)}{r^6}\delta y \tag{A.8}$$

Displacements:

$$u_x = k_d\frac{2x(\nu - x^2/r^2)}{r^2}\delta y \tag{A.9}$$

$$u_y = k_d\frac{2y(-\nu + y^2/r^2)}{r^2}\delta y \tag{A.10}$$

Boundary tractions:

$$T_x = \frac{2}{\pi r^6}[x^2 n_x(x^2 - 3y^2) + 2xy n_y(x^2 - y^2)]\delta y \tag{A.11}$$

$$T_y = \frac{2}{\pi r^6}[2xy n_x(x^2 - y^2) + y^2 n_y(3x^2 - y^2)]\delta y \tag{A.12}$$

Where n_x and n_y are the direction cosines of the normal in x and y directions respectively.

Appendix B

Derivatives of Boundary Stresses on the Normal Direction

Consider an equilibrium structure with traction boundary τ as shown in Fig. B-1. Taking a small block A with one side coincide with boundary τ out from the domain Ω. The stress state of the block is shown in Fig. B-2, in which the polar coordinates are used.

By considering the equilibrium of block A in radial and tangential directions, and taking the dimension of the block A approaching to zero, we obtain

$$\frac{\partial \sigma_r}{\partial r} \quad + \quad \frac{\partial \sigma_{r\theta}}{r\partial \theta} + \frac{\sigma_r - \sigma_\theta}{r} + X_r$$

$$\frac{\partial \sigma_{r\theta}}{\partial r} \quad + \quad \frac{\partial \sigma_\theta}{r\theta} + \frac{2\sigma_{r\theta}}{r} + X_\theta \tag{B.1}$$

(B.1) can be rearranged to obtain the derivatives of the stresses along n^- direction,

$$\frac{\partial \sigma_n}{\partial n^-} \quad = \quad k(\frac{\partial \sigma_{r\theta}}{r\partial \theta} + \frac{\sigma_r - \sigma_\theta}{r} + X_r)$$

$$\frac{\partial \sigma_{r\theta}}{\partial n^-} = k\left(\frac{\partial \sigma_\theta}{r\partial \theta} + \frac{2\sigma_{r\theta}}{r} + X_\theta\right) \tag{B.2}$$

where X_r and X_θ are the components of the body force. r is the radius of the boundary, $k = 1$ if n^+ is in the r direction (i.e. convex boundary), otherwise $k = -1$. σ_r, $\sigma_{r\theta}$ are the boundary tractions, σ_θ is the tangential stress, which can be evaluated by differentiating the displacement field of the BEM solutions on the boundary. Thus once we know the BEM solutions, the above two stress derivative along n^- direction can be obtained numerically.

For straight boundary, (B.2) can be simplified as:

$$\frac{\partial \sigma_{sn}}{\partial n^-} = \frac{\partial \sigma_s}{\partial s} + X_s$$
$$\frac{\partial \sigma_n}{\partial n^-} = \frac{\partial \sigma_{sn}}{\partial s} + X_n \tag{B.3}$$

where σ_s denotes the tangential stress, and σ_{sn} is the tangential traction, which has the positive sign if it is along S^+ direction. X_n and X_s are the components of the body force.
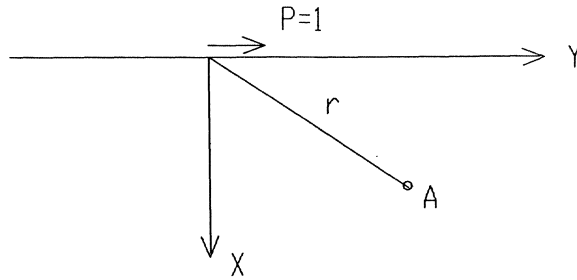
Fig. A-1 Mindlin's Problem
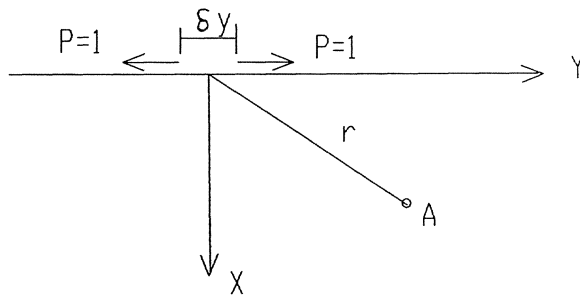
Fig. A-2 Semi-Infinite Plate under a Pair Loads
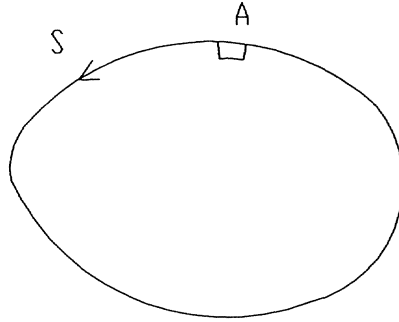
Fig. B-1 An Equilibrium Body

Fig. B-2 The Equilibrium of the Block A

Lecture Notes in Engineering

Edited by C.A. Brebbia and S.A. Orszag